Volume 12, Number 1, 2018

Technical University of Cluj-Napoca
North University Centre of Baia Mare
Faculty of Engineering
Electrical, Electronic and Computer Engineering Department

Volume 12, Number 1, 2018

Carpathian Journal of Electrical Engineering

Carpathian Journal of Electrical Engineering

ISSN 1843 - 7583

UTPRESS PUBLISHER

TECHNICAL UNIVERSITY
OF CLUJ-NAPOCA

NORTH UNIVERSITY CENTRE OF BAIA MARE
FACULTY of ENGINEERING

ELECTRICAL, ELECTRONIC AND
COMPUTER ENGINEERING DEPARTMENT

Carpathian Journal of Electrical Engineering

Volume 12, Number 1, 2018

ISSN 1843 – 7583
http://cee.ubm.ro/cjee.html

CONTENTS

THE REDUCTION OF TOTAL HARMONIC DISTORTION FOR THE MULTILEVEL CONVERTER USING GENETIC ALGORITHMS OPTIMIZATION METHOD

Horatiu Dacian **LASLO**[1], Traian **VARODI**[2]
[1] *SC Electroplus SRL Cluj-Napoca,* [2] *Technical University of Cluj-Napoca.*
office@electroplus-cluj.ro, tvarodi@gmail.com

Keywords*:* **distortion, multilevel converter, algorithms**

Abstract*: Electricity, DC voltage - AC voltage, conversion generated from certain renewable energy sources such as photovoltaic panels should be made with quality factors imposed by the present standards. In the case of multilevel converters the achievement of reasonable distortion factor is realized by optimizing the targeted waveform using Newton Raphson method. This paper presents an optimization solution based on genetic algorithm. Voltage waveforms obtained by this technique and the total harmonic distortion degree of reduction are presented by comparing the results obtained from supplying a consumer with a voltage generated in classical way through DC-AC conversion, using multilevel converter.*

I. INTRODUCTION

In the last decades, the demand of energy produced from renewable sources has increased due to environmental issues and decrease of classics fuel sources: oil, coal and natural gas. Among renewable energy sources the most commonly used for grid connection [1] are photovoltaic panels and wind turbines. The control of the output voltage and frequency are the main problems in the connection of these renewable sources to the grid and therefore for connection, special converters are used in order to make frequency and voltage regulation.

In the case when renewable source produce DC voltage, such as photovoltaic panels or fuel cells the DC-DC converters are used in order to change the level of DC voltage to the required value demanded by application. The converters are also used to improve the voltage quality provided by energy sources. DC-AC converters are used to convert the DC voltage to

AC voltage, at the level of voltage and frequency from the grid. The development of medium and high power renewable sources applications have determined a series of researches in the field of multilevel converters, especially for wind turbine applications, which have as disadvantage the speed variation.

Since the 80s, many power electronics researches have focused on improving the efficiency of current and voltage parameters from semiconductor devices. In order to obtain higher voltage levels electronic converters have been developed. In 1981, converter schematics proposed neutral point-clamped PWM inverter PWM NPC, as well as improved version of multilevel converter with two levels and which today is known as the "diode-clamped multilevel inverter".

Multilevel converter topologies can be divided into three major groups:

• Cascaded multilevel inverters;

• Diode-clamped multilevel inverters;

• Flying-capacitor multilevel inverter.

Along with the converter topology [5], the current researches in the field of multilevel converters are oriented towards finding the optimal solution for commutation. Control strategy aims the minimization of harmonic spectrum for the output sizes and switching losses reduction as low as possible. There are three commutation methods, specifics to multilevel converters such as:

Selective Harmonic Elimination. At this method, each switching device is switched on and off once in one cycle of the connection-disconnection, and the control angles are chosen according to the harmonics that needs to be eliminated in order to minimize the total harmonic distortion factor (THD) for the output voltage.

Carrier-Based PWM. At this method, the switches command signals results from the comparison of reference signal with the signal measured on the AC grid.

Space-Vector PWM. The method is based on command reconfiguration by sampling the command signal according to the inverter output voltage vector.

Multilevel converters allows the growth of output voltage without increasing nominal voltage on the components used by static switches in order to provide direct connection of renewable energy to the grid. In addition it is to be notice that multilevel inverters synthesize sinusoidal waveform with a distortion factor smaller than in the case of two-level inverters.

The technique by which the multilevel inverters synthesizes the waveform, permits the reduction of voltage and current waveforms harmonic content using dimensional reduced filters mounted at the inverter output.

Among the various types of the multilevel converters, cascaded converters are usually used for photovoltaic sources, due to the modular structure, but the number of commutations is higher than in the case of other types of multilevel converters and it is required to have independent voltage sources. The converter with clamped diode is another type of multilevel convertor, widely used in conversion systems for grid connection, due to the minimum

number of active components and the use of common DC sources [2]. The clamped diode converter structure has as disadvantage the imbalance of neutral point, and so equilibrations solutions need to be used for the neutral point potential [3] using capacitors. This method leads to a more complex control system. Also, the existing methods are not applicable to all voltage levels from the system. The utilization of auxiliary devices needed for equilibration or active rectifier leads to increased complexity and value of the equipment [3, 4].

II. MULTILEVEL CONVERTERS IN THE SYSTEMS USING ENERGY CONVERSION

As it is known, the application of DC voltage-AC voltage conversion at fixed frequency and amplitude are: the injection into the system of energy provided by renewable energy sources; energy supplying by interruptible power sources; DC power transmission at high voltage.

The most important problem of the conversion is the fact that the alternative voltage injected need to have a minimal distortion factor and so the harmonics injected are decreased to minimum values. AC-DC voltage conversion is achieved through inverters. Inverter topologies research was influenced by the development of "off-shore" renewable energy sources. The energy transport and energy injection into the power system was another problem studied by the researchers. The energy produced from renewable sources "off-shore" is converted to DC, transported to the mainland, where it is converted into AC voltage and delivered to power system. At the conversion elements, the most important issue is the commutation. The commutation can be "soft" when the waveform is synthesized by the control circuits through pulse width modulation (PWM) or "hard" when the waveform is synthesized [5] by the command of static commutation devices through diagram topology used in the inverter power circuit.

In general is desired to avoid commutation on the inverter force side, but for mentioned applications, this cannot be prevented. Semiconductor devices are usually limited by the reverse voltage at values lower than 10 kV, but on the transport of DC high voltage (HVDC) the 100 kV switching voltage is exceeded and the commutation is achieved by connecting a series of semiconductor devices or using multilevel converters. The simplest topology that can be used for this conversion is the two-level inverter which is made of four switches. Each switch consists of an antiparallel diode, since the configuration needs reverse current diode.

A multilevel inverter is a power electronic system that synthesizes a sinusoidal output voltage from several DC sources. DC sources can be batteries, solar cells or capacitors. Multilevel inverter operation is based on a number of switches connected in series in order to obtain on the output voltage and sinusoidal current. Since multiple switches are connected in

series, the angle of commutation is important for multilevel inverters, because all switches would be operated in such a way that the output voltage and current to have minimum harmonic distortion.

Total harmonic distortion-THD is reduced by increasing the number of levels. It is obvious that an output voltage with a minimum of total harmonic distortion is desirable, but increasing the number of levels requires more commutation devices and so complicates the command and control circuits. The compromise necessity appears for price-weight-complexity for an output voltage with minimum of total harmonic distortion. Previous work in the area of multilevel inverters focused more on total harmonic distortion and on inverters commutation model. The majority were focused in order to obtain at the output a sinusoidal voltage and a current with minimum total harmonic distortion using different commutation models. The commutation angles in multilevel inverters are so important because it can affect the shape of the output voltage and the total harmonic distortion of current. There are several studies on different methods of harmonics elimination which are related to commutation angle calculation [6]. The newest method used to eliminate harmonics is the resultant theory. The harmonics elimination in a multilevel converter using this method focuses on the resultant theory in order to calculate the commutation angles. Some papers have focused on different uses of multilevel inverters, while others relate to different topologies depending on the electricity application for which are used. The paper [6] compares the H-bridge multilevel inverters in the case of high power electric motors. The most common multilevel inverter topologies are: diode-clamped multilevel inverter (DC-MLI); flying capacitor multilevel inverter (FC-MLI); cascaded H-Bridge Multilevel Inverters (CHB MLI).

When the number of levels is larger than three, at DC MLI inverters, the number of clamped diodes and the complexity of the scheme are increased. FC-MLI inverters are based on voltage balancing and can generate different waveforms at the output. It also requires a phase balancing capacitors and leads to increased complexity by increasing the number of capacitors. They are defined as different combinations of capacitors allowing the charging or discharging of the individual flying capacitors in order to produce the same phase leg voltage.

Between these three types of usual multilevel inverters topologies; cascade inverter has the smallest number of components for a given number of levels. Cascade multilevel inverters is made up of a number of cells of H-bridge type in order to synthesize the required voltage from several separated direct voltage sources (SDCS), which may be batteries or fuel cells. All these properties of cascade inverters allow the using of various control strategies using pulse width modulation (PWM) for a more accurate control. In addition for the previously mentioned technologies specific control techniques have been developed for multilevel inverters such as selective harmonic elimination PWM (SHE-PWM), sinusoidal PWM (SPWM), space-vector PWM (SVM) and modulation techniques derived thereof. The modulation methods used for the multi-level inverters can be classified according to the commutation frequency.

III. TOTAL HARMONIC DISTORTION REDUCTION USING GENETIC ALGORITHMS

The genetic algorithms are generally used to solve optimization problems, planning or linear search, multi-criteria. These represent a set of adaptive procedures that finds a solution for a problem investigated by a mechanism of natural selection and genetic evolution. The mechanism was introduced and analyzed by J. Holland, being characterized by the fact that only species (solutions) that are better suited to the environment are able to survive and evolve over generations while those less adapted disappear. The probability of a species to survive and evolve over generations becomes greater while the degree of adaptation increases, which in terms of optimization means that the solution approaches to optimal. To implement the proposed genetic algorithm for optimizing the operation of a multilevel converter in order to reduce the harmonic distortion we use Matlab. The work presented is based on developing a function to perform the optimization based on genetic algorithms:

$$[Param, THD] = f\_GAImplem(ConvLvl, IterNo) \quad (1)$$

The implemented function f_GAImplem receives as input ConvLvl, the level of multilevel converter, whose function is to be optimized and the IterNo represents the number of iterations of the optimization process. The output data provided are: Param, the list of optimization operating parameters for the studied multilevel converter (wave amplitude and pulse width used for the reconstruction of sine wave waveform) and the harmonic distortion THD provided by the converter. The genetic algorithm implemented in the developed Matlab function is based on a population of one hundred individuals, randomly generated, each representing a possible set of operating parameters for the studied multilevel converter. In order to determine the optimal solution for the genetic algorithm implemented for each individual (set of possible operating parameters) it is needed to find the mean square error of the waveform provided by the converter and sinusoidal waveform that is intended to be achieved:

$$MSQ_{err} = \frac{1}{N}\sum_{i=1}^{N}\left[Conv(\omega \cdot t_i) - Sin(\omega \cdot t_i)\right]^2 \quad (2)$$

where: MSQ_{err} is the reconstruction mean square error of the sine wave; N is the number of intermediate points on a period used for the MSQ_{err} evaluation; $Conv\ (\omega \cdot t_i)$ is the effective value at the moment t_i of the waveform signal supplied by the studied converter; N is the pulsation corresponding to the frequency f of the signal provided by the converter.

Also, for each possible converter operating parameters we evaluate the signal harmonic distortion for the given waveform:

$$THD = \frac{\sqrt{V_2^2 + V_3^2 + \cdots + V_n^2}}{V_1} \quad [\%] \tag{3}$$

where: *THD* is the percentage of harmonic distortion for the signal supplied by the converter; V_k is the amplitude of the *k* voltage harmonic obtained from the Fourier decomposition, $k = 1,n$ (where *n* is the number of harmonics under investigation).

In order to achieve the Fourier decomposition of the signal supplied from a possible configuration of multilevel converter investigated on the basis of below relations (3) ÷ (5) we have used Matlab. Here we named a function called f_FourierDeComp(Param), which receives as a input data the signal amplitude and the waveform width of pulses used for the reconstruction of the sinusoidal waveform.

$$V_k = \sqrt{A_k^2 + B_k^2}, \qquad \phi_k = \arctan\left(\frac{B_k}{A_k}\right) \tag{4}$$

where:

$$A_k = \frac{2}{T} \cdot \int_0^T Conv(\omega \cdot t) \cdot Sin\left(\frac{2 \cdot \pi \cdot k \cdot t}{T}\right) dt \tag{5}$$

$$B_k = \frac{2}{T} \cdot \int_0^T Conv(\omega \cdot t) \cdot Cos\left(\frac{2 \cdot \pi \cdot k \cdot t}{T}\right) dt \tag{6}$$

Since harmonic distortion factor *THD* does not provide information regarding the harmonic component of the signal studied in order to determine the multilevel converter configurations which produce waveforms with a low-order harmonics 3, 5 and 7, for each possible solution (individual) the weighted harmonic distortion factor is also evaluate:

$$THD_b = \frac{1}{V_1} \cdot \sum_{k=1}^{n} \sqrt{\left(\frac{V_k}{\log(k)}\right)^2} \quad [\%] \tag{7}$$

In order to determine the optimal solution of multilevel converter (best individual), in terms of those presented above, genetic algorithms implemented within the f_GAImplem function, uses a global cost function that takes into account the weighted value of three factors *THD*, THD_h and MSQ_{err},

$$CostFunc = THD + 1.5 \cdot THD_b + 0.5 \cdot MSQ_{err} \tag{8}$$

Table 1. The Results obtained for the 3 Steps Inverter

Nr. of iterations	Pop	The best values obtained for the THD (%)				
10000	50	27.42	27.42	27.42	27.42	27.42
20000	50	23.59	23.59	23.59	23.59	23.59
1000	500	10.80	10.80	10.80	10.80	10.80

Table 2. The Results obtained for the 4 and 6 Steps Inverter

Nr of steps	The best values obtained for the THD					
4	8.143	18.788	19.623	16.705	19.648	18.408
6	6.347	136.524	45.530	42.171	50.511	56.558
6	5.866	5.881	5.884	50.210	38.126	79.017

Genetic algorithm implemented in Matlab allows through programming mode the selection of the desired number of iterations. Being an iterative process, requires a longer period of running, and in the first phase the program tests the 3 step inverter. At first run for 3 steps we introduce a number of iterations 10000 and then 20000, however, the results do not meet the proposed limits. Therefore, we increase the population of individuals from 100-to 500, 1000 iterations, thus yielding better results, as can be seen from Table 1.

Also, table 1 shows that the solutions obtained are identical. Therefore, a function must be introduced to allow the visualization of intermediate solutions convergence from the algorithm. The graph of convergence is shown in *figure 1*.

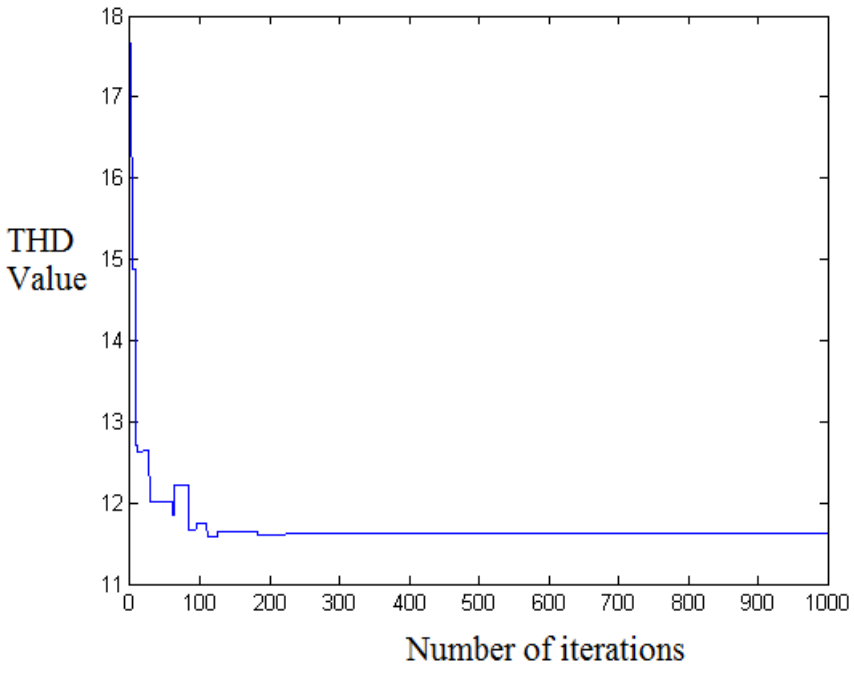

Fig. 1. The solutions convergence graphic for the 3 step inverter.

The results thus obtained were considered superior to those obtained previously. Also should be noted that they within the standard SR EN 50160/2011, which requires the value of THD's to under 8%.

The convergence graphs of THD values for 4 and 6 steps inverter are shown in *figures 2* and *3.*

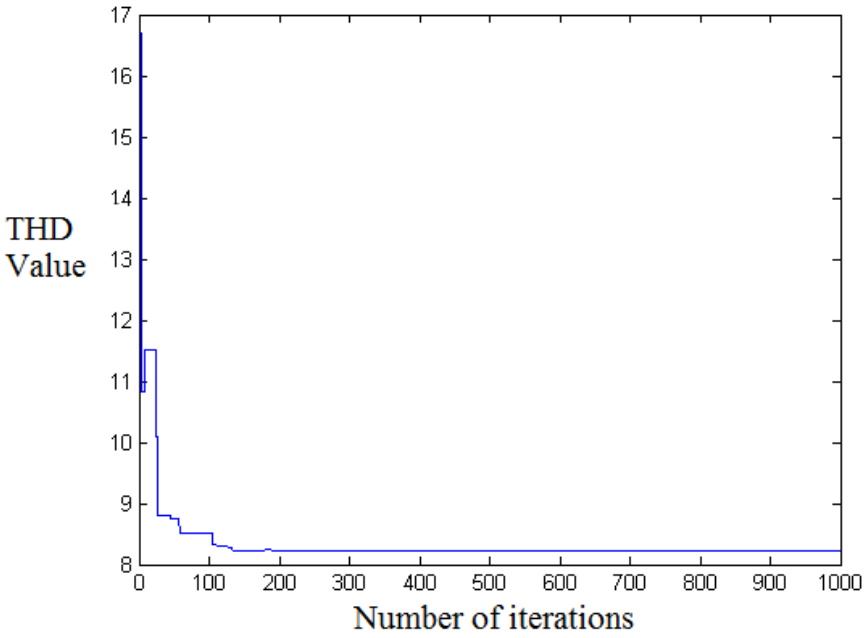

Fig.2. The solutions convergence graphic for the 4 step inverter.

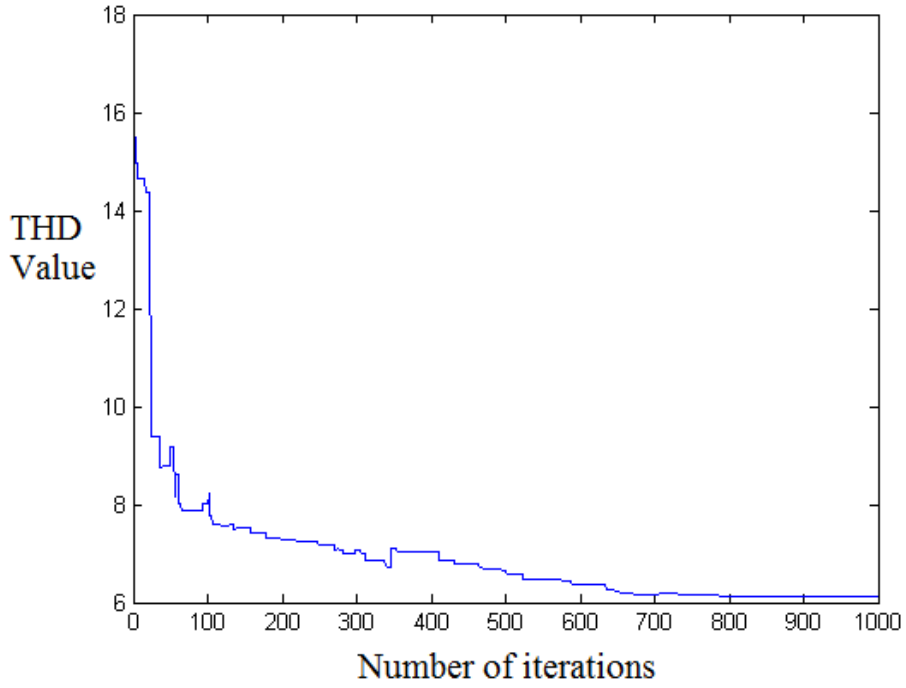

Fig. 3. The solutions convergence graphic for the 6 step inverter.

The goal of the algorithm was to obtain a waveform with the specified number of steps, with a value of THD as low's as possible in order to be inserted into the programmable source. What makes the presented algorithm outperforms other methods is that in the case of three steps, we have six variables, width and height of each step voltage.

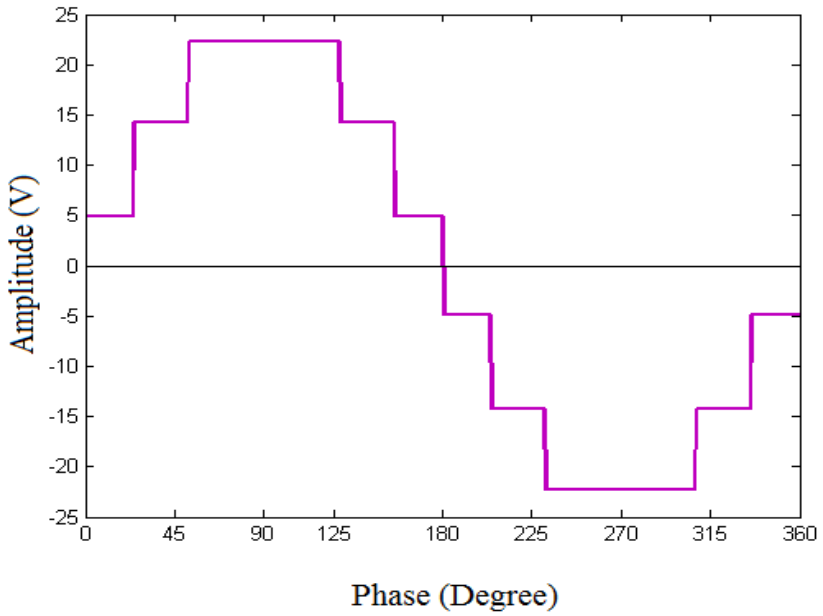

Fig. 4. The waveform shape for 3 steps inverter

Thus, the three waveform width must satisfy the condition that their sum is equal to $\pi/2$, and by testing a number of values which satisfy the basic condition to get the best solution with low THD.

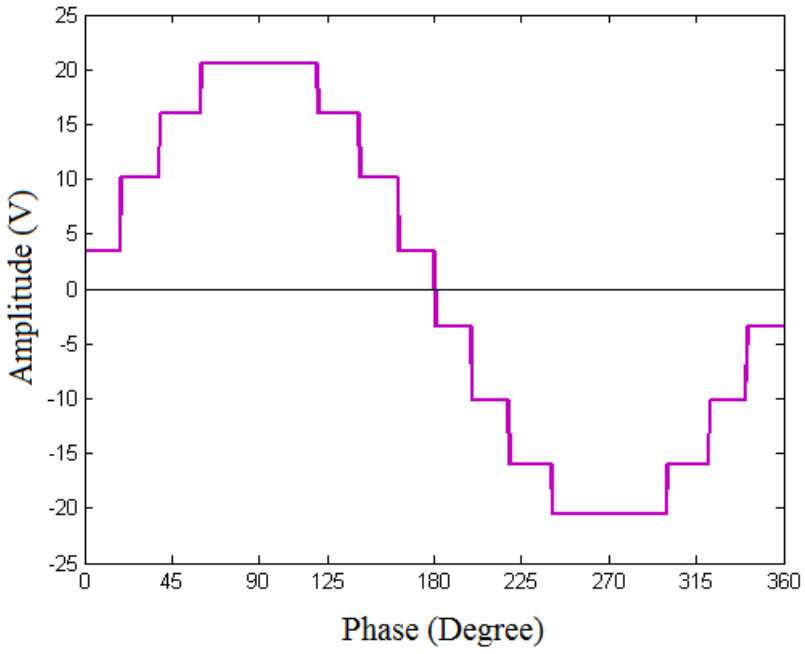

Fig. 5. The waveform shape for the 4 steps inverter

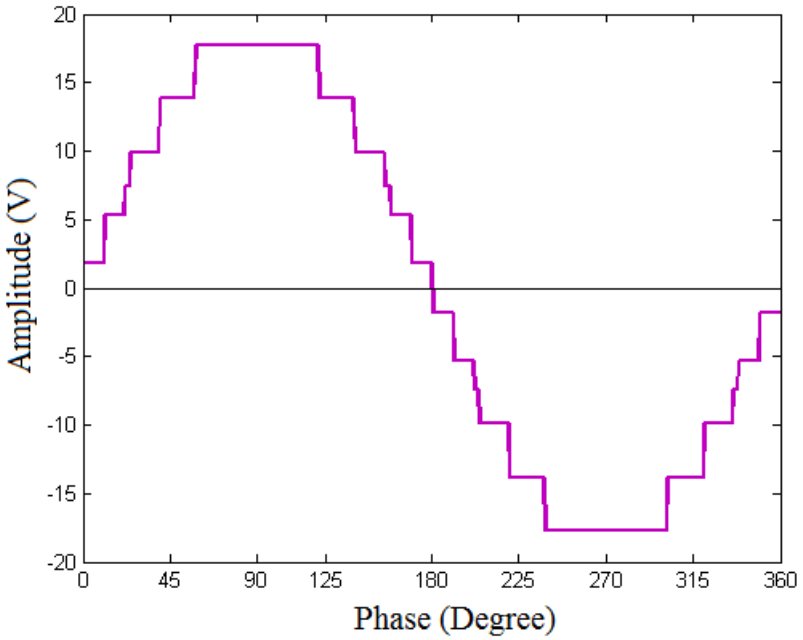

Fig. 6. The waveform shape for 6 steps

IV. EXPERIMENTAL RESULTS

The waveforms thus obtained are plotted in *figures 4, 5* and *6* are there are used for experiments. It must be notice that these waveforms must be processed to be placed in the programmable source [7, 8, 9].

Analyzing the waveforms, it can be seen that what makes them different from most of the literature is the variation of steps not only on the voltage level but also on the value of switching angle. Also, the obtained waveform is not starting from zero like the majority of waveforms in the literature and available in the library of programmable source. THD's values thus obtained are superior to those obtained by other methods.

The programmable source used for testing is an instrument from CTS series produced by California Instruments, which provides an efficient test solution in terms of value for money, which aims to verify the product compliance with a large number of testing standards in ac and dc current. The CTS Series of testing system offers the following advantages: Single-phase and three-phase systems for a wide range of power debited on the load; Data acquisition system with direct access to the PC bus provides high resolution and high sampling rate for accurate measurement and high transfer speeds, even in three phase mode, unlike other IEC test systems that provide a rate transfer limited by the IEEE-488 interface; test software PC-based for harmonics and flicker that offers real-time data color update and continuous monitoring of PASS / FAIL type; Support for European and Japanese standards; Simple utilization under Windows offering IEC test setup, data analysis, display and test reports in MS Word format; High resolution, no gap acquisition data storage to disk in ASCII

format for post-acquisition analysis and reporting. Resumption of recorded test data step or fast - Fast Forward.

Single Step and Fast Forward replay of recorded test data.

Available in a choice of power levels ranging from 1250 VA to 30,000 VA, CTS Systems cover the complete range of single and three phase products that need testing to conform with existing and pending IEC standards.

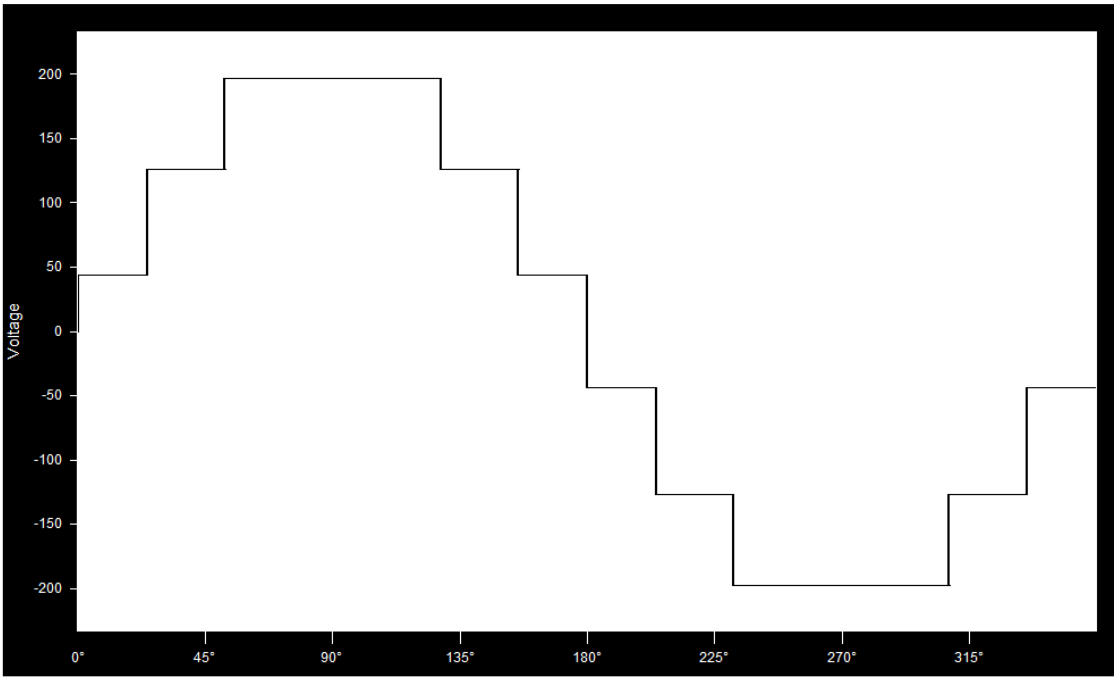

Fig.7. The ideal waveform of three steps inverter functioning with no load

All iX Series AC sources meet IEC requirements for low voltage distortion and offer arbitrary waveform generation, precision measurements, and waveform analysis capabilities for load voltage and current. AC power source real distortion is measured in real time during harmonics testing and any distortion is indicated that could affect the test results. All iX Series based CTS systems support full compliance IEC 61000-4 AC immunity test as well (certain options may be required).

The 1251RP source based on CTS system which can be used for realizing complete harmonics tests and flicker test with low power load and with an peak coefficient of the maximum current.

Source voltage distortion is measured in real-time during the harmonics test and any distortion that could affect the test results is clearly indicated.

A high speed digital signal processor based data acquisition system is used to implement the required IEC compliance measurement system. Direct access to the PC bus ensures a much higher data throughput capability than typically found in single box IEC test systems that use the IEEE-488 instrumentation bus to communicate with the PC.

In harmonics tests, there are available the following determinations: Voltage and Current time domain; Current Harmonics and IEC limits graph; AC Source Voltage Harmonics and IEC; limits graph; Numeric display of F, VRMS, IRMS, IFUND, IPEAK, PF, W, VA, THD.

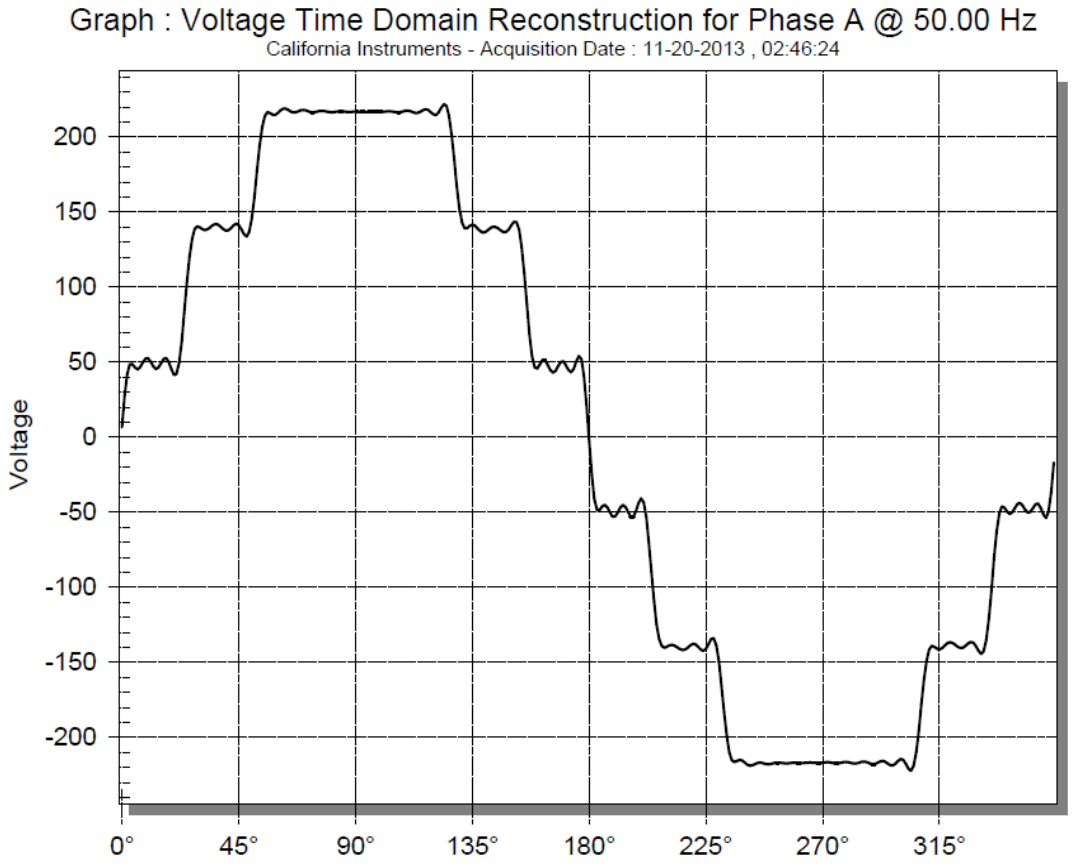

Fig. 8. The waveform obtained through the genetic algorithm, with the 3 steps inverter functioning on load

As load was used an induction motor (asynchronous) single-phase squirrel cage, with the following characteristics: Un=230 Vac; P=460 W; cosφ= 0.8; η=0.8. The load has been provided from the programmable source presented above, with the waveforms generated through the genetic algorithm presented in *figures 3*, *4* and *5*. The waveforms used for controlling the multilevel inverters are also generated from the programmable source library. Using the developed software tool we performed the conversion of voltage levels and the waveforms format obtained from genetic algorithm at the levels and format required for supplying the load. In *figure 7*, the waveform thus obtained and placed into the programmable source. In load operation the waveform deviates from the ideal form presented above, as shown in *figure 8*. The same allure waveform can be noticed, less the existence of a ripple caused by the nonlinearity of the motor.

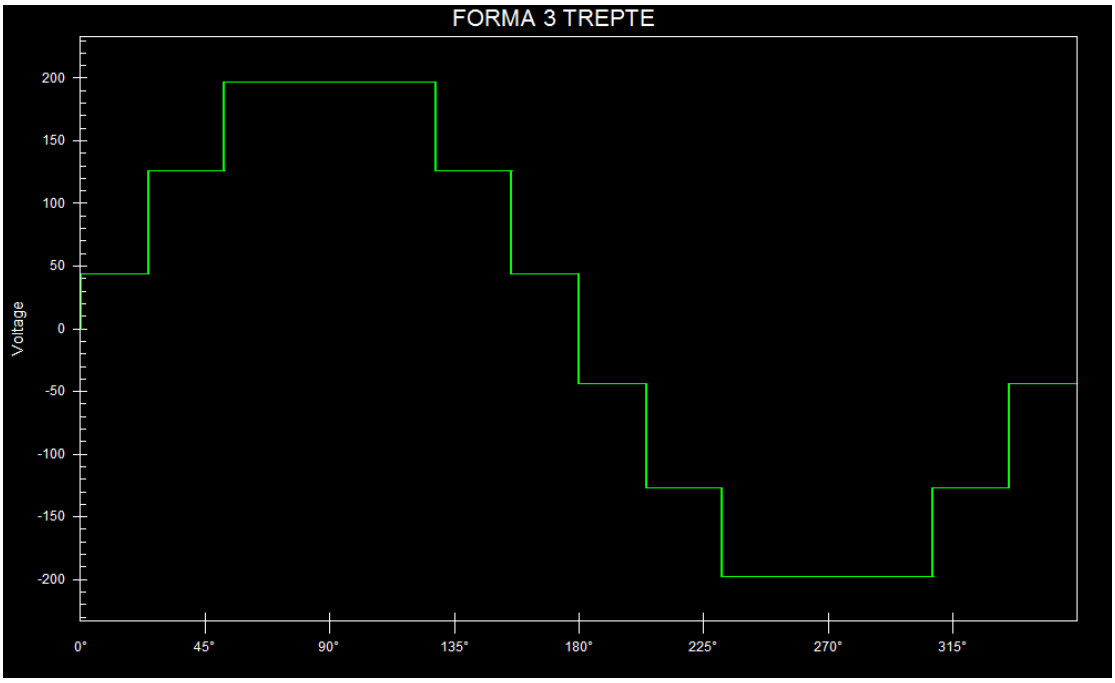

Fig.9. The waveform generated from the programmable source library of the 3 steps inverter operating at no load

In *figure 9* is shown the waveform generated by the programmable source library for the same type of inverter. In *figure 10* the experimental results are presented supplying the motor with the waveform from *figure 9.*

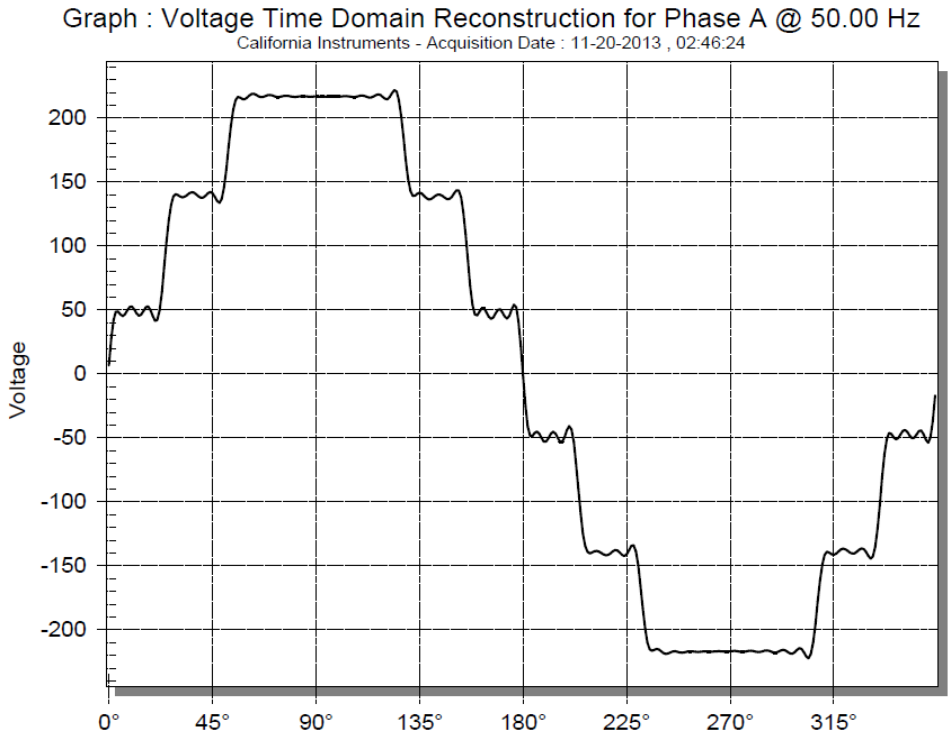

Fig. 10. The waveform generated from the programmable source library of the 3 steps inverter operating in load

V. CONCLUSIONS

In Table 3 the levels of harmonics up to order 49 for supplying the two waveforms are presented [10, 11].

Table 3. The Harmonics Levels

Acquisition Date : 11-20-2013 , 02:46:24
California Instruments
THD Voltage = 11.45 % THD Current = 0.00 %

	rms.	rel. (%)	Phase
Fund	227.890	100.00	0.00
3	1.560	0.68	17.80
5	3.820	1.68	176.00
7	6.450	2.83	358.40
9	6.160	2.70	176.30
11	2.270	1.00	170.00
13	15.930	6.99	358.00
15	14.360	6.30	358.10
17	1.920	0.84	5.40
19	1.170	0.51	4.60
21	2.240	0.98	359.40
23	3.090	1.36	177.10
25	1.810	0.79	175.70
27	5.830	2.56	2.10
29	5.980	2.62	3.60
31	1.460	0.64	9.70
33	1.610	0.71	8.80
35	1.550	0.68	9.30
37	2.000	0.88	185.90
39	1.510	0.66	187.40
41	2.860	1.25	12.90
43	3.180	1.40	15.10
45	1.080	0.47	21.20
47	1.640	0.72	20.60
49	1.390	0.61	22.50

Acquisition Date : 11-20-2013 , 02:54:44
California Instruments
THD Voltage = 16.85 % THD Current = 0.00 %

	rms.	rel. (%)	Phase
Fund	225.840	100.00	0.00
3	11.170	4.95	175.70
5	0.290	0.13	97.30
7	4.410	1.95	169.40
9	24.900	11.03	358.60
11	20.040	8.87	358.10
13	2.550	1.13	164.20
15	0.290	0.13	94.20
17	1.530	0.68	158.10
19	10.590	4.69	358.70
21	9.300	4.12	359.30
23	1.390	0.62	159.80
25	0.260	0.12	95.60
27	0.820	0.36	154.00
29	6.090	2.70	3.40
31	5.530	2.45	5.10
33	0.960	0.43	161.20
35	0.240	0.11	100.10
37	0.550	0.24	156.20
39	4.040	1.79	11.20
41	3.780	1.67	13.60
43	0.760	0.34	165.70
45	0.210	0.09	106.00
47	0.450	0.20	162.40
49	2.950	1.31	20.80

It can be seen that through the developed genetic algorithm, the third harmonic is reduced from 4.95% to 0.68%, which significantly increases the motor operation efficiency (decreasing its operating temperature). On the other hand, there is an increase in the level of

the fifth-order and the seventh voltage harmonics. Fifth order harmonic increases to 1.68%, while the seventh order increases to 2.83%. In view of the fact that the two harmonic components determines the negative sequence and may result in oscillation operation, it is important that the harmonic components to be filtered by means of harmonic filters.

REFERENCES

[1] L. Mihalache, *A high performance DSP controller for three-phase PWM rectifiers with ultra low input current THD under unbalanced and distorted input voltage*, in Conf. Rec. IEEE IAS Annu. Meeting, vol. 1, pp. 138–144, 2005.

[2] Clasis, M., Agelidis, V.G. *Multilevel Converters for Single-phase Grid Connected Photovoltaic Systems-An Overview*, Proceedings of IEEE International Symposium on Industrial Electronics, South Africa, pp. 224-229, 1998.

[3] Alonso, O., Sanchis, P., Gubia, E., Marroyo, L., *Cascade H-Bridge Multilevel Converter for Grid-Connected Photovoltaic Generators with Independent Maximum Power Point Tracking of Each Solar Array*, Proceeding of IEEE Power Electronics Specialist Conference, pp. 731-735, 2003.

[4] Busquets-Monge, S., Rocabert, J., Rodriguez, P., Alepuz, S., Bordonau, J., *Multilevel Diode-Clamped Converter for Photovoltaic Generators with Independent Voltage Control of Each Solar Array*, IEEE Transaction on Industrial Electronics, vol. 53, no. 4, August 2006.

[5] H. Balan, R. Tirnovan, M. I. Buzdugan, *Commutation technique in the supply of electromagnetic actuators*, IET Power Electronics, volume 7, issue 1, pp. 132 – 140, January 2014.

[6] L.M. Tolberg, F.Z. Peng, *Multilevel Converter for Large Electric Drives*, IEEE Transactions on Industry Applications, vol. 35, no. 1, Jan./Feb. 1999, pp. 36-44.

[7] M. Buzdugan, H. Balan, *Power Quality Issues in Electrical Power Distribution Systems*, Bulletin of the Translvania University of Brasov, vol. 8, Special Issue no. , pp , ISSN: 2285-7656-L 2248-7648.

[8] H. Balan, L. Neamt, M. I. Buzdugan, T. E. Pop, *Fault current limiter with solid-state circuit breakers*, Article Book Series: IOP Conference Series-Materials Science and Engineering, volume: 144, article number: 012001, 2016.

[9] M. I. Buzdugan, H. Bălan, *About power quality monitoring in residential grids*, Renewable Energy and Power Quality Journal, vol. 1, no. 15, April 2017.

[10] H. Balan, M. I. Buzdugan, I. Iancau, L. Neamt, *Testing Solutions of the Protection Systems Provided with Delay Maximum Current Relays*, Carpathian Journal of Electrical Engineering, volume 11, number 1, pp. 47-58, 2017.

[11] H. Balan, T. Varodi, M. I. Buzdugan, *Monitoring power breakers using vibro acoustic techniques*, Advances in Science, Technology and Engineering Systems Journal ,vol. 2, no. 3, pp. 1771-1776, 2017.

REAL-TIME TRANSIENT STABILITY STATUS PREDICTION SCHEME AND COMPARATIVE ANALYSIS OF THE PERFORMANCE OF SVM, MLPNN AND RBFNN

Emmanuel Asuming **FRIMPONG**[1], Philip Yaw **OKYERE**[1], Johnson **ASUMADU**[2]
[1]*Kwame Nkrumah University of Science and Technology, Kumasi, Ghana*
[2]*Western Michigan University, Kalamazoo, Michigan, USA*
[1]*eafrimpong.soe@knust.edu.gh,* [2]*pyokyere.soe@knust.edu.gh,* [3] *johnson.asumadu@wmich.edu*

Keywords: neural networks, out-of-step, support vector machine, transient stability

Abstract*:* This paper presents a simple and effective technique for real-time prediction of transient stability status following a large disturbance and compares the performance of three artificial intelligence (AI) techniques commonly employed as decision making tools. The (AI) techniques compared are support vector machine (SVM), multilayer perceptron neural network (MLPNN), and radial basis function neural network (RBFNN). The stability status prediction scheme samples rotor angles of all system generators and extracts the absolute value of the first sampled rotor angle value of each generator. The extracted absolute rotor angle value of all generators are summed and fed as input to a decision tool. The scheme was tested using simulations carried out on the IEEE 39-bus test system. One hundred percent prediction accuracy was obtained when SVM and MLPNN were each employed as decision tools. The use of the RBFNN as decision tool resulted in only sixty-three percent prediction accuracy.

1. INTRODUCTION

Large disturbances such as faults on transmission lines endanger stability of power systems and can lead to wide-scale system outages. This is particularly so when protection schemes are not able to effectively respond to fault conditions. For example, the August 14, 2003 blackouts that occurred in United States and Canada were mainly due to the combined effect of large disturbances and ineffective system protection [1].

Power system faults pose the greatest threat to the maintenance of stability. Severe disturbances could cause large separation of the rotor angles between generators or groups of generators leading to eventual loss of synchronism [2]. The post-disturbance stability status of a system depends on the pre-disturbance system operating condition, the form of disturbance, and the post-disturbance network configuration [3]. Special protective systems (SPSs) which are event based control systems have been developed to address transient instability. SPSs activate controls in response to occurrence of some pre-identified set of disturbances. They are however complicated and expensive; any modifications to the power system requires alteration of their control logic [4].

Researchers have therefore come up with a number of techniques for early detection and prediction of transient instability [2], [4]-[12]. These techniques hinge on the combined ability of phasor measurement units (PMUs) and global positioning system (GPS) to provide real-time capture and transmission of power system data to a centralized location.

Critical issues in transient stability prediction include (i) ease of input data capture, (ii) simplicity, speed and accuracy of input data processing, and (iii) accuracy of final decision making.

The input data used should allow for easy capture and transmission, in real-time, to a centralized point. This should also be done in a short-time window. Rotor angle [5], speed deviation [2], and bus voltage [4] are some of the input parameters that have been used. Using single input data type for each machine or bus is desired. Capturing multiple input data types presents implementation challenges. For example, the work presented in [6] uses 34 input features derived from generator electromagnetic powers, rotor angles and speeds, bus voltages and transmission line power flows, among others. Also, in [7], 10-12 input data samples per generator are required, and in [8], 4 inputs per generator are required. These data requirements will make the volume of data required for large systems huge. Also, the technique presented in [5] uses data captured in a rather long time-window of 120ms.

The processing of input data should be simple, fast and accurate. Significant success has been chalked in this area; but there is still room for improvement. For example, in [4], extensive dynamic simulations are required to establish the stability boundaries of each generator.

The use of pre-determined templates in decision making such as in [4], [9] and [10] is not helpful, considering the fact that changes in system topology may render such templates ineffective. Also, the technique in [11] requires a long period of up to 2.5 seconds after fault clearance to make a decision as to whether or not a system will be stable. Thus, there is the need for an improved transient stability status detection or prediction scheme.

Support vector machine (SVM), multilayer perceptron neural network (MLPNN) and Radial basis function neural network (RBFNN) are artificial intelligence (AI) techniques commonly used for decision making in power system studies. However, their performance in the prediction of transient stability status has not been compared. It is important to highlight

that there is an erroneous perception on the part of some researchers about AI techniques. Some researchers perceive them as black-box type decision making tools [4]. Contrary to this perception, AI techniques are based on sound mathematical principles. Their decisions (outputs) are mathematically determined from given inputs. This has been demonstrated in this paper.

This paper proposes an improved scheme to predict transient stability or otherwise and also compares the performance of the aforementioned AI tools. The scheme uses generator rotor angles as input data. The rotor angles are sampled at a rate of 60 samples per second. This sampling rate is practically feasible in the capture of rotor angles [13]. Also, phasor measurement units do operate at this sampling rate [14]. Only the first sampled rotor angle value of each generator is required by the scheme. For each sampled rotor angle value, the absolute value is extracted. The extracted absolute rotor angle values (one for each generator) are then summed. The summed value is then fed into one of the decision making tools which predicts the stability status.

Compared to schemes existing in literature, the proposed technique uses single input data for each generator, captured in a shorter time window ($1/60^{th}$ of a second), requires minimal training data (less than 2% of data generated), uses minimal input data (number of inputs equals number of generators), does not require predetermined templates, and its implementation does not require complex computations.

The rest of the paper is organized as follows: Section 2 discusses the use of rotor angle as input parameter. Section 3 discusses SVM, MLPNN and RBFNN. Section 4 presents the proposed scheme while Section 5 highlights the test system used and simulations done. Results obtained are presented and discussed in Section 6. Conclusions drawn are highlighted in Section 7.

2. USE OF ROTOR ANGLE AS INPUT PARAMETER

Rotor angle has been extensively used as power system input parameter for various studies. Rotor angle is a key parameter in the fundamental equation governing generator rotor dynamics [15]. The equation is given as [15]:

$$M\frac{d^2\delta}{dt^2} = P_m - P_e \tag{1}$$

where M is the inertia coefficient, δ is the rotor angle, P_m is the mechanical power and P_e is the electrical power. It can also be shown that [2],

$$\frac{d\delta}{dt} = \left[\frac{\omega_0}{H}\int_{\delta_0}^{\delta} P_a d\delta\right]^{\frac{1}{2}} \tag{2}$$

where H is the inertia constant and P_a is the difference between input mechanical power and output electromagnetic power. For stability to be attained after a disturbance, it is expected that $\frac{d\delta}{dt}$ will be zero in the first swing [15]. This condition gives rise to the equal area criterion which is a well-known classical transient stability criterion.

Rotor angles are normally expressed relative to a common reference. This reference cannot be based on a single generator, since any instability in the reference generator makes the relative angles meaningless. In order to overcome this difficulty, the concept of system centre of inertia (COI) angle is used to obtain a reference angle [9].

Many researchers discourage the use of rotor angles in algorithms [9]. This is because the COI values, in practice, require continuous updates using real time measurements. This requires extra pre-processing and has significant errors. However, recent work by engineers from Schweitzer Engineering Laboratories, Inc. and San Diego Gas & Electric point to a breakthrough in capturing rotor angle data [13]. The researchers [13] have successfully installed and commissioned a rotor angle measurement system on the generators in a 740 MVA combined cycle plant. No reference angle value is required in the measurement. This has offered a tremendous boost to the continuing use of rotor angles as input parameter for power system studies. This significant success motivated the use of rotor angle as input parameter in this work.

3. DECISION MAKING TOOLS

3.1. Support Vector Machine

Support vector machine (SVM) is an extremely powerful machine learning algorithm that focuses on classifying data [16], [17]. SVMs are inherently two-class classifiers. The main idea of a support vector machine is to construct a hyperplane as the decision surface in such a way that the margin of separation between two data categories is maximized. SVMs can be used when the data to be classified has two classes. They separate the data into two categories, namely positive (+1) and negative (-1).

SVMs can provide good generalization performance on pattern classification problems despite the fact that they do not incorporate problem-domain knowledge. This attribute is unique to SVMs [17]. In addition to using separating hyperplanes, SVMs use support vectors to aid in data classification. Support vectors are points that are closest to the separating hyperplane; these points are on the boundary of the slab [16]. The building of a support vector machine hinges on the following two mathematical operations: (a) nonlinear mapping of an input vector into a high-dimensional feature space that is hidden from both the input and the

output, and (b) construction of an optimal hyperplane for separating the features discovered in (a) [17].

Figure 1 illustrates these definitions, with + indicating data points of type 1, and – indicating data points of type –1 [18].

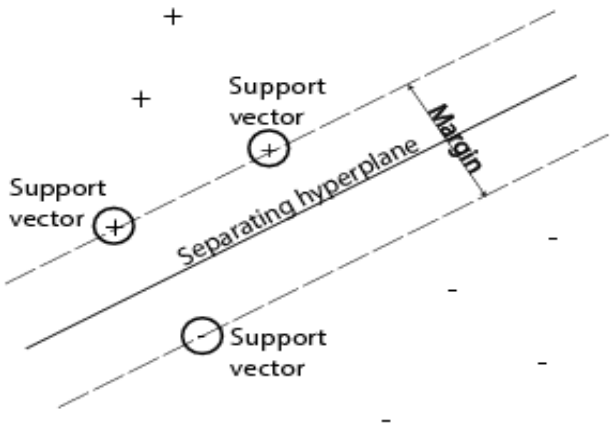

Fig. 1. Data points of SVM

Figure 2 shows the general architecture of an SVM [17]. The input layer consists of the input signal vector. In the hidden layer, an inner-product kernel is computed between the input signal vector (**x**) and support vector ($\mathbf{s_i}$). The linear outputs of the hidden layer neurons are summed in the output neuron. The output neuron has a bias.

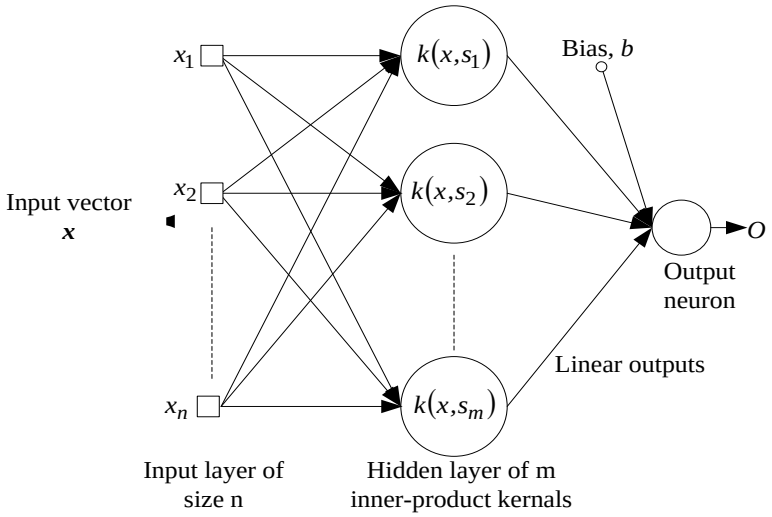

Fig. 2: General architecture of support vector machine

The interim output, O of a support vector machine can be computed as [18]:

$$O = \sum_i \mathbf{w}_i \, k(\mathbf{x}, \boldsymbol{s}_i) + b \tag{3}$$

where **x** is the input vector, $\mathbf{s}_i$ is the support vector, b is the bias, and $\mathbf{w}_i$ is the weight vector. The function $k(\mathbf{x}, \mathbf{s}_i)$ is a kernel of **x** and $\mathbf{s}_i$. The weight and bias values are obtained in the training phase. A linear kernel, meaning dot product, was used in this work. The linear kernel was selected because the classification required is a two-class one. Other possible kernel functions are quadratic, polynomial, Gaussian or radial basis function, and multilayer perceptron [18].

SVMs are trained with input-output pairs to give targets of either +1 or -1. An output of $+1$ is given when $O \geq 0$ while -1 is recorded when $O < 0$. In this work, the SVM was trained to produce a target of +1 for a condition that will lead to transient stability and -1 for a condition that will lead to transient instability. In other words, stability status, t, from SVM output, O is obtained as follows:

$$O \geq 0 \quad \Rightarrow \quad t = +1 \Rightarrow system\ is\ stable \tag{4}$$

$$O < 0 \quad \Rightarrow \quad t = -1 \Rightarrow system is unstable \tag{5}$$

The training was done using the sequential minimal optimisation method [16].

3.2. Multilayer perceptron and Radial basis function neural networks

Artificial Neural Networks (ANNs) mimic the human brain and have remarkable ability to derive meaning from complicated or imprecise data. They can be used to extract patterns and detect trends that are too complex to be noticed by humans or other computer techniques [19]. Two commonly used neural networks are radial basis function (RBF) and multilayer perceptron (MLP) neural networks [20], [21].

3.2.1. Multilayer perceptron neural network

Multilayer perceptron neural network is one of the artificial neural networks that have gained wide application in power system studies [22], [5]. It can be used to extract patterns and detect trends that are too complex to be noticed by humans or other computer techniques [22], [5]. Typically, the MLPNN is organized as a set of interconnected layers of artificial neurons, namely input, hidden and output layers. When a neural group is provided with data through the input layer, the neurons in this first layer propagate the weighted data and randomly selected bias, through the hidden layers. Once the net sum at a hidden node is determined, an output response is provided at the node using a transfer (activation) function. Commonly used transfer functions are: linear, log-sigmoid and hyperbolic tangent sigmoid [23], [24]. MLPNN, like any other neural network, has to be trained [23]. In this work, the MLPNN was trained using the Levenberg–Marquardt algorithm [25].

The MLPNN used in this work has the architecture shown in *Fig. 3*.

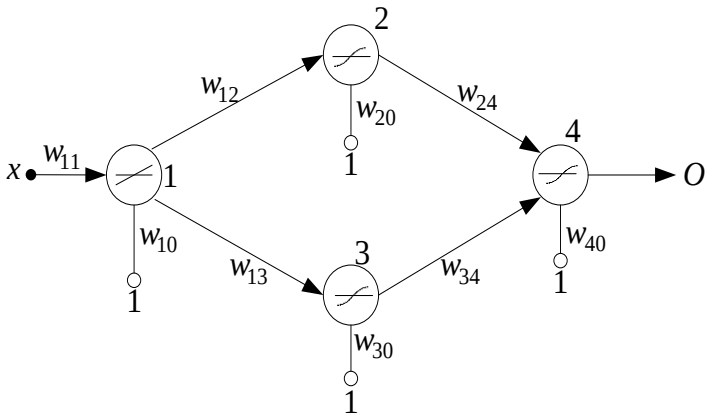

Fig. 3: Architecture of used MLPNN

where x is the input data, w_{ij} is the weight between neurons i and j, w_{i0} is the weight of the bias of neuron i, and O is the output of the neural network. Biases have fixed input values of 1. The input neuron has linear transfer functions while the hidden layer and output neurons have tangent sigmoid transfer functions. The output O of the MLPNN is determined as follows:

The output, y_1, of neuron 1 is given by:

$$y_1 = f\left(xw_{11} + w_{10}\right) = xw_{11} + w_{10} \tag{6}$$

The output, y_2, of neuron 2 is given by:

$$\begin{aligned} y_2 &= f\left(y_1 w_{12} + w_{20}\right) \\ &= \frac{e^{2\left(y_1 w_{12} + w_{20}\right)} - 1}{e^{2\left(y_1 w_{12} + w_{20}\right)} + 1} \\ &= \frac{e^{2\left(\left(xw_{11} + w_{10}\right)w_{12} + w_{20}\right)} - 1}{e^{2\left(\left(xw_{11} + w_{10}\right)w_{12} + w_{20}\right)} + 1} \end{aligned} \tag{7}$$

The output, y_3, of neuron 3 is given by:

$$\begin{aligned} y_3 &= f\left(y_1 w_{13} + w_{30}\right) \\ &= \frac{e^{2\left(y_1 w_{13} + w_{30}\right)} - 1}{e^{2\left(y_1 w_{13} + w_{30}\right)} + 1} \\ &= \frac{e^{2\left(\left(xw_{11} + w_{10}\right)w_{13} + w_{30}\right)} - 1}{e^{2\left(\left(xw_{11} + w_{10}\right)w_{13} + w_{30}\right)} + 1} \end{aligned} \tag{8}$$

The output, O, of MLPNN is thus given by:

$$O = f\left(w_{24}y_2 + w_{34}y_3 + w_{40}\right) = \frac{e^{2\left(w_{24}y_2 + w_{34}y_3 + w_{40}\right)} - 1}{e^{2\left(w_{24}y_2 + w_{34}y_3 + w_{40}\right)} + 1} \tag{9}$$

The MLPNN was trained to give an output of 0 if a disturbance will lead to transient stability, and an output of 1 if a disturbance will result in transient instability.

In practice, neural networks do not always give exact outputs of 0 or 1. For example, an expected output of 0 may be presented as 0.017 while a value of say 0.819 may be obtained instead of 1. As a result, in this work, (10) and (11) are used to round the output of the MLPNN to either 0 or 1.

$$O \geq 0.5 \rightarrow O = 1 \tag{10}$$

$$O < 0.5 \rightarrow O = 0 \tag{11}$$

3.2.2. Radial basis function neural network

Radial basis function neural network (RBFNN) is also an extremely powerful neural network [26]. It is a two-layered neural network having an input (or hidden) layer and output layer. The neurons in the input layer have Gaussian transfer function while those in the output layer have linear transfer function. The number of neurons in the output layer is predetermined by the user. The number of input neurons is however determined in the training process. Fig. 4 shows the architecture of a RBFNN with one input and one output.

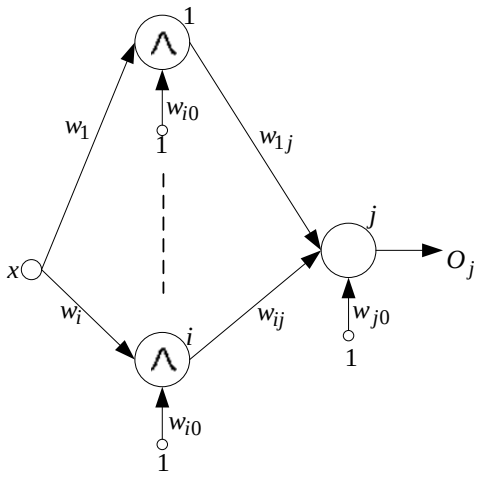

Fig. 4: Architecture of RBFNN

The output Y_i of a radial basis neuron *i* in the input (or hidden) layer can be obtained as [26]:

$$Y_i = R\left(\|w_i.x\|w_{i0}\right) \tag{12}$$

where x is the input vector (signal), w_i is the weight vector of radial neuron i, $\|w_i.x\|$ is the Euclidean distance between the two vectors, w_{i0} is the bias weight of neuron i, and R is a Gaussian function. In MATLAB, R is given as [27]:

$$R(n) = e^{-n^2} \tag{13}$$

The output O_j of neuron j in the output layer is given as:

$$O_j = Y_i w_{ij} + w_{j0} \tag{14}$$

where w_{ij} is the weight of the connection between neuron i in the input layer and neuron j in the output layer, and w_{j0} is the bias weight of neuron j. The RBFNN was trained to give an output of 0 if a disturbance will lead to transient stability, and an output of 1 if a disturbance will result in transient instability.

4. PROPOSED TRANSIENT STABILITY STATUS PREDICTION SCHEME

Figure 5 shows a functional block diagram of the proposed technique. The scheme is activated upon a large disturbance such as the tripping of a loaded line, generator or transformer and operates by sampling the rotor angle of each generator in the system using a sampling rate of 60 samples per second. It then extracts only the first sample of each generator. The absolute value of each extracted sample is then obtained. The obtained absolute values are then summed and used as input to a trained decision-making tool (which is either SVM, MLPNN or RBFNN). The decision-making tool then outputs the predicted transient stability status of the system.

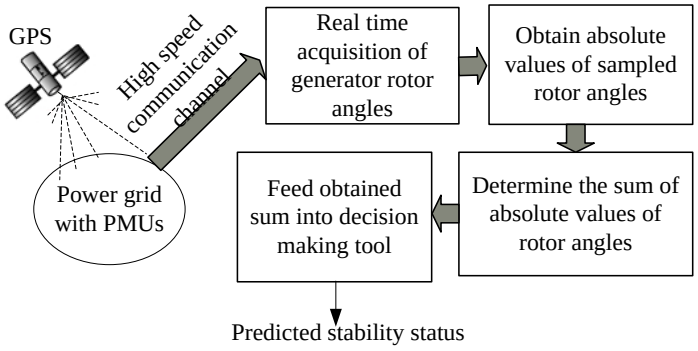

Fig. 5: Functional block diagram of the proposed technique

The operating procedure is further outlined as follows:

- For every generator *i*, sample the rotor angle and extract only the first rotor angle sample, δ_i:

$$\delta_i = \delta_{i,1} \quad i = 1,2,...,N \tag{15}$$

where N is the number of generators of the system

- For each extracted rotor angle sample, obtain the absolute value $|\delta_i|$.
- Obtain the input, *x*, to the decision making tool (MLPNN, RBFNN or SVM) by summing the absolute values as follows:

$$x = \sum_{i=1}^{N} |\delta_i| , \; i = 1,2,...,N \tag{16}$$

5. TEST SYSTEM USED

The IEEE 39-bus test system was used to test the proposed scheme. It is shown in Fig. 6.

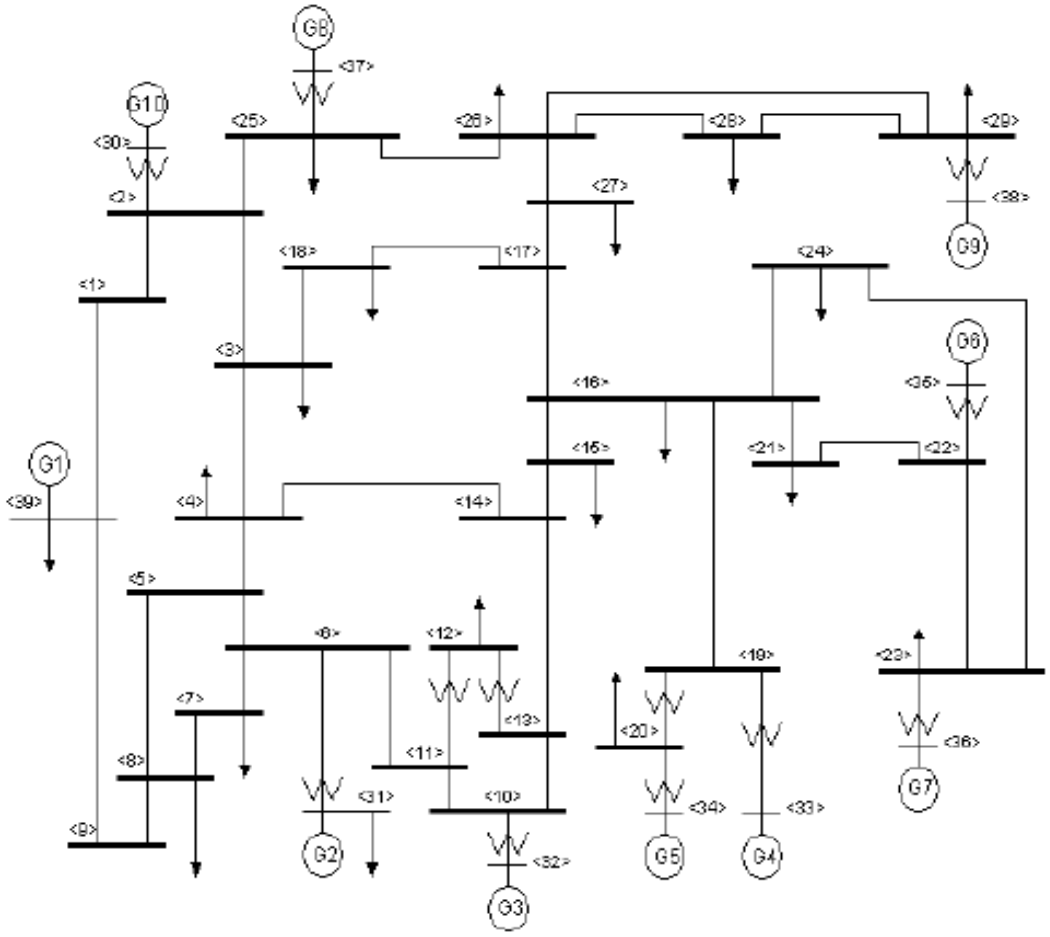

Fig. 6: IEEE 39-bus test system

This test system, also known as the New England test system, is a very popular test system for transient stability studies. Several researchers have used it for their work [4], [9], [10] for these main reasons: it is a model of a practical system; and it can be modeled and simulated using several non-commercial versions of simulation tools. The system consists of 10 generators, one of which is a generator representing a large system. Data for its model was obtained from [28], [29].

Transient stability analysis of the test system was performed using the PSS®E software. A detailed dynamic model which includes prime mover and excitation system dynamics was used. Several fault simulations were obtained by varying the fault location, fault duration, system loading, network topology, and generator availability.

About fault location, bus and line faults at different locations were simulated. Fault durations were also varied by starting with short durations which resulted in transient stability and extending them gradually until instability occurred. The effect of shutting down a generator due to low loading conditions or for purposes of maintenance was also considered. For example, for a loading level of 80% base load, generator 2 (G2) was removed from circuit before disturbances were applied. Additionally, the effect of changes in network topology was investigated by considering N-1 contingency. For example, for some of the simulations, the line between bus 25 and bus 26 was removed before the application of faults.

A total of 210 fault simulations were done to obtain 105 cases of transient stability and 105 cases of transient instability. The following criterion was used to determine the stability status of the system following a simulated disturbance: A system was seen as being transiently unstable if the rotor angle difference between any two generators exceeded 180 degrees within a typical study period of 3 seconds following fault clearance, otherwise, the system was seen to be stable [3].

Sampling of rotor angles was done allowing for a trigger delay time of 2 ms after fault clearance. The sampling and analysis of data were done using the MATLAB software.

6. RESULTS OBTAINED

6.1. Rotor angle trajectories

Two representative cases are presented here to show rotor angle trajectories obtained for the simulated cases. *Figure 7* shows time responses of rotor angles for a case of transient stability. The fault was applied on the line between buses 13 and 14 of the test system at 110% base loading. The fault was applied at $t = 0.1s$ and the line tripped at $t = 0.2s$. Figure 8 shows time responses of rotor angles for an unstable case. The system and fault conditions were the same as those for the stable case except that the fault duration was extended by 0.2 seconds to make the system transiently unstable. *Table 1* shows absolute values of sampled

rotor angles for each machine for the two fault cases.

The input to decision making tool using (16) is obtained as follows:

$$x(stable) = 103.1633$$

$$x(unstable) = 350.2648$$

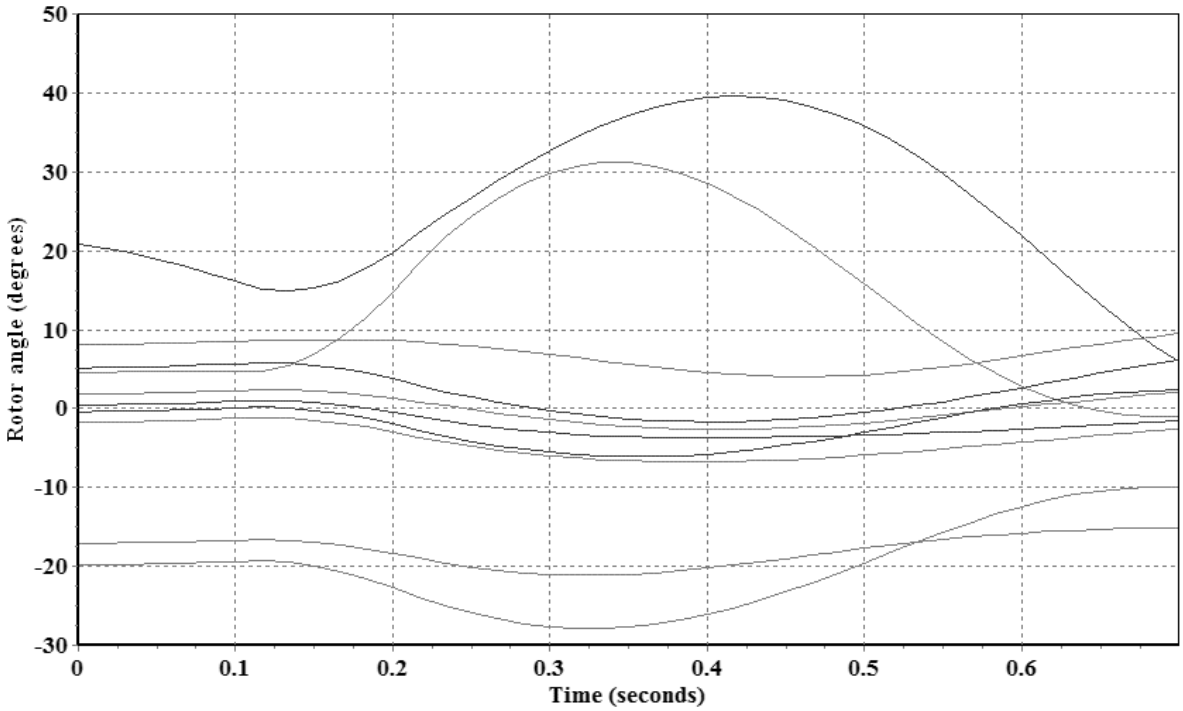

Fig. 7: Rotor angle trajectories for a stable condition

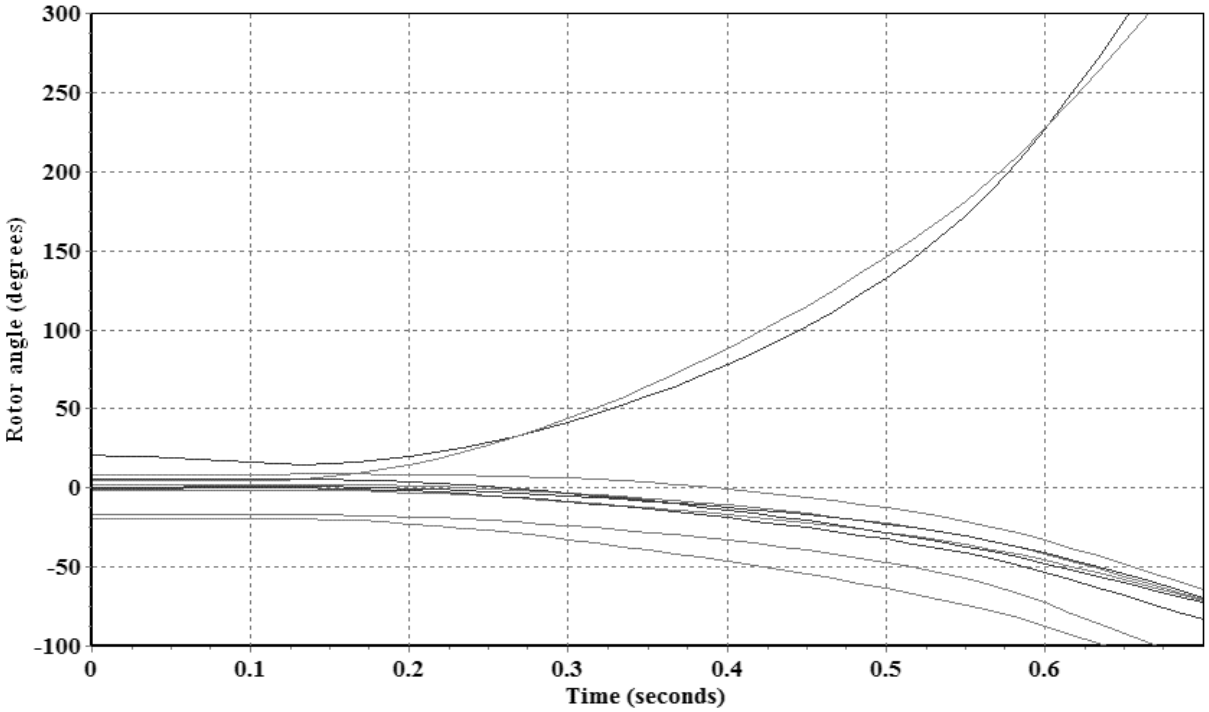

Fig. 8: Rotor angle trajectories for an unstable condition

Table 1: Absolute values of sampled rotor angles

Generator	Absolute values of rotor angles (degrees)	
	Stable	Unstable
1	23.9276	49.0633
2	22.2254	85.5155
3	18.3866	96.6407
4	0.8698	12.5067
5	3.6542	18.5483
6	8.4008	2.2257
7	1.0094	13.7294
8	2.7970	20.8451
9	2.9092	16.0681
10	18.9833	35.1220

6.2. Support vector machine (SVM)

6.2.1. Training

Rotor angle data from two cases of transient stability, and two cases of transient instability, representing 1.90% of data generated, were used to train the SVM. The remaining 98.10% of the data generated (103 cases of instability and another 103 cases of stability) were then used to test the proposed scheme. The training data of 1.90% is very low when compared with the training data of 75% used for some stability status prediction schemes existing in literature [9].

6.2.2. Structure of SVM

The characteristic data of the SVM after training is presented below:

$$\text{Support vector, } s_i = \begin{pmatrix} 145.1524 \\ 167.7435 \end{pmatrix}$$

$$\text{Weight vector, } w_i = \begin{pmatrix} 0.0039 \\ -0.0039 \end{pmatrix}$$

$$\text{Bias, } b = 13.8504$$

For the above SVM structure, the interim output, 0 given by (3) becomes

$$O(x) = x\left(s_1 \times w_1 + s_2 \times w_2\right) + b =$$

$$= x\left(145.1524 \times 0.0039 + 167.7435 \times -0.0039\right) + 13.8504 =$$

$$= -0.08811x + 13.8504 \quad (17)$$

6.2.3. Performance

The prediction accuracy of the scheme using SVM as decision making tool was found to be 100%. A sample calculation of the SVM output is presented using input value, *x*, obtained from *Table 1*.

Transient stable case

Interim output, *O*, of SVM using (17) is obtained as:

$$O(x=103.1633) = -0.08811 \times 103.1633 + 13.8504 = 4.7607 \quad (18)$$

Stability status, t, using (4) is +1 which means transient stable.

Transient unstable case

Interim output, O, of SVM using (17) is obtained as:

$$O(x=350.2648) = -0.08811 \times 350.2648 + 13.8504 = -17.0114 \quad (19)$$

Stability status, t, using (5) is -1 which means transient unstable.

6.3. Multilayer perceptron neural network (MLPNN)

6.3.1. Training

Initially, the MLPNN was trained with the same data used to train the SVM. However, this did not yield satisfactory test results. Desired performance was achieved only after training with higher volume of training data; which is 4.76% of total generated data.

6.3.2. Architecture of MLPNN

The MLPNN had three layers (as shown in *fig. 3*). The input layer had one neuron with a linear transfer function while the hidden layer had 2 neurons with tangent sigmoid transfer functions. The output layer had one neuron, also with a tangent sigmoid transfer function. The characteristic data is presented in *Table 2*.

Table 2: Weight values of MLPNN

Input signal – Input layer	Input layer – Hidden layer	Hidden layer – output
$w_{11} = -4.882$	$w_{12} = -5.892$	$w_{24} = 6.864$

$w_{10} = -2.7$	$w_{13} = 2.7856$ $w_{20} = 3.8567$ $w_{30} = 2.829$	$w_{34} = -0.25914$ $w_{40} = 0.32231$

6.3.3 Performance

Applying (6) to (9), the MLPNN outputs are obtained as follows:

Transient stable case

$$O(x = 103.1663) = 0.0000012 \tag{20}$$

Using (11), *O* is 0 which means transient stable.

Transient unstable case

$$O(x = 350.2648) = 1 \tag{21}$$

This means that the system will be transient unstable.

6.4. Radial basis function neural network (RBFNN)

The RBFNN was also initially trained with the same input data used to train the SVM. However, this did not yield satisfactory performance. The highest performance of 63% prediction accuracy was obtained only after increasing the volume of training data samples to 9.05% of total data. Beyond this, it was observed that the prediction accuracy remained the same. Thus, the RBFNN offered poor performance.

7. CONCLUSION

A novel technique for real-time prediction of transient stability status has been presented. The technique does not require any large volume of input data. The data processing approach is also simple. Its operation is also fast considerating the fact that it requires minimal input data captured in a very short time window. It can also be easily implemented. The performance of three artificial intelligence decision making tools namely support vector machine, multilayer perceptron neural network, and radial basis function neural network have also been evaluated. The support vector machine has been found to be most effective followed by the multilayer perceptron neural network. The radial basis function neural network gave the least performance.

REFERENCES

[1] U.S.-Canada Power System Outage Task Force, *Final Report on the August 14, 2003 Blackout in the United States and Canada: Causes and Recommendations*, Apr. 2004. Available: http://www.nerc.com/filez/blackout.html

[2] E. A. Frimpong, A. Johnson, and P. Y. Okyere, *Neural network and speed deviation based generator out-of-step prediction scheme*, Journal of Electrical Engineering, vol.15, no.2, pp.1-8, June 2015.

[3] P. Kundur, J. Paserba, V. Ajjarapu, G. Andersson, A. Bose, C. Canizares, N. Hatziargyriou, D. Hill, A. Stankovic, C. Taylor, T. Van Cutsem, and V. Vittal: *Definition and classification of power system stability*, IEEE Transactions on Power Syststems, vol. 19, no. 2, pp. 1387–1401, May 2004.

[4] D. R. Gurusinghe and A. D. Rajapakse, *Post-disturbance transient stability status prediction using synchrophasor measurements*, IEEE Transactions on Power Systems, vol. 31, no. 5, pp. 3656-3664, Sept. 2016.

[5] N. Amjady and S. F. Majedi, *Transient stability prediction by a hybrid intelligent system*, IEEE Transaction on Power Systems, vol. 22, no. 3, pp. 1275 -1283, August 2007.

[6] Y. Zhou, J. Wu, Z. Yu, L Ji. and L. Hao, A *hierarchical method for transient stability prediction of power systems using the confidence of a svm-based ensemble classifier*, Energies, vol. 9, pp. 1-20, 2016.

[7] J. Hazra, R. K. Reddi, K. Das, D. P. Seetharam and A. K. Sinha, *Power grid transient stability prediction using wide area synchrophasor measurements*, Proceeding of 3rd IEEE PES Innovative Smart Grid Technologies Europe (ISGT Europe), Berlin, China, pp. 1-8, 2012.

[8] A. N. AL-Masri, M. Z. A. A. Kadir, H. Hizam and N. Mariun, A *novel implementation for generator rotor angle stability prediction using an adaptive artificial neural network application for dynamic security assessment*, IEEE Transactions on Power Systems, vol. 28, no.3, p. 2516-2525, 2013.

[9] A.D. Rajapakse, F. Gomez, O.M.K.K. Nanayakkara, P.A. Crossley and V.V. Terzija, *Rotor angle stability prediction using post-disturbance voltage trajectory patterns*, IEEE Transactions on Power Systems, vol. 25, no. 2, pp. 945-956, 2010.

[10] F. Gomez, A. Rajapakse, U. Annakkage and I. Fernando, *Support vector machine-based algorithm for post-fault transient stability status prediction using synchronized measurements*, IEEE Transactions on Power Systems, vol. 26, no. 3, pp. 1474-1483, 2011.

[11] T. Guo, and J. V. Milanović, O*n-line prediction of transient stability using decision tree method — sensitivity of accuracy of prediction to different uncertainties*, Proceedings of the IEEE Grenoble PowerTech, Grenoble, 2013.

[12] D. E. Echeverría, J. L. Rueda, J. C. Cepeda, D. G. Colomé and I. Erlich, *Comprehensive approach for prediction and assessment of power system transient stability in real-time*, Proceedings of the 4th IEEE PES Innovative Smart Grid Technologies Europe (ISGT Europe), Copenhagen, pp. 1-5, 2013.

[13] T. Rahman, S. Sankaran, N. Seeley and K. Garg, *Capturing generator rotor angle and field*

quantities – SDG&E experience and approach to using nontraditional generator measurements, Proceedings of the 42nd Annual Western Protective Relay Conference, Spokane, Washington, p. 1-9, 2015.

[14] *IEEE Standard for Synchrophasor Measurements for Power Systems*, IEEE Std. C37.118.1-2011, Dec. 2011.

[15] I. J. Nagrath and D. P. Kothari, *Power System Stability*, Power System Engineering, New Delhi, India; Tata Mcgraw-Hill, ch. 12, sec. 12.2, pp. 486-489, 1994.

[16] Statistics and Machine Learning Toolbox™, User's Guide, Matlab R2015a.

[17] Support Vector Machine [Online]. Available: https://www.fer.unizg.hr /_download/repository/ 07-SupportVectorMachine, 2016.

[18] Matrix Laboratory software, MATLAB R2013a.

[19] C. W. Liu, M. C. Su, S. S. Tsay, and Y. J. Wang, *Application of a novel fuzzy neural network to real-time transient stability swings prediction based on synchronized phasor measurements*, IEEE Transactions on Power Syststems, vol 14, no. 2, pp. 685-692, May 1999.

[20] K. J, McGarry, S. Wermter and J. MacIntyre, *Knowledge extraction from radial basis function networks and multi-layer perceptrons*, International Joint Conference on Neural Networks, Washington D.C., p. 1-4, 2009.

[21] A. Kavousifard and H. Samet, *Consideration effect of uncertainty in power system reliability indices using radial basis function network and fuzzy logic theory*, *Neurocomputing*, vol. 74, no. 17, pp. 3420-3427, 2011.

[22] E. A. Frimpong, J. A. Asumadu and P.Y. Okyere, S*peed deviation and multilayer perceptron neural network based transient stability status prediction scheme*, Journal of Electrical and Electronic Engineering, vol. 15, no. 2, pp. 9-16, 2015.

[23] A. N. Fathian, and M.R. Gholamian, *Using MLP and RBF neural networks to improve the prediction of exchange rate time series with ARIMA*, International Journal of Information and Electronics Engineering, vol. 2, no. 4, pp. 543-546, 2012,

[24] H. Memarian, and S. K. Balasundram, C*omparison between multi-layer perceptron and radial basis function networks for sediment load estimation in a tropical watershed*, Journal of Water Resource and Protection, vol. 4, pp. 870-876, 2012.

[25] H. Yu, and B. M. Wilamowski, *Intelligent Systems*, Industrial Electronics Handbook, 2nd Edition, CRC press, pp. 12-1 to 12-15, 2011.

[26] A. Kavousifard and H. Samet: *Consideration effect of uncertainty in power system reliability indices using radial basis function network and fuzzy logic theory*, Neurocomputing, vol. 74, No. 17, 2011, p. 3420-3427.

[27] M. H. Beale, M. T. Hagan and H. B. Demuth, *Neural Network Toolbox™, User Guide*, MATLAB, R2016b, pp. 6-3 – 6-4, 2016.

[28] E. A. Frimpong: P*rediction of transient stability status and coherent generator groups*, PhD dissertation, Dept. of Elect. and Elec. Eng., Kwame Nkrumah University of Science and Technology, Kumasi, Ghana, 2015. [Available online]

[29] Y. Song, *Design of secondary voltage and stability controls with multiple control objectives*, PhD dissertation, Sch. of Elect. and Compt. Eng., Georgia Institute of Technology, Georgia, USA, 2009. [Available online]

FRAGARIA DALTONIANA ALGORITHM FOR SOLVING OPTIMAL REACTIVE POWER DISPATCH PROBLEM

Lenin **KANAGASABAI**
Prasad V.Potluri Siddhartha Institute of Technology, Kanuru, Vijayawada, 520007, Andhra Pradesh, India
gklenin@gmail.com

Keywords: optimization, reactive power, transmission loss, Fragaria Daltoniana plant

Abstract*: This paper projects Fragaria Daltoniana Algorithm (FDA) to solve optimal reactive power dispatch problem. Fragaria Daltoniana plant develops sprinter, roots for spread and pursuit for water resources & mineral deposit. In Fragaria Daltoniana plant sprinter, roots are whispered as implement for global and local searches. The planned Fragaria Daltoniana Algorithm (FDA) will replicate the computational agents at all iterations, revealing all agents to both minute and big movements from the begin to end & data exchange between agents. The proposed Fragaria Daltoniana Algorithm (FDA) has been tested on standard IEEE 30 bus test system and simulation results show evidently the better performance of the projected FDA in reducing the real power loss & enhancement of static voltage stability margin.*

1. INTRODUCTION

In recent years the optimal reactive power dispatch (ORPD) problem has received great attention as a result of improving in economy and security of power system operation. Solutions of ORPD problem aim to minimize object functions such as fuel cost, power system loses, etc. while satisfying a number of constraints like limits of bus voltages, tap settings of transformers, reactive and active power of power resources and transmission lines and a number of controllable Variables. Various numerical methods like the gradient method [1-2], Newton method [3] and linear programming [4-7] have been implemented to solve the optimal reactive power dispatch problem. Both the gradient and Newton methods have the intricacy in managing inequality constraints. The problem of voltage stability and

collapse play a key role in power system planning and operation [8]. Evolutionary algorithms such as genetic algorithm have been already projected to solve the reactive power flow problem [9-11]. Evolutionary algorithm is a heuristic methodology used for minimization problems by utilizing nonlinear and non-differentiable continuous space functions. In [12], Hybrid differential evolution algorithm is projected to increase the voltage stability index. In [13] Biogeography Based algorithm is projected to solve the reactive power dispatch problem. In [14], a fuzzy based method is used to solve the optimal reactive power scheduling method. In [15], an improved evolutionary programming is used to elucidate the optimal reactive power dispatch problem. In [16], the optimal reactive power flow problem is solved by integrating a genetic algorithm with a nonlinear interior point method. In [17], a pattern algorithm is used to solve ac-dc optimal reactive power flow model with the generator capability limits. In [18], F. Capitanescu proposes a two-step approach to calculate Reactive power reserves with respect to operating constraints and voltage stability. In [19], a programming based approach is used to solve the optimal reactive power dispatch problem. In [20], A. Kargarian et al present a probabilistic algorithm for optimal reactive power provision in hybrid electricity markets with uncertain loads. This paper projects Fragaria Daltoniana Algorithm (FDA) to solve optimal reactive power dispatch problem. In the iteration's the capacity of computational agents is imitated in a suitable manner & prejudice the weakest agents. Computational agent is endangered to both minute and big movements repeatedly from begin to end & it conceivably achieve the local and global explorations synchronously. In the projected Fragaria Daltoniana Algorithm (FDA) the computational agents do not communicate with each other, and the above said duplication-elimination procedure are united with a kind of sifter that influence the agents on the path to the global best solution. The proposed Fragaria Daltoniana Algorithm (FDA) has been evaluated on standard IEEE 30 bus test system. The simulation results show that the projected Fragaria Daltoniana Algorithm (FDA) surpasses all the entitled reported algorithms in minimizing the real power loss and static voltage stability margin also enhanced.

2. VOLTAGE STABILITY EVALUATION

2.1. Modal analysis for voltage stability evaluation

Modal analysis is one among best methods for voltage stability enhancement in power systems. The steady state system power flow equations are given by:

$$\begin{bmatrix}\Delta P\\ \Delta Q\end{bmatrix} = \begin{bmatrix} J_{p\theta} & J_{pv} \\ J_{q\theta} & J_{QV} \end{bmatrix} \begin{bmatrix}\Delta\theta\\ \Delta V\end{bmatrix} \quad (1)$$

where:

ΔP = Incremental change in bus real power.

ΔQ = Incremental change in bus reactive Power injection

$\Delta\theta$ = Incremental change in bus voltage angle.

ΔV = Incremental change in bus voltage Magnitude

$J_{p\theta}$, J_{PV} , $J_{Q\theta}$, J_{QV} Jacobian matrix are the sub-matrixes of the system voltage stability is affected by both P and Q.

To reduce (1), let $\Delta P = 0$, then:

$$\Delta Q = \left[J_{QV} - J_{Q\theta}J_{P\theta^{-1}}J_{PV}\right]\Delta V = J_R\Delta V \tag{2}$$

$$\Delta V = J^{-1} - \Delta Q \tag{3}$$

where:

$$J_R = \left(J_{QV} - J_{Q\theta}J_{P\theta^{-1}}JPV\right) \tag{4}$$

J_R is called the reduced Jacobian matrix of the system.

2.2. Modes of Voltage instability

Voltage Stability characteristics of the system have been identified by computing the eigenvalues and eigenvectors.

Let

$$J_R = \xi\wedge\eta \tag{5}$$

where,

ξ = right eigenvector matrix of JR

η = left eigenvector matrix of JR

Λ = diagonal eigenvalue matrix of JR

and

$$J_{R^{-1}} = \xi\wedge^{-1}\eta \tag{6}$$

From (5) and (8), we have,

$$\Delta V = \xi\wedge^{-1}\eta\Delta Q \tag{7}$$

or

$$\Delta V = \sum_I \frac{\xi_i\eta_i}{\lambda_i}\Delta Q \tag{8}$$

where ξ_i is the ith column right eigenvector and η the ith row left eigenvector of JR and λ_i is the ith eigenvalue of JR.

The *i*th modal reactive power variation is,

$$\Delta Q_{mi} = K_i \xi_i \tag{9}$$

where,

$$K_i = \sum_j \xi_{ij^2} - 1 \tag{10}$$

with ξ_{ji} is the *j*th element of ξ_i.

The corresponding *i*th modal voltage variation is

$$\Delta V_{mi} = [1/\lambda_i]\Delta Q_{mi} \tag{11}$$

If $|\ \lambda_i\ | = 0$ then the *i*th modal voltage will collapse.

In (10), let $\Delta Q = e_k$, where e_k has all its elements zero except the *k*th one being 1. Then,

$$\Delta V = \sum_i \frac{\eta_{1k}\ \xi_1}{\lambda_1} \tag{12}$$

η_{1k} being the kth element of η_1 .

V –*Q* sensitivity at bus *k*,

$$\frac{\partial V_K}{\partial Q_K} = \sum_i \frac{\eta_{1k}\ \xi_1}{\lambda_1} = \sum_i \frac{P_{ki}}{\lambda_1} \tag{13}$$

3. PROBLEM FORMULATION

The objectives of the reactive power dispatch problem is to minimize the system real power loss and maximize the static voltage stability margins (SVSM).

3.1. Minimization of Real Power Loss

Minimization of the real power loss (P_{loss}) in transmission lines is mathematically stated as follows:

$$P_{loss} = \sum_{\substack{k=1 \\ k=(i,j)}}^{n} g_{k(V_i^2 + V_j^2 - 2V_i V_j \cos\theta_{ij})} \tag{14}$$

where *n* is the number of transmission lines, g_k is the conductance of branch k, V_i and V_j are voltage magnitude at bus *i* and bus *j*, and θ_{ij} is the voltage angle difference between bus *i* and bus *j*.

3.2. Minimization of Voltage Deviation

Minimization of the voltage deviation magnitudes (*VD*) at load buses is mathematically stated as follows:

$$\text{Minimize } VD = \sum_{k=1}^{nl} |V_k - 1.0| \tag{15}$$

where *nl* is the number of load busses and V_k is the voltage magnitude at bus *k*.

3.3. System Constraints

Objective functions are subjected to these constraints shown below.

Load flow equality constraints:

$$P_{Gi} - P_{Di} - V_i \sum_{j=1}^{nb} V_j \begin{bmatrix} G_{ij} & cos\,\theta_{ij} \\ +B_{ij} & sin\,\theta_{ij} \end{bmatrix} = 0, i = 1,2 \ldots., nb \tag{16}$$

$$Q_{Gi} - Q_{Di} - V_i \sum_{j=1}^{nb} V_j \begin{bmatrix} G_{ij} & sin\,\theta_{ij} \\ +B_{ij} & cos\,\theta_{ij} \end{bmatrix} = 0, i = 1,2 \ldots., nb \tag{17}$$

where, *nb* is the number of buses, P_G and Q_G are the real and reactive power of the generator, P_D and Q_D are the real and reactive load of the generator, and G_{ij} and B_{ij} are the mutual conductance and susceptance between bus *i* and bus *j*.

Generator bus voltage (VGi) inequality constraint:

$$V_{Gi}^{min} \leq V_{Gi} \leq V_{Gi}^{max}, i \in ng \tag{18}$$

Load bus voltage (VLi) inequality constraint:

$$V_{Li}^{min} \leq V_{Li} \leq V_{Li}^{max}, i \in nl \tag{19}$$

Switchable reactive power compensations (QCi) inequality constraint:

$$Q_{Ci}^{min} \leq Q_{Ci} \leq Q_{Ci}^{max}, i \in nc \tag{20}$$

Reactive power generation (QGi) inequality constraint:

$$Q_{Gi}^{min} \leq Q_{Gi} \leq Q_{Gi}^{max}, i \in ng \tag{21}$$

Transformers tap setting (Ti) inequality constraint:

$$T_i^{min} \leq T_i \leq T_i^{max}, i \in nt \tag{22}$$

Transmission line flow (SLi) inequality constraint:

$$S_{Li}^{min} \leq S_{Li}^{max}, i \in nl \tag{23}$$

where, *nc*, *ng* and *nt* are numbers of the switchable reactive power sources, generators and transformers.

4. FRAGARIA DALTONIANA PLANT

Fragaria Daltoniana plant (*fig. 1*) which promulgates through runners will do to augment its survival. If it is in an upright spot of the ground, with enough water, nutrients, and light, then it is sound to undertake that there is no stress on it to leave that spot to promise its survival. So, it will propel numerous short runners that will give new Fragaria Daltoniana plant and inhabit the locality as greatest they can. If, on the other hand, the mother plant is in a spot that is meagre in water, nutrients, light, or any one of these essential for a plant to endure, then it will try to find a healthier spot for its offspring. So, it will propel few runners further afield to explore distant areas. One can also assume that it will propel only a limited, since sending a long runner is a large venture for a plant which is in a meagre spot. We may further assume that the class of the spot (abundance of nutrients, water, and light) is imitated in the development of the plant.

Fig. 1. Fragaria Daltoniana plant

A plant p_i is in spot X_i in dimension n. This means $X_i = \{x_{i,}$ *for* $j = 1, \ldots, n\}$. Let NP be the number of Fragaria Daltoniana plant to be used initially:

i. Fragaria Daltoniana plant which are in noble spots propagate by engendering numerous short runners.
ii. Those in poor spots promulgate by producing few long runners.

It is clear that, in the above explanation, exploitation is applied by sending many short runners by plants in noble spots, while exploration is applied by sending fewlong runners by plants in meagre spots.

The parameters used in Fragaria Daltoniana plant are the population size NP which is the number of Fragaria Daltoniana plant, the maximum number of generations $g_{\max}$, and the maximum number of possible runners $n_{\max}$ per plant. $g_{\max}$ is effectively the stopping criterion.

The algorithm uses the objective function value at different plant positions X_i, $i = 1, \ldots, NP$, in a regularized form N_i, to rank them as would a fitness function in a standard genetic algorithm.

The number of plant runners n_α^i, calculated according to (24), has length dx^icalculated using the regularized form of the objective value at X_i, each giving a $dx^i \in (-1,1)^n$, as calculated with (25). Afterward all plants in the population have sent out their apportioned runners, new plants are appraised and the whole increased population is sorted. To keep the population continuous, individuals with lower growth are eradicated.

The number of runners allocated to a given plant is proportionate to its fitness as in:

$$n_\alpha^i = [n_{max} N_i \alpha], \alpha \in (0,1) \tag{24}$$

Each solution X_i engenders at least one runner and the length of each such runner [21-24] are contrariwise proportionate to its growth as in (25) below:

$$dx_j^i = 2(1 - N_i)(\alpha - 0.5), for\ j = 1, .., n \tag{25}$$

where n is the problem dimension.

Having calculated dx_j^i, the extent to which the runner will reach, the exploration equation that finds the next area to discover is as follows:

$$y_{i,j} = x_{i,j} + \left(b_j - a_j\right) dx_j^i\ , for\ j = 1, .., n \tag{26}$$

If the bounds of the exploration domain are desecrated, the point is accustomed to be within the domain $[a_j, b_j]$, where a_j and b_j are lower and upper bounds demarcating the exploration space for the jth coordinate.

5. FRAGARIA DALTONIANA ALGORITHM (FDA)

In application of Fragaria Daltoniana Algorithm (FDA), the preliminary population is vital. We run the algorithm number of times from arbitrarily produced populations. The finest individual from each run forms a member of the preliminary population. The amount of runs to produce the preliminary population is NP; so, the population size is$r = NP$. When this number is greater than a definite threshold, the variables are fixed for the rest of the run. Let pop be a common matrix containing the population of a given run. Its rows correspond to individuals. The following equation is used to produce an arbitrary population for each of the preliminary runs:

$$x_{i,j} = a_j + \left(b_j - a_j\right)\alpha \, , j = 1, .. , n \tag{27}$$

where $x_{i,j} \in [a_j, b_j]$ is the jth entry of solution X_i and a_j and b_j are the jth entries of the lower and upper bounds defining the exploration space of the problem and $\alpha \in (0, 1)$.

In the chief frame of the algorithm, before updating the population we produce a provisional population Φ to clutch new solutions produced from each individual in the population. Then we implement three rules with fixed amendment parameter P_m, chosen here, as $P_m = 0.789$.The first two rules are applied if the population is initialized arbitrarily.

Regulation one uses the following equation to modernize the population:

$$x^*_{i,j} = x_{i,j}(1 + \beta), j = 1, .. , n \tag{28}$$

where $\beta \in [-1, 1]$ and $x^*_{i,j} \in [a_j, b_j]$.

The produced individual $X^*_i$is calculated according to the objective function and is stored in Φ.

In regulation two another individual is produced with the same modification parameter$P_m = 0.789$ as in the following equation:

$$x^*_{i,j} = x_{i,j} + \left(x_{l,j} - x_{k,j}\right)\beta \, , j = 1, .. , n \tag{29}$$

where $\beta \in [-1, 1]$, $x^*_{i,j} \in [a_j, b_j]$. l, k are conjointly special indices and are different from i.

The created individual X^*_i is appraised according to the objective function and is stored in Φ. The first two regulations are valid for $r \leq NP$ the number of runs. For $r > NP$ the algorithm also attempts to identify entries which are settling to their ultimate values through a counter IN. If the jth entry in existing population has a low IN value, then it is adapted by

implementing (23); or else it is left as it is. The following equation is used when modification is essential:

$$x_{i,j}^{*} = x_{i,j} + \left(x_{i,j} - x_{k,j}\right)\beta \, , j = 1, .., n \tag{30}$$

where $\beta \in [-1, 1]$, $x_{i,j}^{*} \in [a_j, b_j]$, and k is different from i.

To preserve the size of the population constant, the extra plants at the bottom of the organized population are eradicated.

Fragaria Daltoniana Algorithm (FDA) for solving optimal reactive power dispatch problem:

Initialization: g_{max}, NP, r

If $r \leq NP$ at that juncture; Produce an arbitrary population of plants $pop = \{Xi \mid i = 1, 2, \ldots, NP\}$, using (27) and collect the best solutions.

End if

While $r > NP$ do

Use population pop_g formed by congregation all best solutions from preceding runs. Compute IN_j value for each column j of pop_g

End while

Estimate the population. In case of pop_g the algorithm does not need to estimate the population,

Set number of runners

While ($ngen < gmax$) do

Generate Φ:

for i = 1 to NP do

for k = 1 to n_r do

if $r \leq NP$ then

If rand $\leq P_m$ then

Produce a new-fangled solution $x_{i,j}^{*}$ according to (28);

Calculate it and store it in Φ;

End if

If rand $\leq P_m$ then

Produce a new-fangled solution $x_{i,j}^{*}$ according to (29);

Estimate it and store it in Φ;

End if

Else

For j = 1: n do

If (rand $\leq P_m$) then

Modernize the jth entry of X_i, i = 1,2,..,NP, according to (30);

End if

Calculate new-fangled solution and store it in Φ;
End for
End if
End for
Augment Φ to existing population;
Arrange the population in uphill order of the objective values;
Modernize current best;
End while
Revisit: updated population.

6. SIMULATION RESULTS

The efficiency of the proposed Fragaria Daltoniana Algorithm (FDA) is demonstrated by testing it on standard IEEE-30 bus system. The IEEE-30 bus system has 6 generator buses, 24 load buses and 41 transmission lines of which four branches are (6-9), (6-10), (4-12) and (28-27) - are with the tap setting transformers. The lower voltage magnitude limits at all buses are 0.95 p.u. and the upper limits are 1.1 for all the PV buses and 1.05 p.u. for all the PQ buses and the reference bus. The simulation results have been presented in *Tables 1, 2, 3 &4*. And in the *Table 5* shows the proposed algorithm powerfully reduces the real power losses when compared to other given algorithms. The optimal values of the control variables along with the minimum loss obtained are given in *Table 1*. Corresponding to this control variable setting, it was found that there are no limit violations in any of the state variables.

Table 1. Results of FDA – ORPD Optimal Control Variables

Control variables	***Variable setting***
V1	*1.041*
V2	*1.046*
V5	*1.044*
V8	*1.030*
V11	*1.000*
V13	*1.030*
T11	*1.00*
T12	*1.00*
T15	*1.00*
T36	*1.00*
Qc10	*2*
Qc12	*3*

Table 2.Results of FDA -Voltage Stability Control Reactive Power Dispatch Optimal Control Variables

Control variables	***Variable setting***
V1	*1.049*
V2	*1.048*
V5	*1.045*
V8	*1.036*
V11	*1.002*
V13	*1.034*
T11	*0.090*
T12	*0.090*
T15	*0.090*
T36	*0.090*
Qc10	*3*
Qc12	*2*

Control variables	*Variable setting*
Qc15	*2*
Qc17	*0*
Qc20	*2*
Qc23	*2*
Qc24	*3*
Qc29	*2*
Real power loss	*4.2632*
SVSM	*0.2472*

Control variables	*Variable setting*
Qc15	*2*
Qc17	*3*
Qc20	*0*
Qc23	*2*
Qc24	*2*
Qc29	*3*
Real power loss	*4.9885*
SVSM	*0.2489*

Optimal reactive power dispatch problem together with voltage stability constraint problem was handled in this case as a multi-objective optimization problem where both power loss and maximum voltage stability margin of the system were optimized simultaneously. *Table 2* indicates the optimal values of these control variables. Also it is found that there are no limit violations of the state variables. It indicates the voltage stability index has increased from 0.2472 to 0.2489, an advance in the system voltage stability. To determine the voltage security of the system, contingency analysis was conducted using the control variable setting obtained in case 1 and case 2. The eigenvalues equivalents to the four critical contingencies are given in *Table 3*. From this result it is observed that the eigenvalue has been improved considerably for all contingencies in the second case.

Table 3. Voltage Stability under Contingency State

Sl.No	***Contingency***	***ORPD Setting***	***VSCRPD Setting***
1	*28-27*	*0.1419*	*0.1434*
2	*4-12*	*0.1642*	*0.1650*
3	*1-3*	*0.1761*	*0.1772*
4	*2-4*	*0.2022*	*0.2043*

Table 4. Limit Violation Checking Of State Variables

State variables	***limits***		***ORPD***	***VSCRPD***
	lower	***upper***		
Q1	*-20*	*152*	*1.3422*	*-1.3269*
Q2	*-20*	*61*	*8.9900*	*9.8232*
Q5	*-15*	*49.92*	*25.920*	*26.001*
Q8	*-10*	*63.52*	*38.8200*	*40.802*
Q11	*-15*	*42*	*2.9300*	*5.002*
Q13	*-15*	*48*	*8.1025*	*6.033*
V3	*0.95*	*1.05*	*1.0372*	*1.0392*
V4	*0.95*	*1.05*	*1.0307*	*1.0328*
V6	*0.95*	*1.05*	*1.0282*	*1.0298*
V7	*0.95*	*1.05*	*1.0101*	*1.0152*

State variables	*limits*		*ORPD*	*VSCRPD*
	lower	*upper*		
V9	*0.95*	*1.05*	*1.0462*	*1.0412*
V10	*0.95*	*1.05*	*1.0482*	*1.0498*
V12	*0.95*	*1.05*	*1.0400*	*1.0466*
V14	*0.95*	*1.05*	*1.0474*	*1.0443*
V15	*0.95*	*1.05*	*1.0457*	*1.0413*
V16	*0.95*	*1.05*	*1.0426*	*1.0405*
V17	*0.95*	*1.05*	*1.0382*	*1.0396*
V18	*0.95*	*1.05*	*1.0392*	*1.0400*
V19	*0.95*	*1.05*	*1.0381*	*1.0394*
V20	*0.95*	*1.05*	*1.0112*	*1.0194*
V21	*0.95*	*1.05*	*1.0435*	*1.0243*
V22	*0.95*	*1.05*	*1.0448*	*1.0396*
V23	*0.95*	*1.05*	*1.0472*	*1.0372*
V24	*0.95*	*1.05*	*1.0484*	*1.0372*
V25	*0.95*	*1.05*	*1.0142*	*1.0192*
V26	*0.95*	*1.05*	*1.0494*	*1.0422*
V27	*0.95*	*1.05*	*1.0472*	*1.0452*
V28	*0.95*	*1.05*	*1.0243*	*1.0283*
V29	*0.95*	*1.05*	*1.0439*	*1.0419*
V30	*0.95*	*1.05*	*1.0418*	*1.0397*

Table 5. Comparison of Real Power Loss

Method	*Minimum loss*
Evolutionary programming [25]	*5.0159*
Genetic algorithm [26]	*4.665*
Real coded GA with Lindex as SVSM [27]	*4.568*
Real coded genetic algorithm [28]	*4.5015*
Proposed FDA method	*4.2632*

7. CONCLUSION

In this paper, the Fragaria Daltoniana Algorithm (FDA) has been successfully solved optimal reactive power dispatch problem. The planned Fragaria Daltoniana Algorithm (FDA) will replicate the computational agents at all iterations, revealing all agents to both minute and big movements from the begin to end & data exchange between agents. The proposed Fragaria Daltoniana Algorithm (FDA) has been tested on standard IEEE 30 bus test system and simulation results show evidently the better performance of the projected FDA in reducing the real power loss & enhancement of static voltage stability margin.

REFERENCES

[1] O. Alsac and B. Scott, *Optimal load flow with steady state security*,,IEEE Transaction. PAS , pp. 745-751, 1973.

[2] Lee K. Y, Paru Y. M, Oritz J. L, *A united approach to optimal real and reactive power dispatch* , IEEE Transactions on power Apparatus and systems: PAS-104 : 1147-1153, 1985.

[3] A. Monticelli, M .V. F Pereira and S. Granville, *Security constrained optimal power flow with post contingency corrective rescheduling*, IEEE Transactions on Power Systems :PWRS-2, No. 1, pp.175-182,1987.

[4] Deeb N, Shahidehpur S. M, *Linear reactive power optimization in a large power network using the decomposition approach*, IEEE Transactions on power system: 5(2) : pp 428-435, 1990.

[5] E. Hobson, *Network constrained reactive power control using linear programming*, IEEE Transactions on power systems, 99 (4), pp 868-877, 1980.

[6] K. Y Lee ,Y. M Park , and J. L Oritz, *Fuel –cost optimization for both real and reactive power dispatches*, IEE Proc; 131C,(3), pp.85-93,1984.

[7] M. K. Mangoli, K. Y. Lee, *Optimal real and reactive power control using linear programming*, Electric Power System, vol.26, pp.1-10,1993.

[8] C. A. Canizares, A. C. Z.de Souza, V. H. Quintana, *Comparison of performance indices for detection of proximity to voltage collapse*, vol. 11. no.3, pp.1441-1450, 1996.

[9] K. Anburaja, *Optimal power flow using refined genetic algorithm*, Electric Power Component System, Vol. 30, 1055-1063, 2002.

[10] D. Devaraj, B. Yeganarayana, *Genetic algorithm based optimal power flow for security enhancement*, IEE proceedings on Generation.Transmission and. Distribution; 152, 2005.

[11] Berizzi, C. Bovo, M. Merlo, M. Delfanti, *A GA approach to compare ORPF objective functions including secondary voltage regulation*, Electric Power Systems Research, vol. 84, no. 1, pp. 187 – 194, 2012.

[12] C.-F. Yang, G. G. Lai, C.-H.Lee, C.-T. Su, G. W. Chang, *Optimal setting of reactive compensation devices with an improved voltage stability index for voltage stability enhancement*, International Journal of Electrical Power and Energy Systems, vol. 37, no. 1, pp. 50 – 57, 2012.

[13] P. Roy, S. Ghoshal, S. Thakur, *Optimal VAR control for improvements in voltage profiles and for real power loss minimization using biogeography based optimization*, International Journal of Electrical Power and Energy Systems, vol. 43, no. 1, pp. 830 – 838, 2012.

[14] B. Venkatesh, G. Sadasivam, M. Khan, *A new optimal reactive power scheduling method for loss minimization and voltage stability margin maximization using successive multi-objective fuzzy LP technique*, IEEE Transactions on Power Systems, vol. 15, no. 2, pp. 844 – 851, 2000.

[15] W. Yan, S. Lu, D. Yu, *A novel optimal reactive power dispatch method based on an improved hybrid evolutionary programming technique*, IEEE Transactions on Power Systems, vol. 19, no. 2, pp. 913 – 918, 2004.

[16] W. Yan, F. Liu, C. Chung, K. Wong, *A hybrid genetic algorithm interior point method for optimal reactive power flow*, IEEE Transactions on Power Systems, vol. 21, no. 3, pp. 1163 – 1169, 2006.

[17] J. Yu, W. Yan, W. Li, C. Chung, and K. Wong, *An unfixed piecewise optimal reactive power-flow model and its algorithm for ac-dc systems*, IEEE Transactions on Power Systems, vol. 23, no. 1, pp. 170 –176, 2008.

[18] F. Capitanescu, *Assessing reactive power reserves with respect to operating constraints and voltage stability*, IEEE Transactions on Power Systems, vol. 26, no. 4, pp. 2224–2234, 2011.

[19] Z. Hu, X. Wang, and G. Taylor, *Stochastic optimal reactive power dispatch: Formulation and solution method*, International Journal of Electrical Power and Energy Systems, vol. 32, no. 6, pp. 615 – 621, 2010.

[20] Kargarian, M. Raoofat, M. Mohammadi, *Probabilistic reactive power procurement in hybrid electricity markets with uncertain loads*, Electric Power Systems Research, vol. 82, no. 1, pp. 68 – 80, 2012.

[21] X.-S. Yang, *Nature-Inspired Metaheuristic Algorithms*, Luniver Press, 2011.

[22] Salhi, E. S. Fraga, *Nature-inspired optimization approaches and the new plant propagation algorithm*, in Proceedings of the International Conference on Numerical Analysis and Optimization (ICeMATH '11), Yogyakarta, Indonesia, 2011.

[23] J. Brownlee, Clever Algorithms: *Nature-Inspired Programming Recipes*, 2011.

[24] Muhammad Sulaiman, Abdellah Salhi, Birsen Irem Selamoglu, Omar Bahaaldin Kirikchi, *A Plant Propagation Algorithm for Constrained Engineering Optimisation Problems*, Mathematical Problems in Engineering Volume 2014.

[25] Wu Q H, Ma J T, *Power system optimal reactive power dispatch using evolutionary programming*, IEEE Transactions on power systems; 10(3): 1243-1248 , 1995.

[26] S.Durairaj, D.Devaraj, P.S.Kannan, *Genetic algorithm applications to optimal reactive power dispatch with voltage stability enhancement*, IE(I) Journal-EL Vol 87, 2006.

[27] D.Devaraj, *Improved genetic algorithm for multi – objective reactive power dispatch problem*, European Transactions on electrical power; 17: 569-581, 2007.

[28] P. Aruna Jeyanthy and Dr. D. Devaraj, *Optimal Reactive Power Dispatch for Voltage Stability Enhancement Using Real Coded Genetic Algorithm*, International Journal of Computer and Electrical Engineering, Vol. 2, No. 4, 1793-8163, 2010.

CLOSED FORM FORMULAS FOR ELF INDUCTIVE COUPLING BETWEEN FINITE LENGTH WIRES WITH EARTH RETURN

Giovanni **LUCCA**
SIRTI S.p.A, Milano, Italy
G.Lucca@sirti.it

Keywords: electromagnetic interference, electromagnetic compatibility, electromagnetic coupling

Abstract*: This paper deals with the evaluation of the inductive coupling between an overhead finite length wire circuit and a buried wire circuit, both with earth return, in the range of Extremely Low Frequencies (ELF). In particular, the attention is focused on the key parameter for this kind of problems i.e. the per unit length (p.u.l.) mutual impedance between the two circuits. Starting from the exact formula involving a Sommerfeld's integral, two new approximated analytical formulas, having different levels of approximation, are derived; the advantage of these formulas is that, in such a way, the p.u.l. mutual impedance is expressed only by means of elementary functions so avoiding numerical calculations of the Sommerfeld's integral. Finally, a comparison between the two proposed formulas is made.*

1. INTRODUCTION

It is known that the issue of Extremely Low Frequency electromagnetic interference from power lines/electrified railway lines on pipelines is an important topic related to the electrical safety for staff getting in touch with accessible parts of the pipeline. Risks for safety exist whether the power line/railway line is both in faulty condition or is in normal operating condition; moreover, overvoltage and overcurrent induced on the pipeline may produce damages to the pipeline itself (e.g. insulating coating perforation) or to devices and apparatuses connected to it (e.g. cathodic protection devices). Finally, one has not to forget the AC corrosion risk that is related to the electromagnetic induction generated on the pipe-earth circuit under normal operating condition of the inducing line [1-2].

This paper focuses on the inductive interference generated on long buried metallic structures such as pipelines, ducts, telecommunication cables; the frequencies considered are the typical ones used for transmission and distribution of electrical power i.e. 50-60Hz.

The key parameter for the evaluation of the inductive coupling is the p.u.l. mutual impedance which is directly proportional to the inductive component of the electric field generated by the power line conductors. Such conductors, hung, between two consecutive towers, can be represented, in first approximation, as long horizontal and finite length wires parallel to the soil surface.

In literature, only few contributions, concerning the approach to this problem by means of the finite length wires model, exist; in fact, most of the works are focused on the infinite length wires model whose progenitor is the famous paper by Carson published in 1926 [3].

For a comparison between the two approaches (i.e. finite and infinite length wire models) one can have a look at [4].

It is also worth to mention alternative approaches involving the Finite Element Method [5-8], but they are out of the scope of the present paper.

Among the papers, dealing with mutual coupling between finite length wires with earth return, one has to mention [9-14] where the mutual impedance is expressed by means of the so called "Neumann formulas" involving integrals along the wires path. A different technique is adopted in [15] where the author, by considering an overhead linear horizontal antenna and by applying the "complex image theory", obtained approximated closed form formulas for electric and magnetic fields valid in the quasi-static range and in the upper semi-space. Nevertheless, no formulas were given for evaluating the field in the lower semi-space i.e. in the soil.

This paper proposes new closed form formulas, built up by means of elementary functions, for evaluating, the inductive component of the electric field in the soil in the ELF range. In particular, thanks to these formulas, one can avoid numerical integration of Sommerferld's integral.

2. DERIVATION OF THE FORMULAS

2.1. General

The starting point is evaluating the inductive component of the electric field generated by a finite length overhead wire with earth return carrying a harmonic constant current given by the phasor I_{pl}. The overhead wire, assumed having constant height H over the soil, is a representation of a generic power line conductor hung between two consecutive towers (See *fig.1*).

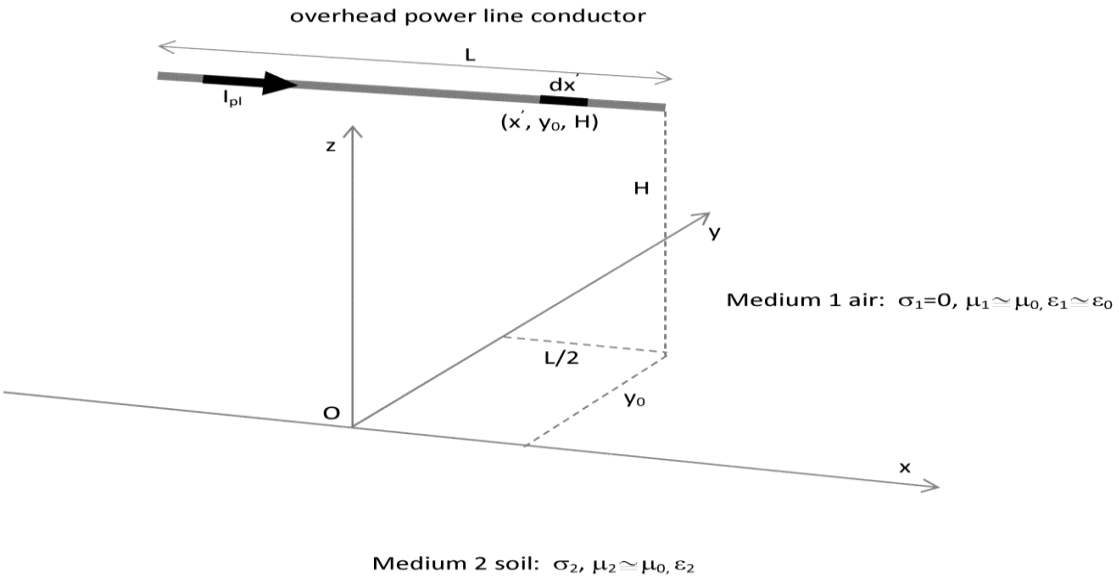

Fig. 1. Representation of a power line conductor as an overhead finite wire length

It is convenient to suppose the wire, having length *L*, as composed by infinitesimal horizontal electric dipoles each one of length *dx*'; thus, the field produced by the whole wire can be calculated as sum of all the contributions generated by the single dipoles.

According to [16], the inductive x-component of the electric field produced in the soil (medium 2, $z<0$) in the generic point (x, y, z) by a single dipole placed in (x', y_0, H) is proportional to the *x*-component of the electric Hertz potential Π *i.e.*:

$$dE_{2x}^{ind}(x,y,z) = k_2^2 \Pi_{2x}(x,y,z) =$$
$$= \frac{j\omega\mu_0 I dx'}{4\pi} \int_0^{\infty} \frac{2\lambda e^{-\sqrt{\lambda^2-k_1^2}H} e^{\sqrt{\lambda^2-k_2^2}z}}{\sqrt{\lambda^2-k_1^2}+\sqrt{\lambda^2-k_2^2}} J_0\left(\lambda\sqrt{(x-x')^2+(y'-y_0)^2}\right) d\lambda \quad (1)$$

Note that (1) is expressed by means of a Sommerfeld's integral. In (1), j is the imaginary unit, J_0 is the Bessel function of the first kind and order 0 and k_1, k_2 are respectively given by:

$$k_1^2 = -j\omega\mu_0(j\omega\varepsilon_0) \quad (2)$$

$$k_2^2 = -j\omega\mu_0(\sigma_2 + j\omega\varepsilon_2) \quad (3)$$

In order to obtain the field produced by the wire, one has to integrate expression (1) over the whole wire length, i.e.:

$$E_{2x}^{ind}(x,y,z)$$
$$= \int_{-\frac{L}{2}}^{\frac{L}{2}} \left[\frac{j\omega\mu_0 I}{4\pi} \int_0^{\infty} \frac{2\lambda e^{-\sqrt{\lambda^2-k_1^2}H} e^{\sqrt{\lambda^2-k_2^2}z}}{\sqrt{\lambda^2-k_1^2}+\sqrt{\lambda^2-k_2^2}} J_0\left(\lambda\sqrt{(x-x')^2+(y'-y_0)^2}\right) d\lambda \right] dx' \quad (4)$$

2.2. Approximated formulas

By introducing suitable hypotheses, it is possible to simplify (1), so that the field $E_{2x}^{ind}(x,y,z)$ can be expressed by means of an analytical expression much simpler than (4).

The simplifying assumptions can be listed as follows:

- Neglecting displacement currents i.e.: $k_1 \cong 0$ (in the air) and $k_2^2 = -j\omega\mu_0\sigma_2$ (in the earth)
- Due to the extremely low frequencies considered (50-60Hz), to the typical range of values for the soil conductivity σ_2 (i.e.: [10^{-4}, 10^{-1}]S/m) and to the typical range of values for the burial depth of pipes (i.e.: [0.5, 2]m), it is possible to write with good approximation:

$$e^{\sqrt{\lambda^2-k_2^2}z} \cong e^{\lambda z} \tag{5}$$

Therefore, by defining $\gamma^2 = k_2^2$, formula (1) can be simplified as follows:

$$dE_{2x}^{ind}(x,y,z) = \frac{j\omega\mu_0 I}{4\pi}\int_0^\infty \frac{2\lambda e^{-\lambda H}e^{\lambda z}}{\lambda+\sqrt{\lambda^2+\gamma^2}} J_0\left(\lambda\sqrt{(x-x')^2+(y'-y_0)^2}\right)d\lambda \tag{6}$$

In (6), according to [17] a further simplification can be introduced:

$$\frac{2\lambda}{\lambda+\sqrt{\lambda^2+\gamma^2}} = 1 - e^{2\frac{\lambda}{\gamma}}\left[1+\frac{1}{3}\left(\frac{\lambda}{\gamma}\right)^3+\cdots\right] \tag{7}$$

By substituting (7) into (6) and after some algebric steps, that have been omitted for brevity, one obtains, by the help of certain identities, [18]:

$$dE_{2x}^{ind}(x,y,z) = \frac{j\omega\mu_0 I dx'}{4\pi}\left\{\begin{array}{c} \frac{1}{\sqrt{(x-x')^2+(y-y_0)^2+(|z|+H)^2}} + \\ +\frac{-1}{\sqrt{(x-x')^2+(y-y_0)^2+\left(|z|+H+\frac{2}{\gamma}\right)^2}} + \\ -\frac{(-1)^3}{\gamma^3}\frac{3\left(|z|+H+\frac{2}{\gamma}\right)\left[(x-x')^2+(y-y_0)^2\right]-2\left(|z|+H+\frac{2}{\gamma}\right)^3}{\left(\sqrt{(x-x')^2+(y-y_0)^2+\left(|z|+H+\frac{2}{\gamma}\right)^2}\right)^7} \end{array}\right\} \tag{8}$$

In particular, the following identity has been used:

$$\frac{1}{3\gamma^3}\int_0^\infty \lambda^3 e^{-\left(|z|+H+\frac{2}{\gamma}\right)\lambda} J_0\left(\lambda\sqrt{(x-x')^2+(y'-y_0)^2}\right)d\lambda =$$
$$\frac{(-1)^3}{3\gamma^3}\frac{d^3}{d\left(|z|+H+\frac{2}{\gamma}\right)^3}\left(\frac{1}{\sqrt{(x-x')^2+(y-y_0)^2+\left(|z|+H+\frac{2}{\gamma}\right)^2}}\right) \tag{9}$$

In order to obtain the total electric field produced by the overhead wire, one has to integrate expression (8), over whole wire length so obtaining:

$$E_{2x}^{ind}(x,y,z) =$$

$$\frac{j\omega\mu_0 I}{4\pi}\left\{\begin{array}{l} \ln\left(\frac{\frac{L}{2}-x+\sqrt{\left(\frac{L}{2}-x\right)^2+(y-y_0)^2+(|z|+H)^2}}{-\left(\frac{L}{2}+x\right)+\sqrt{\left(\frac{L}{2}+x\right)^2+(y-y_0)^2+(|z|+H)^2}}\right)+ \\ -\ln\left(\frac{\frac{L}{2}-x+\sqrt{\left(\frac{L}{2}-x\right)^2+(y-y_0)^2+\left(|z|+H+\frac{2}{\gamma}\right)^2}}{-\left(\frac{L}{2}+x\right)+\sqrt{\left(\frac{L}{2}+x\right)^2+(y-y_0)^2+\left(|z|+H+\frac{2}{\gamma}\right)^2}}\right)+ \\ +\frac{(-1)^3}{\gamma^3}\frac{3\left(|z|+H+\frac{2}{\gamma}\right)}{\left[(y-y_0)^2+\left(|z|+H+\frac{2}{\gamma}\right)^2\right]^2}\sum_{k=0}^{1}\frac{(-1)^k}{2k+3}\binom{1}{k}\frac{(x'-x)^{2k+3}}{\left[\sqrt{(x-x')^2+(y-y_0)^2+\left(|z|+H+\frac{2}{\gamma}\right)^2}\right]^{2k+3}}\Bigg|_{x'=\frac{-L}{2}}^{x'=\frac{L}{2}}+ \\ +\frac{(-1)^3}{\gamma^3}\frac{\left[3\left(|z|+H+\frac{2}{\gamma}\right)(y-y_0)^2-2\left(|z|+H+\frac{2}{\gamma}\right)^3\right]}{\left[(y-y_0)^2+\left(|z|+H+\frac{2}{\gamma}\right)^2\right]^3}\sum_{k=0}^{2}\frac{(-1)^k}{2k+1}\binom{2}{k}\frac{(x'-x)^{2k+1}}{\left[\sqrt{(x-x')^2+(y-y_0)^2+\left(|z|+H+\frac{2}{\gamma}\right)^2}\right]^{2k+1}}\Bigg|_{x'=\frac{-L}{2}}^{x=\frac{L}{2}} \end{array}\right\} \quad (10)$$

Also in this case, all the mathematical passages leading from (8) to (10) have been omitted for brevity.

The p.u.l. mutual impedance between the overhead wire with earth return and a buried parallel wire with earth return evaluated in the generic point *(x, y, z)* belonging to the wire axis is defined by:

$$Z_m(x,y,z) = \frac{E_{2x}^{ind}(x,y,z)}{I} =$$

$$\frac{j\omega\mu_0}{4\pi}\left\{\begin{array}{l} \ln\left(\frac{\frac{L}{2}-x+\sqrt{\left(\frac{L}{2}-x\right)^2+(y-y_0)^2+(|z|+H)^2}}{-\left(\frac{L}{2}+x\right)+\sqrt{\left(\frac{L}{2}+x\right)^2+(y-y_0)^2+(|z|+H)^2}}\right)+ \\ +\ln\left(\frac{\frac{L}{2}-x+\sqrt{\left(\frac{L}{2}-x\right)^2+(y-y_0)^2+\left(|z|+H+\frac{2}{\gamma}\right)^2}}{-\left(\frac{L}{2}+x\right)+\sqrt{\left(\frac{L}{2}+x\right)^2+(y-y_0)^2+\left(|z|+H+\frac{2}{\gamma}\right)^2}}\right)+ \\ +\frac{(-1)^3}{\gamma^3}\frac{3\left(|z|+H+\frac{2}{\gamma}\right)}{\left[(y-y_0)^2+\left(|z|+H+\frac{2}{\gamma}\right)^2\right]^2}\sum_{k=0}^{1}\frac{(-1)^k}{2k+3}\binom{1}{k}\frac{(x'-x)^{2k+3}}{\left[\sqrt{(x-x')^2+(y-y_0)^2+\left(|z|+H+\frac{2}{\gamma}\right)^2}\right]^{2k+3}}\Bigg|_{x'=\frac{-L}{2}}^{x'=\frac{L}{2}}+ \\ +\frac{(-1)^3}{\gamma^3}\frac{\left[3\left(|z|+H+\frac{2}{\gamma}\right)(y-y_0)^2-2\left(|z|+H+\frac{2}{\gamma}\right)^3\right]}{\left[(y-y_0)^2+\left(|z|+H+\frac{2}{\gamma}\right)^2\right]^3}\sum_{k=0}^{2}\frac{(-1)^k}{2k+1}\binom{2}{k}\frac{(x'-x)^{2k+1}}{\left[\sqrt{(x-x')^2+(y-y_0)^2+\left(|z|+H+\frac{2}{\gamma}\right)^2}\right]^{2k+1}}\Bigg|_{x'=\frac{-L}{2}}^{x=\frac{L}{2}} \end{array}\right\} \quad (11)$$

Thus, from (11) one gets a function $Z_m=Z_m(x, y, z)$ that it is composed by four addends; the first and second addends represent the basic contribution (logarithmic terms) while the third and fourth ones may be considered as additional corrective terms; in particular, it can be interesting to estimate their influence on the results.

To this aim, it is convenient to define the p.u.l. mutual impedance $Z_m'=Z_m'(x, y,z)$ without additional terms, i.e.:

$$Z'_m(x,y,z)=\frac{j\omega\mu_0 I}{4\pi}\left\{\begin{array}{l}\ln\left(\dfrac{\frac{L}{2}-x+\sqrt{\left(\frac{L}{2}-x\right)^2+(y-y_0)^2+(|z|+H)^2}}{-\left(\frac{L}{2}+x\right)+\sqrt{\left(\frac{L}{2}+x\right)^2+(y-y_0)^2+(|z|+H)^2}}\right)+\\ -\ln\left(\dfrac{\frac{L}{2}-x+\sqrt{\left(\frac{L}{2}-x\right)^2+(y-y_0)^2+\left(|z|+H+\frac{2}{\gamma}\right)^2}}{-\left(\frac{L}{2}+x\right)+\sqrt{\left(\frac{L}{2}+x\right)^2+(y-y_0)^2+\left(|z|+H+\frac{2}{\gamma}\right)^2}}\right)\end{array}\right\} \tag{12}$$

Note that formula (12) is obtained by considering only the first addend, inside square brackets, in formula (7).

3. COMPARISON BETWEEN THE MUTUAL IMPEDANCE FORMULAS

In order to calculate the influence of the corrective terms, it is useful to define the following quantities:

$$\Delta Z_{m\,\%}(x,y,z)=\frac{|Z_m(x,y,z)|-|Z'_m(x,y,z)|}{|Z_m(x,y,z)|}100 \tag{13}$$

$$\Delta\phi(x,y,z)=arg\big(Z_m(x,y,z)\big)-arg\big(Z'_m(x,y,z)\big) \tag{14}$$

Being $\Delta Z_{m\%}$ the per cent relative difference between the modulus of Z_m and Z_m' while $\Delta\phi$ is the difference between their arguments.

It is convenient to express the results by means of polar plots being the polar radius $R=R(x, y)$ given by the formula:

$$R(x,y)=\sqrt{x^2+(y-y_0)^2} \tag{15}$$

The polar plots that follow have been obtained for $y_0 = 0$, $H = 20$m, and $h_{pipe} = -1.5$m (typical burial depth of a pipeline), $L = 250$m (typical distance between two consecutive towers for a High Voltage power line) and the polar angle is counter-clockwise measured starting from the positive x semi-axis. They have been drawn for different values of soil

conductivity and in correspondence of different values for the polar radius R, i.e.: $\delta/100$, $\delta/10$, $\delta/2$, δ, 2δ, 3δ, 5δ. Being δ the skin depth in the earth at the frequency f = 50Hz.

For convenience, the formula for the skin depth in the earth is reported:

$$\delta = \frac{1}{\sqrt{\pi f \mu_2 \sigma_2}} \tag{16}$$

Figures 2-4 show the polar plots of $\Delta Z_{m\%}$ and $\Delta\phi$ evaluated for different values of soil conductivity and it can be noticed that:

- The per cent relative difference $\Delta Z_{m\%}$ ranges approximatively in the interval [-20%, 25%]
- The difference $\Delta\phi$ ranges approximatively in the interval [-3^0, 13^0]

These differences occur essentially in the range [$\delta/2$, 3δ] for the polar radius while, on the contrary they are negligible outside that range. Therefore, one has:

- if $R << \delta$ or $R >> \delta$, then the use of Z_m or Z_m' is essentially equivalent
- on the contrary, when $R \sim \delta$, a certain not negligible difference between Z_m and Z_m' can be noticed.

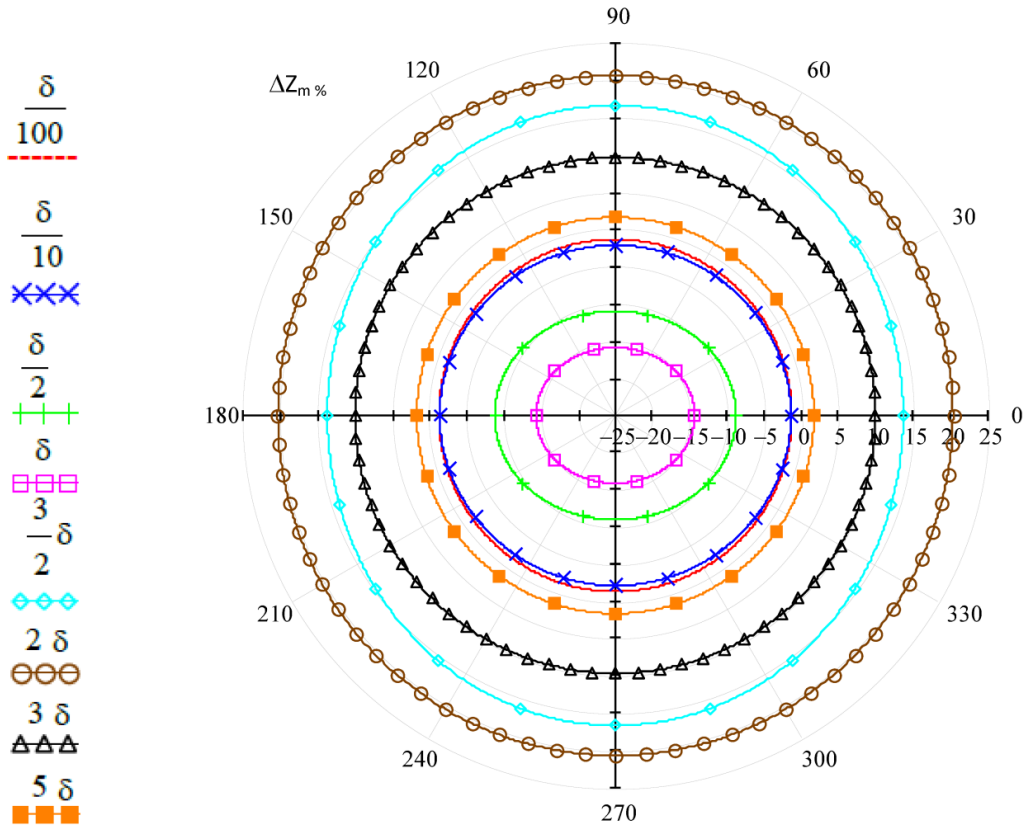

Fig. 2a. Polar plot of $\Delta Z_{m\%}$ for different values of polar radius; $\sigma_2 = 2 \cdot 10^{-2}$ S/m

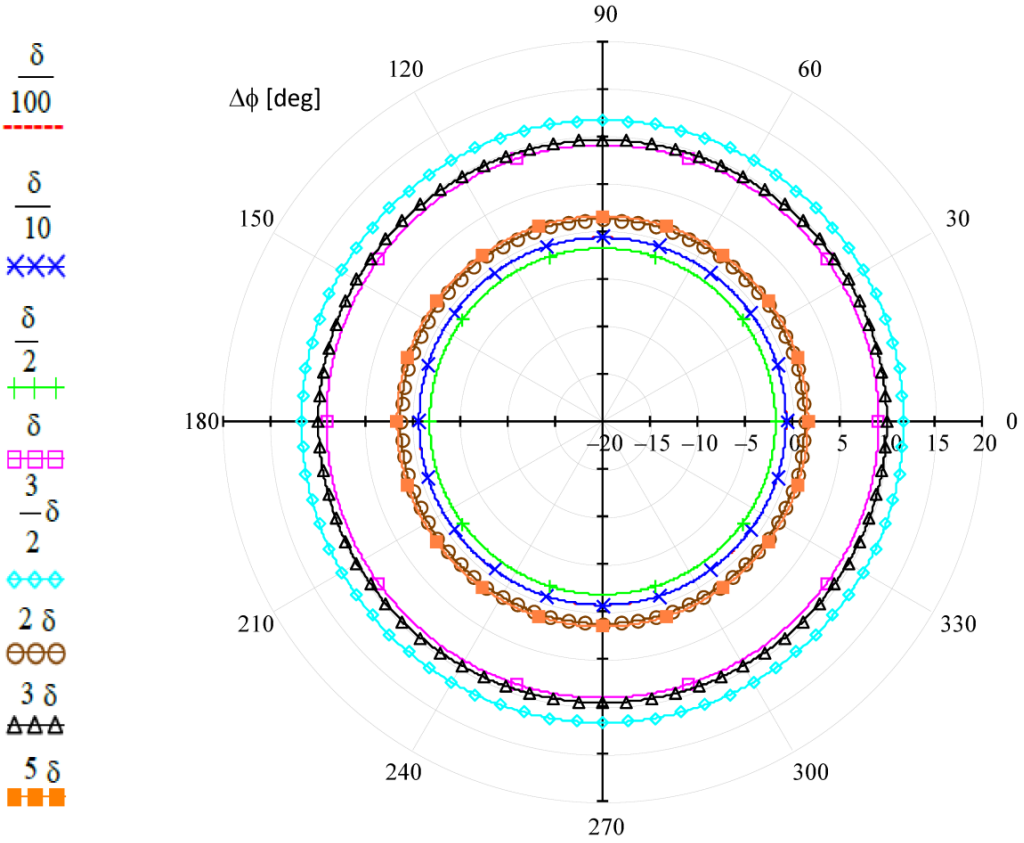

Fig. 2b. Polar plot of $\Delta\phi$ for different values of polar radius; $\sigma_2=2\cdot10^{-2}$S/m

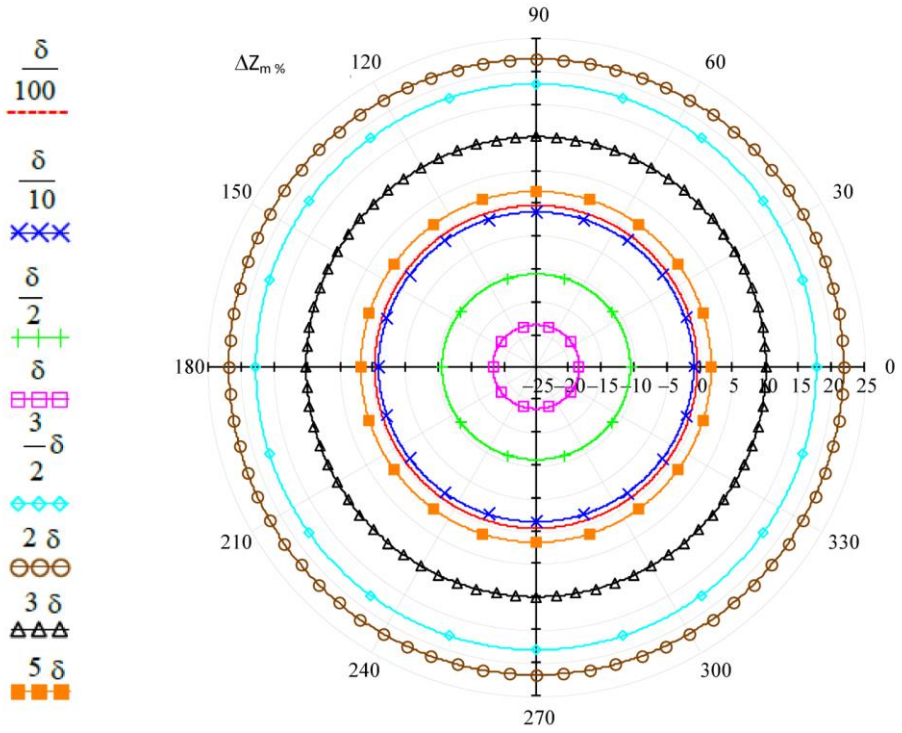

Fig. 3a. Polar plot of $\Delta Z_{m\%}$ for different values of polar radius; $\sigma_2=2\cdot10^{-3}$S/m

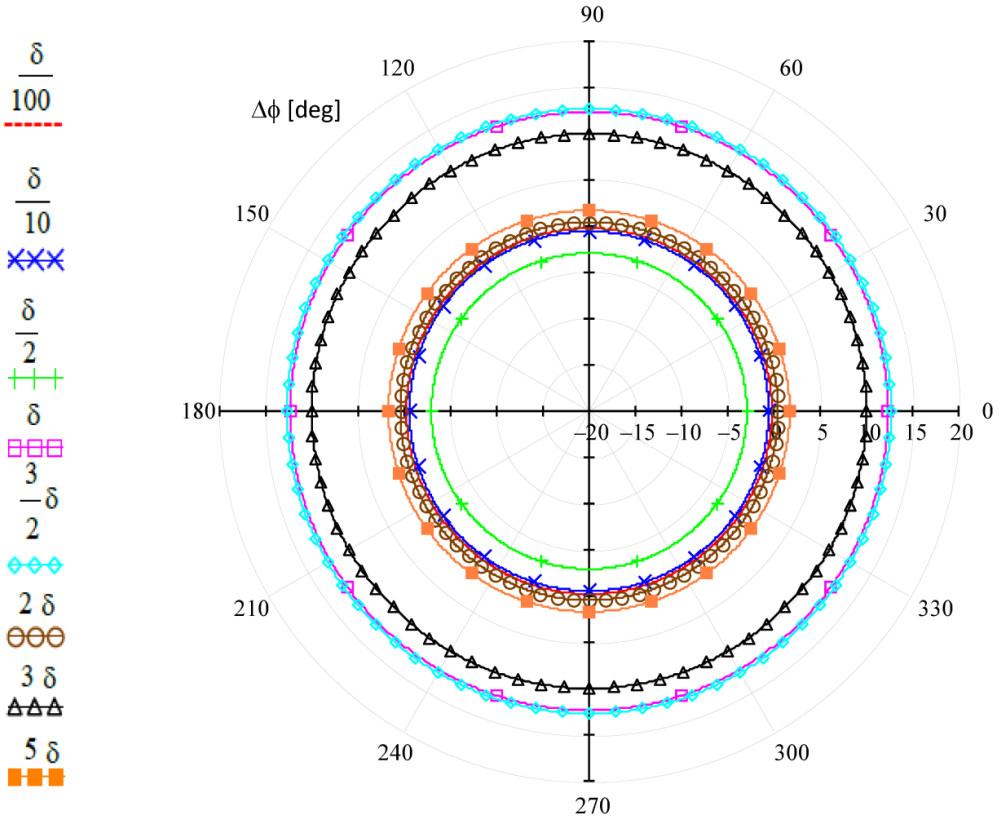

Fig. 3b. Polar plot of $\Delta\phi$ for different values of polar radius; $\sigma_2=2\cdot10^{-3}$S/m

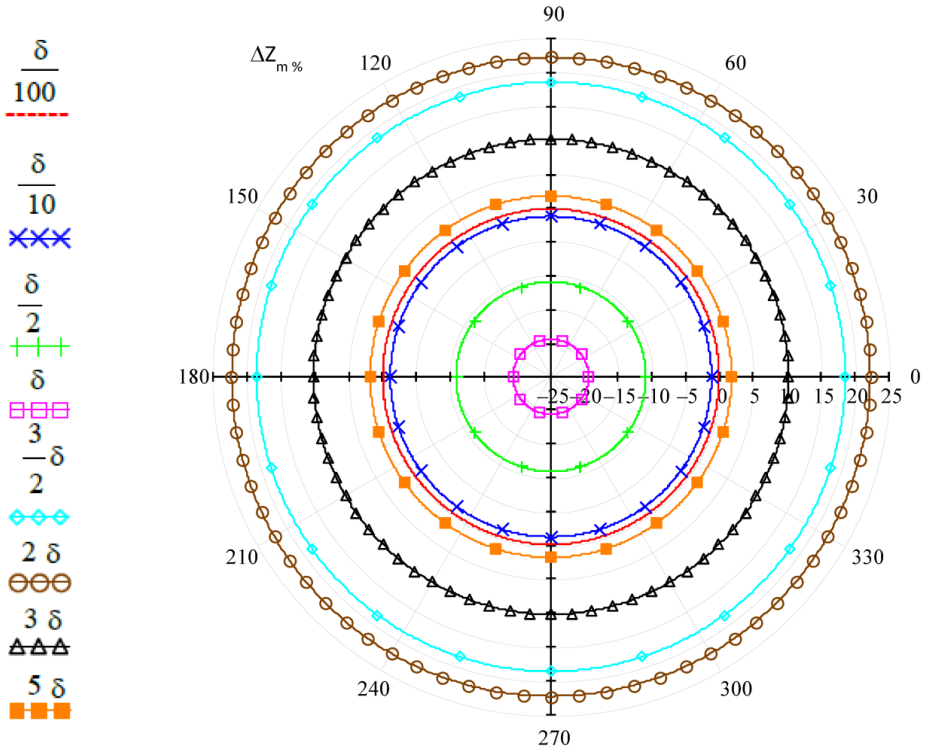

Fig. 4a. Polar plot of $\Delta Z_{m\%}$ for different values of polar radius; $\sigma_2=2\cdot10^{-4}$S/m

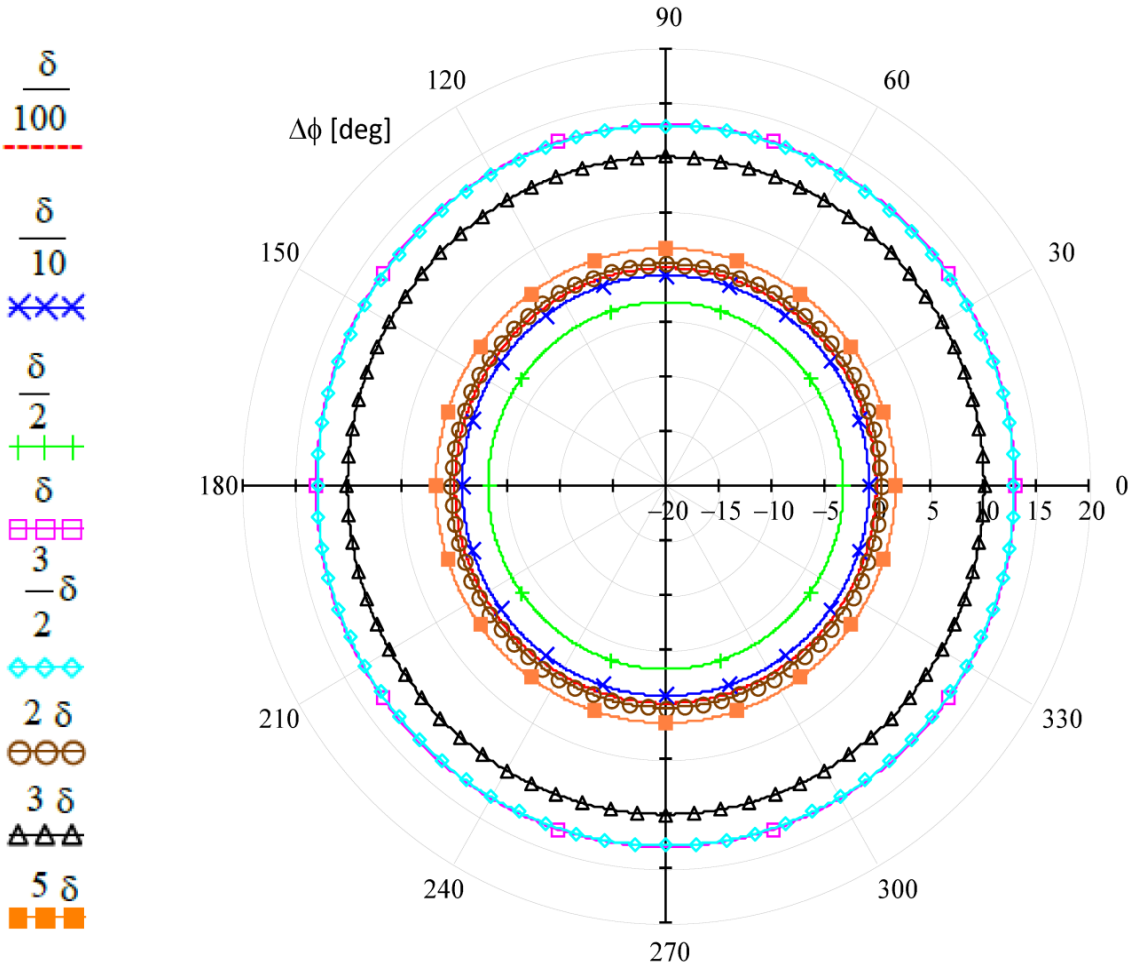

Fig. 4b. Polar plot of $\Delta\phi$ for different values of polar radius; $\sigma_2=2\cdot10^{-4}$S/m

4. INFLUENCE OF ADDITIONAL TERMS IN INTERFERENCE CALCULATIONS

A typical and straightforward application of the proposed formulas consists in evaluating the p.u.l. electromotive force (emf) induced on a pipeline-earth circuit under the inductive influence of nearby power lines and then calculating the induced voltage and current on the circuit itself.

Thus, it is interesting to check the influence in using Z_m' instead of Z_m when calculating induced voltage and current on a buried pipeline subjected to the 50Hz inductive coupling from a power line. To this purpose, a simple example consisting of a parallelism between an overhead power line conductor 10km long and a pipeline 5km long is considered. See *fig.5* for a simple sketch. The power line conductor-earth circuit carries a constant inducing current I_{pl} while the pipe-earth circuit is closed at its boundaries on the characteristic impedance.

By treating the pipeline-earth circuit as a transmission line circuit, the influence of the electromagnetic field produced by the power line is modelled by a p.u.l. distributed emf generator applied along the pipeline-earth circuit. In the present example, being inducing and induced line parallel, such a generator is related to the above defined p.u.l. mutual impedances respectively by:

$$e(x) = Z_m(x, D)I_{pl} \qquad e'(x) = Z'_m(x, D)I_{pl} \tag{17}$$

The theory and the formulas for evaluating induced voltage and current on a transmission line circuit under the influence of external electromagnetic fields can be found in [19] and to it one can refer for details.

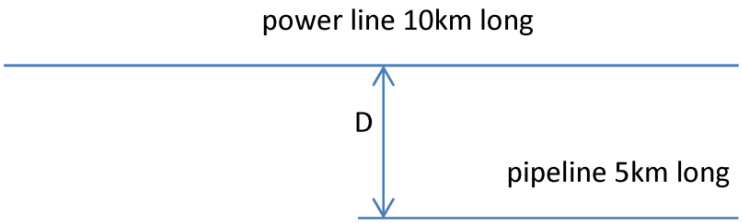

Fig. 5. Sketch of power line and pipeline layouts

In order to compare the results, it is worthwhile to define the following quantities:

- *U(x)* and *I(x)* induced voltage and current obtained when applying the generator *e(x)* to the pipeline-earth circuit
- *U'(x)* and *I'(x)* induced voltage and current obtained when applying the generator *e'(x)* to the pipeline-earth circuit
- *ΔU%(x)* the per cent relative difference relevant to the voltage that is:

$$\Delta U_{\%}(x) = \frac{|U(x)| - |U'(x)|}{|U(x)|} 100 \tag{18}$$

- *ΔI%(x)* the per cent relative difference relevant to the current that is:

$$\Delta I_{\%}(x) = \frac{|I(x)| - |I'(x)|}{|I(x)|} 100 \tag{19}$$

In *figures 6-8* the quantities $\Delta U_{\%}(x)$ and $\Delta I_{\%}(x)$ have been plotted versus pipeline progressive for different values of soil conductivity and in correspondence of different values for the lateral distance *D* (see *fig. 5*) between inducing and induced circuit i.e.: $\delta/100$, $\delta/10$, $\delta/2$, δ, 2δ, 3δ, 5δ.

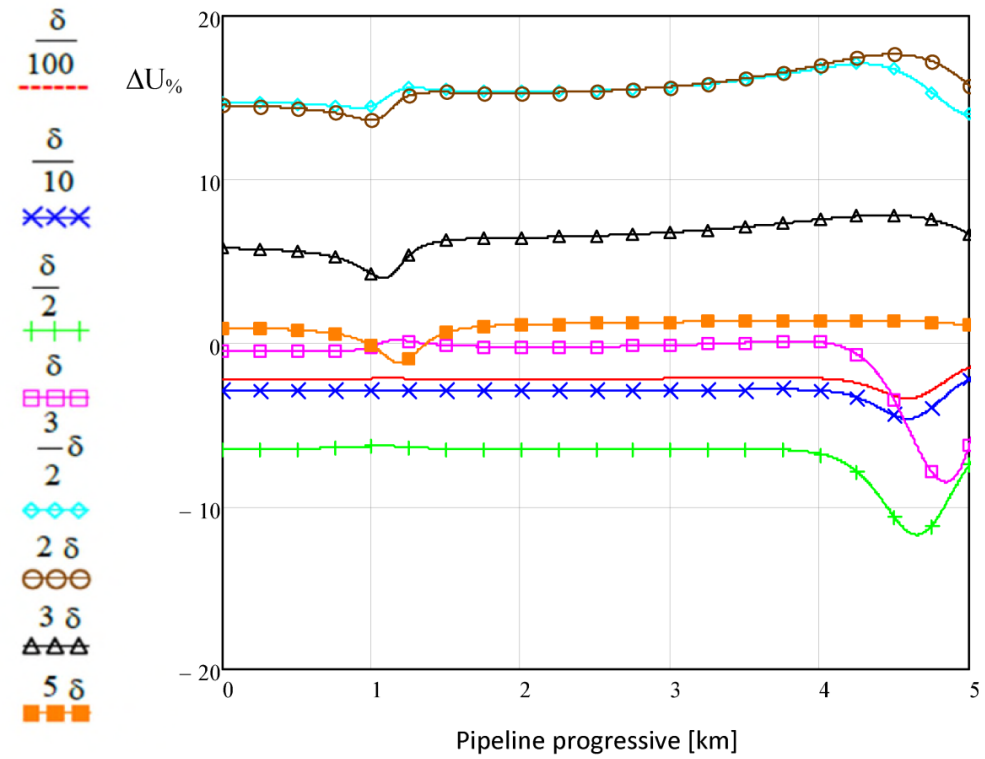

Fig. 6a. $\Delta U_{\%}$ versus pipeline progressive for different values of D; $\sigma_2=2\cdot10^{-2}$S/m

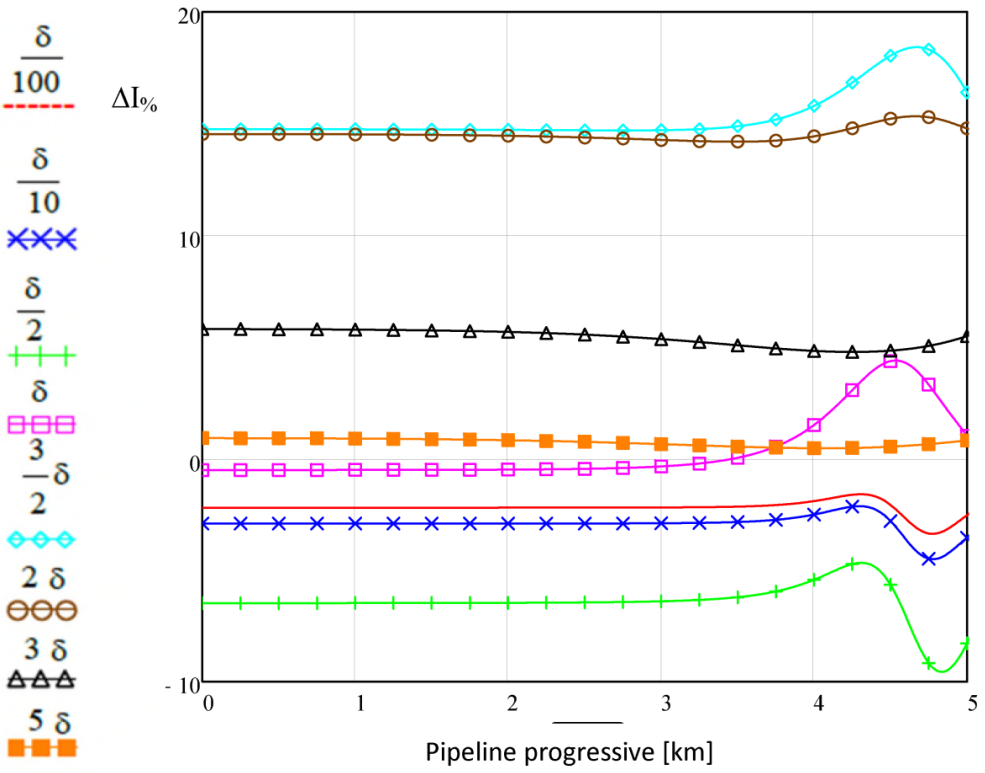

Fig. 6b. $\Delta I_{\%}$ versus pipeline progressive for different values of D; $\sigma_2=2\cdot10^{-2}$S/m

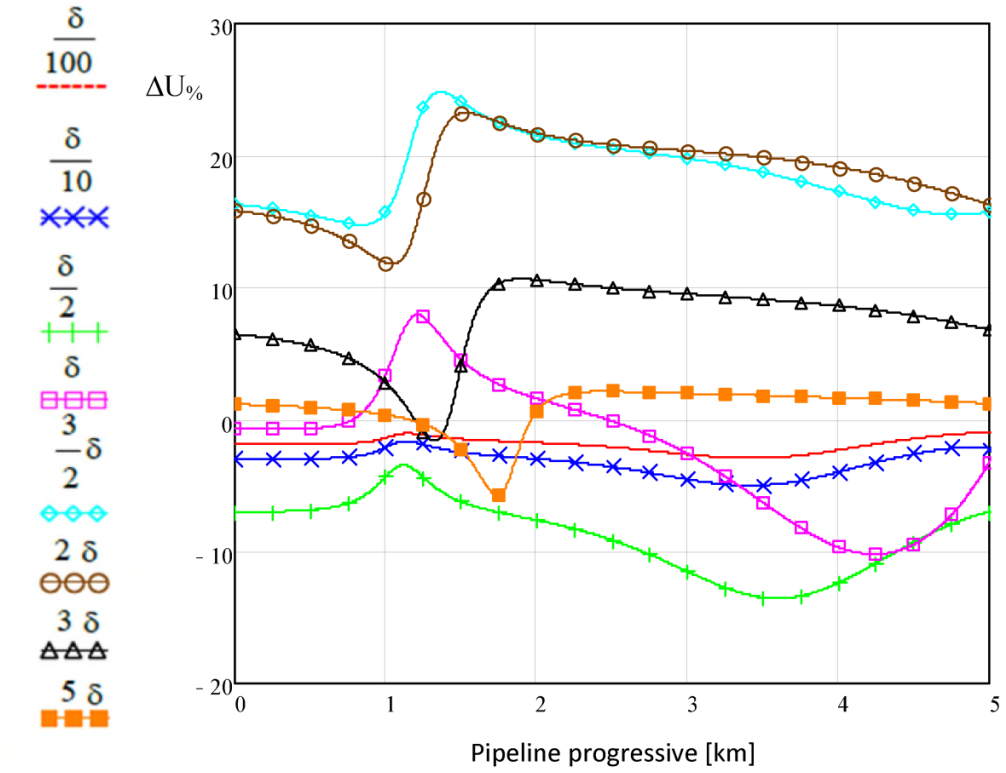

Fig. 7a. $\Delta U_{\%}$ versus pipeline progressive for different values of D; $\sigma_2=2\cdot10^{-3}$S/m

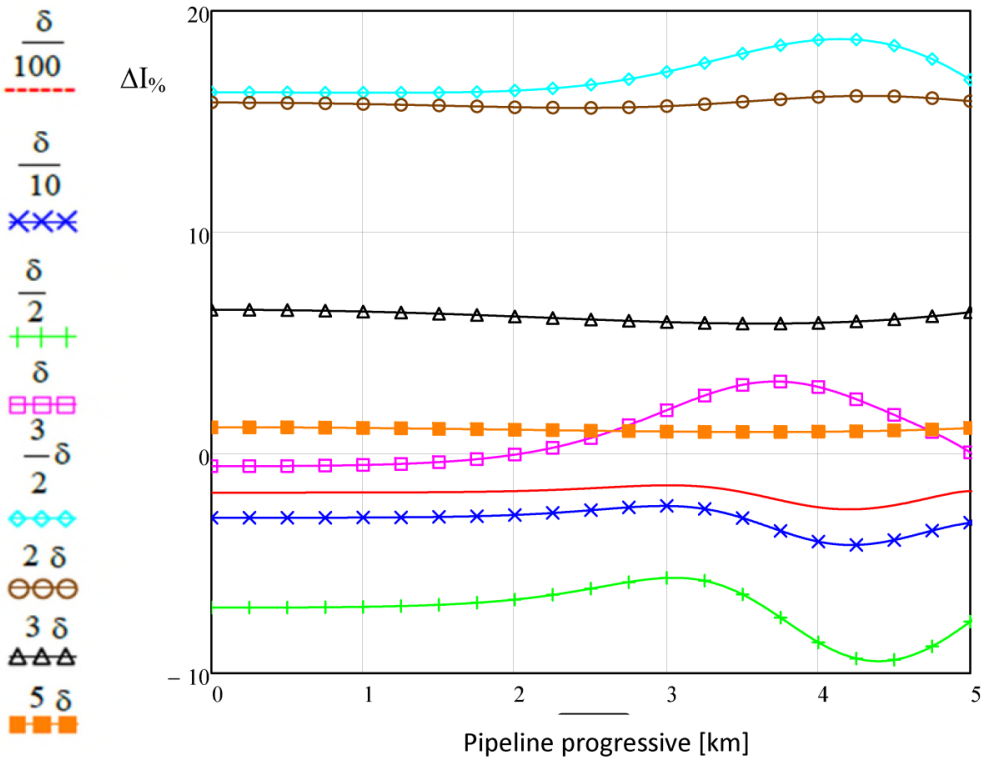

Fig. 7b. $\Delta I_{\%}$ versus pipeline progressive for different values of D; $\sigma_2=2\cdot10^{-3}$S/m

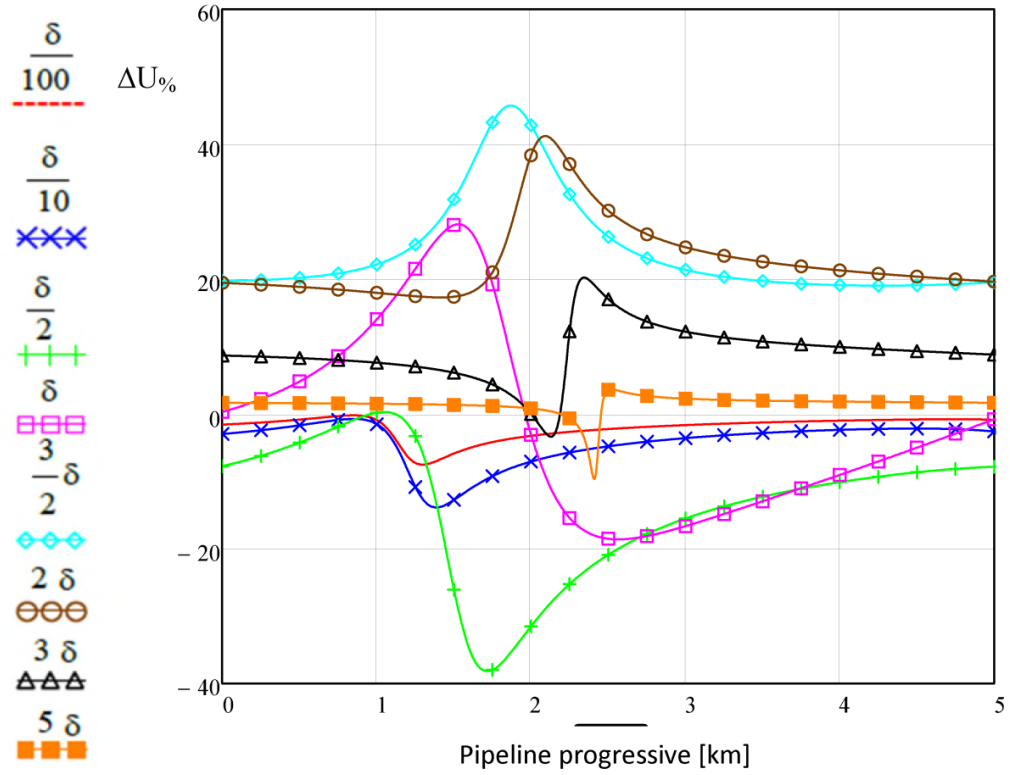

Fig. 8a. $\Delta U_{\%}$ versus pipeline progressive for different values of D; $\sigma_2=2\cdot10^{-4}$S/m

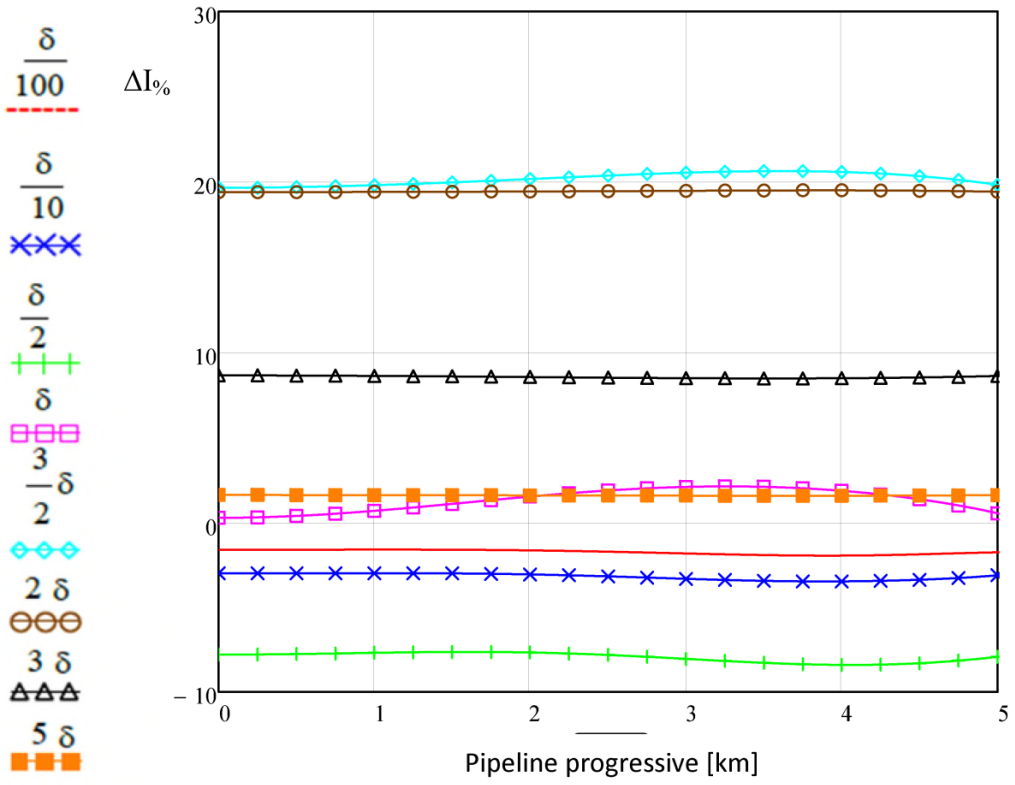

Fig. 8b. $\Delta I_{\%}$ versus pipeline progressive for different values of D; $\sigma_2=2\cdot10^{-4}$S/m

Figures 6-8 show that, in case of parallelism between power line and pipeline, depending on the lateral distance *D* and on the earth conductivity, the relative per cent difference in evaluating the interference results by using formula (10) or (11) can range approximatively:

- in the interval [-40%, 40%] for the induced voltage
- in the interval [-10%, 20%] for the induced current

Hence, in certain specific cases, depending on the lateral distance between power line and pipeline and especially with soil having low-medium conductivity, not negligible differences in using Z_m' instead of Z_m can be found when calculating induced voltage and current.

Furthermore, it is useful to notice that in [4] it is shown that the results obtained by using Z_m are consistent with the ones coming from the application of the formulas reported in [9] and [11].

The main advantage in using formulas (11) or (12) instead of the ones given in References [9-13] which are based on Neumann integrals, consists in their greater simplicity and in an easier evaluation of the induced emf on the pipeline-earth circuit.

5. CONCLUSIONS

In this paper two new and convenient closed form formulas for evaluating, in the ELF range, the p.u.l. mutual impedance between an overhead finite length wire and a buried wire, both with earth return, are proposed. The two different formulas yield values having per cent relative differences in the range [-20%, 25%].

Moreover, when evaluating the interference on the victim circuit (i.e. induced voltage and current), the use of the formula without corrective terms instead of the one with corrective terms may lead, in specific cases, to not negligible differences in the results. Thus, in applications, it is preferable to use the formula (12) instead of (11).

REFERENCES

[1] CIGRE, *Guide on the influence of High Voltage AC Power Systems on Metallic Pipelines,* Publication n. 95, 1995.

[2] CIGRE, *AC Corrosion on metallic pipelines due to interference froma AC power lines-Phenomenon modelling and countermeasures,* Publication n. 290, 2006.

[3] J. R. Carson, *Wave Propagation in Overhead Wires with Ground Return*, Bell System Technical Journal, Vol.5, p. 539-554, 1926.

[4] G. Lucca, *Different approaches in calculating AC inductive interference from power lines on*

pipelines, IET Science, Measurements & Technology, vol. 12, 2018.

[5] A. Cristofolini, A. Popoli, L. Sandrolini, *A comparison between Carson's formulae and a 2D FEM approach for the evaluation of AC interference caused by overhead power lines on buried metallic pipelines*, Prog. Electromagn. Res. C, vol.79, p.39-48, 2017.

[6] G. C. Christoforidis, D. P. Labridis, P. S. Dokopoulos: *A Hybrid Method for Calculating the Inductive Interference Caused by Faulted Power Lines to Nearby Buried Pipelines*, IEEE Trans. on Power Deliv., vol. 20, pp.1465-1473, 2005.

[7] D. D Micu, L. Czumbil, G. Christoforidis , A. Ceclan: *Layer Recurrent Neural Network Solution for an Electromagnetic Interference Problem* , IEEE Trans on Magnetics, vol. **47**, pp. 1410-1413, 2011.

[8] D. D Micu, L. Czumbil, G. Christoforidis : *AC interference on pipelines due to double circuit power lines: A detailed study*, Electric Power Systems Research, Vol. 103, pp. 1-8, 2013.

[9] R. M. Foster, *Mutual Impedance of Grounded Wires Lying on the Surface of the Earth*, Bell System Technical Journal, Vol.10, p. 408-419, 1931.

[10] R. M. Foster, *Mutual Impedance of Grounded Wires Lying on or Above the Surface of the Earth*, Bell System Technical Journal, Vol.12, p. 264-287, 1933.

[11] E. D. Sunde, *Earth Conduction Effects in Transmission System*, D. Van Nostrand Company Inc., 1949.

[12] L. J. Lacey, *The mutual impedance of earth-return circuits*, Proc. of the I.E.E., Vol. 99, Part IV, p. 156-167, 1952.

[13] M. V. Kostenko, K. E. Mihailov, E. L. Portinov, L. G. Pozdnjakov, V. B. Sokolov, I. M. Zarkhi, *Resistive and Inductive Interference on Communication Lines Entering Large Power Plants*, CIGRE Session 36-02, Paris, France, 1970.

[14] ITU, *Directives concerning the protection of telecommunication lines against harmful effects from electric power and electrified railway lines*, Vol. II: *Calculating induced voltages and currents in practical cases*, ITU, Geneva, 1999.

[15] P. R. Bannister, *Summary of Image Theory Expressions for the Quasi-Static Fields of Antennas at or Above the Earth's Surface*, Proceedings of the IEEE, vol.67, No. 7, p. 1001-1008, July 1979.

[16] J. R. Wait , *The electromagnetic fields of a horizontal dipole in the presence of a conducting half-space*, Canadian Journal of Physics, vol. 39, p. 1017-1028, 1961.

[17] J. R. Wait, K. P. Spies, *On the image representation of the quasi-static fields of a line current source above the ground*, Canadian Journal of Physics, vol. 47, p. 2731-2733, 1969.

[18] I. S. Gradshteyn, I. M. Ryzhik, *Table of Integrals, Series, and Products* Seventh Edition, Elsevier, 2007.

[19] ITU, *Directives concerning the protection of telecommunication lines against harmful effects from electric power and electrified railway lines*, Vol. III: *Capacitive, inductive and conductive coupling: physical theory and calculation methods*, ITU, Geneva, 1989.

ELECTRICITY CONSERVATION AND SAFETY AWARENESS AMONG SENIOR HIGH SCHOOL STUDENTS

Emmanuel Asuming **FRIMPONG**, Elvis **TWUMASI**
Department of Electrical and Electronic Engineering, Kwame Nkrumah University of Science and Technology, Kumasi, Ghana
eafrimpong.soe@knust.edu.gh, elvistwumasi@gmail.com

Keywords: energy conservation, energy efficiency, electric safety

Abstract*:* Awareness of conservation and safety issues regarding electrical energy use among students is critical. This study has determined the level of electricity conservation and safety awareness among senior high school students in the Ashanti Region of Ghana. The study was carried out through the administration of questionnaires to eight hundred and eighty-three students in five selected schools in the study region. The study assessed awareness levels based on gender, programme of study and academic study level. The questionnaires were developed to establish student's knowledge of specific energy conservation practices relating to various consumer appliances, their motivation or otherwise to support institutional efforts to reduce energy consumption as well as their awareness of specific issues regarding electric shocks and electric fires. Analysis of the administered questionnaires point to the fact that a very high percentage of the students in all the three categories considered are aware of most of the issues presented to them. Also, a high percentage of them are inclined towards factors that motivate energy savings. Of the categories evaluated, females, students in the first level of study, and those studying Home Economics had the highest average awareness levels. The findings of this study will be very useful for educational campaigns concerning electricity use.

1. INTRODUCTION

Electric energy is of much importance to the world. Notwithstanding the huge benefits of electric energy, the lack of adherence to basic rules associated with electricity use has caused many adverse effects including electric shocks and electric fires. Additionally, inefficient use of electric energy has dire financial consequences. Therefore, electrical energy

conservation and electric safety awareness is of utmost importance in all areas of electricity usage; be it residential, educational, commercial or industrial. Educational institutions are of great concern when it comes to safe and efficient utilization of electricity because they bring together hundreds and thousands of individuals from diverse backgrounds [1]. The lack of awareness of energy saving measures and electrical safety amongst students can spell doom for educational institutions.

Efficient lighting control through behavioural change, including the use of efficient daylighting strategies alone, has the potential of reducing electrical energy consumption of educational institutions by up to 30% [2]. On a wider scale, energy efficiency and conservation awareness in schools can curb the need for expanded generation capacity. Moreover, electrical safety awareness among students would help to reduce the hazards due to electric shocks and electric fires. It is reported that most of the fire outbreaks in schools occur due to the misuse of electricity by students [3]. Students are found of engaging in unsafe activities such as overloading extension cables, using frayed cables or exposed conductors and connecting appliance cables directly to sockets without using plugs [4].

The issues highlighted above necessitate awareness of the right use of electric energy among students [5]. Of importance in this awareness drive are students in the second cycle institutions. This is partly because of their inexperience and the fact that several of them are housed in one dormitory. Furthermore, in developing countries with high illiteracy levels, many young students may be the only literates in their families. Therefore, their acquisition of sound knowledge in electric energy utilization will go a long way towards the enlightenment of their families in efficient and safe electric energy use. The more knowledgeable people are, the more interested they are in adopting energy saving practices and in participating in energy saving policies and programmes [6].

Efforts toward educating young students are bound to fail if they are not based on knowledge of their current levels of awareness of energy conservation and electric safety issues. Knowledge of their level of awareness will determine the issues to stress on as well as the overall approach to use. Thus, there is the need for research into the electric energy conservation and electric safety perspective of students in secondary schools. Most published journal articles about electric energy awareness among secondary school students have focused on awareness on renewable energy sources [7]. Only few research works have been published in electric energy efficiency, electric energy conservation, and electric safety awareness among students of secondary schools. The prominent work amongst the few is the work presented in [5]. The work in [5] determined the level of awareness of secondary school students in the Aegean region of Turkey with regards to renewable energy sources and energy saving. The study concluded that the 400 hundred students interviewed had a high level of awareness about renewable energy sources and energy saving. The study however failed to evaluate the levels of awareness of the students on specific energy saving activities, which is critical for any education. Furthermore, electric safety issues were not considered.

This study therefore sought to address this knowledge gap. It among others determined the level of awareness of secondary school students about electric safety, energy efficiency and specific energy saving activities. The study was conducted by administering questionnaires to senior high school (formally called senior secondary school) students in the Ashanti Region of Ghana. The questionnaires asked various questions that required students to indicate their knowledge of specific energy efficiency and energy conservation measures related to various consumer loads. Their current level of engagement in energy conservation was also determined. Their willingness to engage in energy savings was also assessed. The reasons for their willingness or the lack of it was also determined. Again, their knowledge about electric safety was established. The findings presented will inform the specific issues to place greater emphasis on when educating students in secondary schools about safe and effective use of electricity, to ensure desired outcomes.

2. METHODOLOGY

The study was done by administering questionnaires to the target group. The target group was senior high school students in the Ashanti Region of Ghana. Schools in the Ashanti Region admit students from diverse social, ethnic, cultural, religious and economic backgrounds. The questions were administered to students in five senior high schools. One of the schools admits only male students, one admits only female students while the remaining three are mixed schools. The questionnaires were distributed to eight hundred and eighty-three (883) students, in a controlled environment (that is in their classrooms). This ensured that all distributed questionnaires were completed and returned. The administration of the questionnaires was largely supervised by the teachers of the schools. Explanations were offered to students who had difficulty understanding any of the questions asked. In all, four hundred and sixty-one (461) males and four hundred and twenty-two (422) females participated in the survey. The questionnaires were carefully distributed to capture students studying various programmes and at different study levels. The programmes covered were Business, General Arts, Home Economics, Science and Visual Arts. Senior High Schools in Ghana have three study levels namely, SHS1, SHS2 and SHS3. SHS3 is the highest level. The study covered male and female students studying the various programmes at all the different levels. Table 1 shows details of the socio-demographic characteristics of students that were involved in the study.

The questionnaires were designed to draw the following information from the students: (i) their energy efficiency awareness about various consumer loads including lighting, electronic devices, heating appliances and refrigerators (ii) their knowledge and application of appliance ratings and energy efficiency labels, (iii) their current engagement in energy saving practices, (iv) their motivation or otherwise to embark on energy conservation,

(v) their awareness of the causes of electric shocks and electric fires, and (vi) their knowledge of preventive measures against electric shocks and electric fires. Before the mass distribution of the questionnaires, a pretest was done in one of the schools to ascertain the suitability, reliability and validity of the questionnaires.

Table 1. Socio-demographic characteristics of students

		Number	*Percentage(%)*
Gender	Male	461	52.2
	Female	422	47.8
Programme	Business	148	16.8
	General Arts	285	32.3
	Home economics	161	18.2
	Science	180	20.4
	Visual Arts	109	12.3
Level	SHS1	235	26.6
	SHS2	365	41.3
	SHS3	283	32.0

3. RESULTS AND ANALYSIS

The analysis of the collected data was done using the Statistical Package for Social Sciences (SPSS) software. The descriptive statistics model in SPSS was employed to summarize the data into figures, tables and charts. It is worth noting that a few of the questions were not answered by some of the students. For example, whereas all 283 SHS3 students answered the question relating to their awareness of energy saving by not overloading refrigerators, a slightly reduced number of 281 gave responses to knowledge of the fact that allowing hot food to cool before putting them in refrigerators saves energy. The reason for this is unknown since it was not possible to identify and interview the students who did not answer those questions. The sub-sections that follow discusses the results obtained.

3.1. Energy efficiency awareness in the use of refrigerators

It was determined whether the students knew that energy will be saved if the following are done: refrigerators are not overloaded, foods are made to cool before being put in refrigerators, refrigerator doors are kept closed, adequate ventilation is provided around refrigerators to facilitate heat transfer, and freezer compartments are regularly defrosted.

Figure 1 summarizes the levels of awareness of students based on gender. Three hundred and eighty-five males representing 84.5% of the male respondents indicated awareness of the fact that energy is saved by not overloading refrigerators. For the females, 84.6% knew that energy is saved when refrigerators are not overloaded. With regards to the issue of allowing hot food to cool before being put in refrigerators, 86.1% of the males indicated awareness of this while a higher percentage of 93.1% of the females indicated knowledge of this fact. Nearly ninety-four percent (93.7%) of the males indicated knowledge of the fact that keeping refrigerator doors closed save energy while 97.6% of their female counterparts also indicated awareness of this. A rather low percentage of 66.2% of the males knew that, to conserve energy, adequate ventilation must be provided around refrigerators. Similarly, 63.0% of the females had knowledge of this fact. Lastly, only 56.4% of the males knew that defrosting freezer compartments regularly lead to energy saving while a higher percentage of 62.6% of the females knew this. Both male and female students showed very high levels of awareness in saving energy by not overloading refrigerators and not putting hot foods in them. However, the same cannot be said of their levels of awareness when it comes to positioning refrigerators and defrosting freezers to reduce electricity consumption. Their levels of awareness in these latter areas are relatively low. Averagely, the female students have higher level of awareness than their male counterparts.

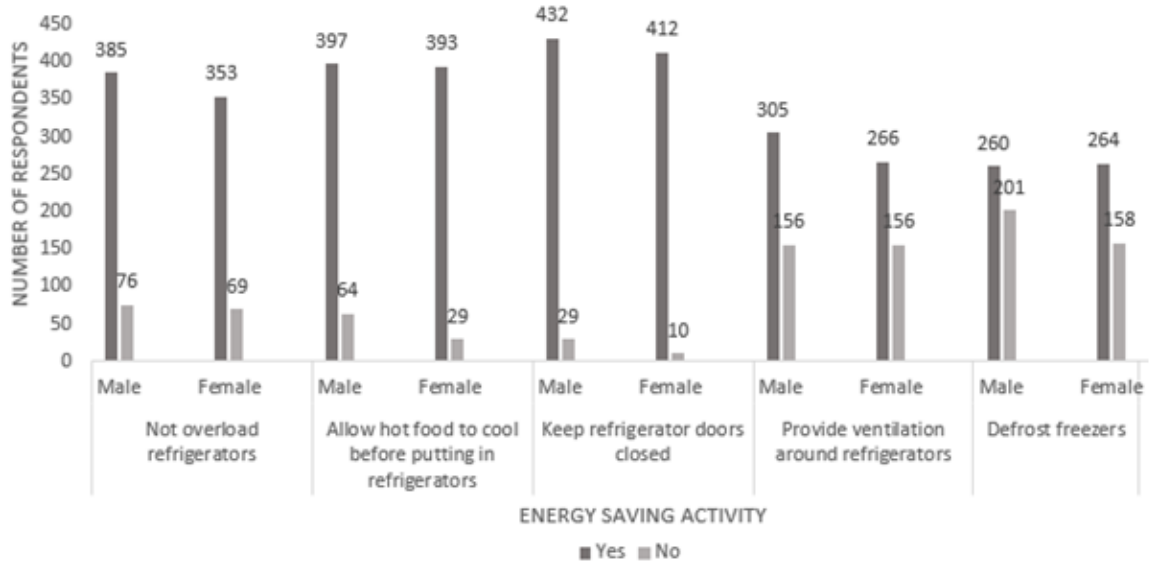

Fig. 1: Awareness in the use of refrigerators based on gender

Figure 2 shows the awareness levels for energy saving issues regarding the use of refrigerators, based on the study levels. The percentages of SHS1, SHS2 and SHS3 students who knew that energy is saved when refrigerators are not overloaded are 91.1%, 80.5% and 81.3% respectively. With regards to awareness of the fact that allowing hot foods to cool before putting them in refrigerators is energy saving, the percentages that answered in the affirmative are 89.4%, 91.0% and 88.3% for SHS1, SHS2 and SHS3 respectively. In terms of

energy saving awareness relating to keeping refrigerator doors closed, 95.3% of SHS1 students, 95.1% of SHS2 students and 96.5% of SHS3 answered yes. The percentages relating to providing enough ventilation around refrigerators to save energy are 69.6%, 61.9% and 64% for SHS1, SHS2 and SHS3 respectively. Pertaining to energy saving due to defrosting freezer compartments, the percentages which indicated awareness are 67.2% for SHS1, 55.3% for SHS2 and 59.6% for SHS3. All study levels demonstrated very high degrees of awareness in the areas assessed except having to provide enough ventilation around refrigerators and defrosting freezes to save energy. Contrary to expectation, the SHS1 students had averagely higher degree of awareness than all other levels. This may be due to some education they had at Junior High School level or during freshmen orientation sessions at the Senior High Schools. Whatever the reason may be, this goes to show that early education yields positive outcomes.

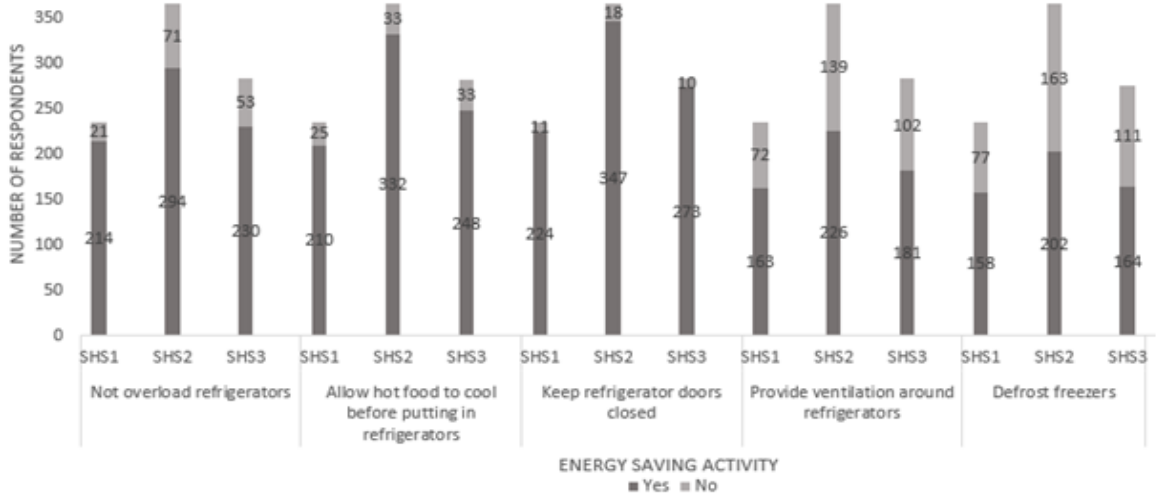

Fig. 2: Awareness in the use of refrigerators based on study level

Figure 3 summarizes the level of awareness of students, based on programme of study. Of the 148 students in the Business programme who gave responses as to whether they were aware that energy is saved when refrigerators are not overloaded, 88.5% indicated awareness. For the same question, the percentages of those who responded in the affirmative for the General Arts, Home Economics, Science and Visual Arts programmes are 78.9%, 87.2%, 83.3% and 86.1% respectively. Regarding knowledge of the fact that allowing hot food to cool before putting them in refrigerators save energy, the percentages that indicated knowledge of this are 82.4% for students studying Business, 91.9% for students studying General Arts, 94.4% for students studying Home Economics, 88.3% for students studying Science and 87.2% for students studying Visual Arts. Almost 97% of the Business students knew that keeping refrigerator doors closed saved energy. Likewise, 95.1% of the General Arts students are aware that keeping refrigerator doors closed is energy saving. The percentages for the other programmes are 96.2%, 97.8 and 91.7% for Home Economics,

Science and Visual Arts respectively. The percentages of Business, General Arts, Home Economics, Science and Visual Arts students who specified awareness of the fact that adequate ventilation must be provided around refrigerators for them to consume less energy are 59.4%, 64.1%, 67.7%, 62.6% and 75.9% respectively. With regards to defrosting freezers to conserve energy, the percentage affirmative responses are 57.0%, 55.7%, 66.5%, 59.8% and 69.4% for Business, General Arts, Home Economics, Science and Visual Arts programmes respectively. The Home Economics students showed the highest average awareness.

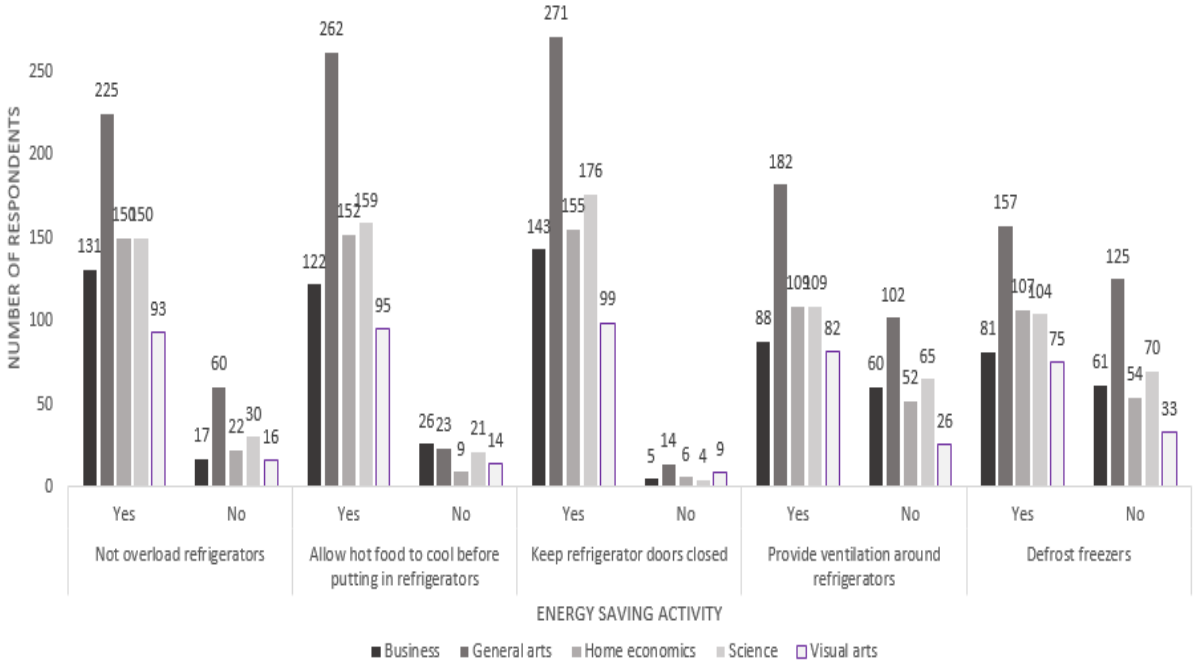

Fig. 3: Awareness in the use of refrigerators based on programme of study

3.2. Energy saving awareness relating to heating loads

Here, students were asked to indicate whether they knew that engaging in the following activities save energy: (i) heating only the required amount of water instead of always filling the kettle, (ii) bathing with cold water instead of warm water where possible, and (iii) ironing clothes in bulk, say over the weekend, instead of ironing daily.

Figure 4 provides details of responses received, based on gender. Approximately 81% of the male students knew that heating only the required amount of water would save energy. For the females, the percentage awareness was 88.6%. Thus, more females than males are aware of this. With regards to bathing with cold water instead of warm water to save energy, the percentage awareness was 64.2% of males and 64.0% of females. In terms of ironing in bulk instead of in bits, the percentages that indicated awareness are 83.1% and 91.0% of

males and females respectively. Here too, the females demonstrated greater awareness than their male counterparts.

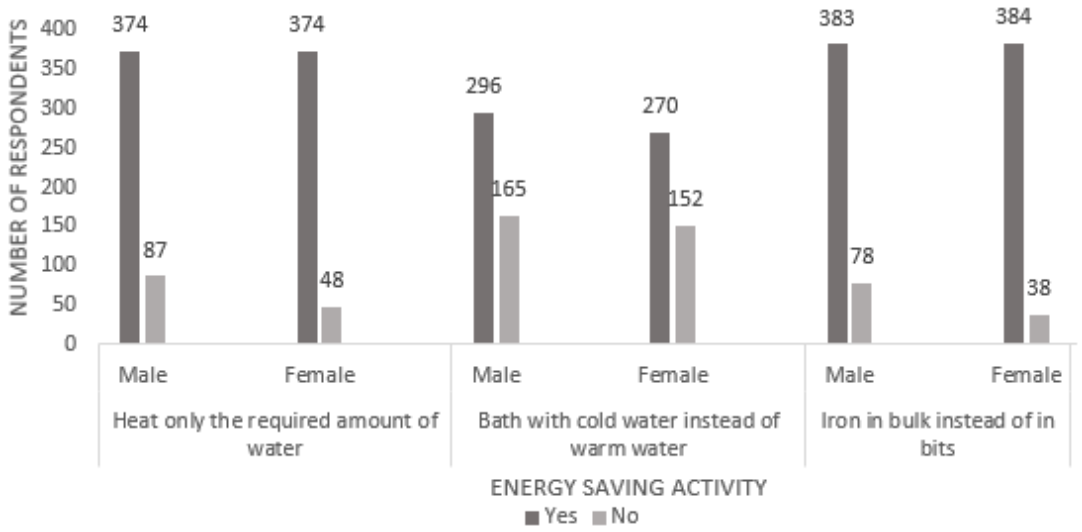

Fig. 4: Awareness in the use of heating loads based on gender

Shown in *figure 5* are the responses, in terms of study level. The percentages for knowing that heating only the required amount of water saves energy are 85.1% for SHS1, 83.8% for SHS2 and 85.5% for SHS3. For energy saving by bathing with cold water instead of heated water, the percentages are 63.4%, 67.7% and 60.1% for SHS1, SHS2 and SHS3 respectively. Lastly, 88.9% of SHS1 students, 83.3% of SHS2 students and 89.8% of SHS three students knew that bulk ironing is energy conserving. Again, the SHS1 students had the highest average percentage awareness.

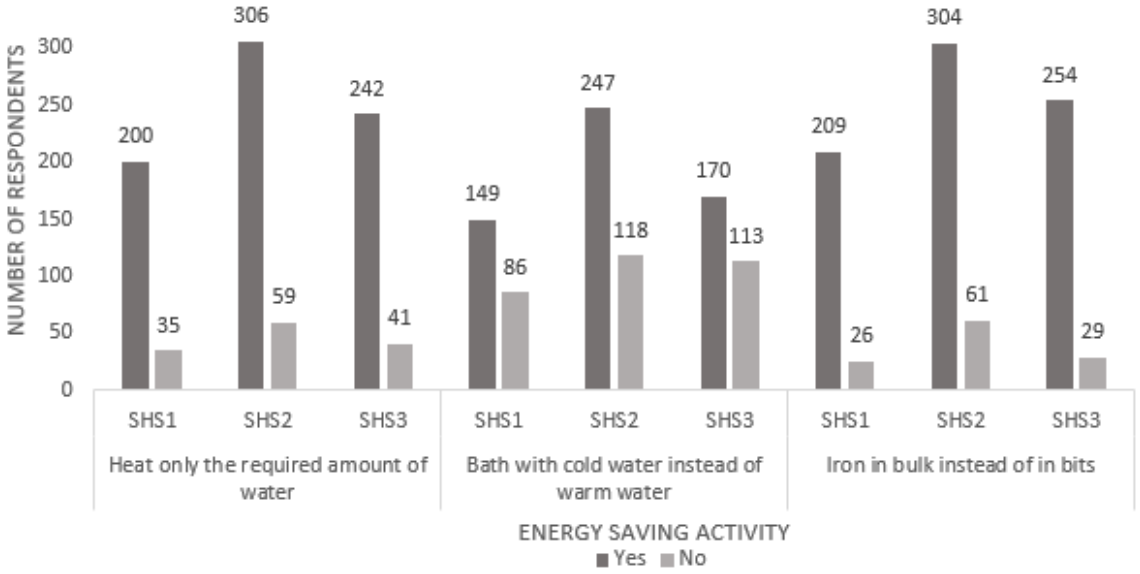

Fig. 5: Awareness in the use of heating loads based on study level

Figure 6 captures the responses, in terms of programme of study. The percentages for knowing that heating only the required amount of water saves energy are 75.0% for Business students, 87.4% for General Arts students, 87.6% for Home Economics students, 87.8% for Science and 81.7% for Visual Arts students. For energy saving by bathing with cold water instead of heated water, the percentages are 56.1%, 69.5% and 57.1%, 65.6%, and 68.8% for students studying Business, General Arts, Home Economics, Science and Visual Arts respectively. Lastly, 86.5% of students studying Business, 84.2% of students studying General Arts, 92.5% of students studying Home Economics, 90.6% of students studying Science, and 79.8% of students studying Visual Arts knew that bulk ironing is energy saving. In terms of awareness in energy saving associated with heating loads, the General Arts student had the highest average level of awareness.

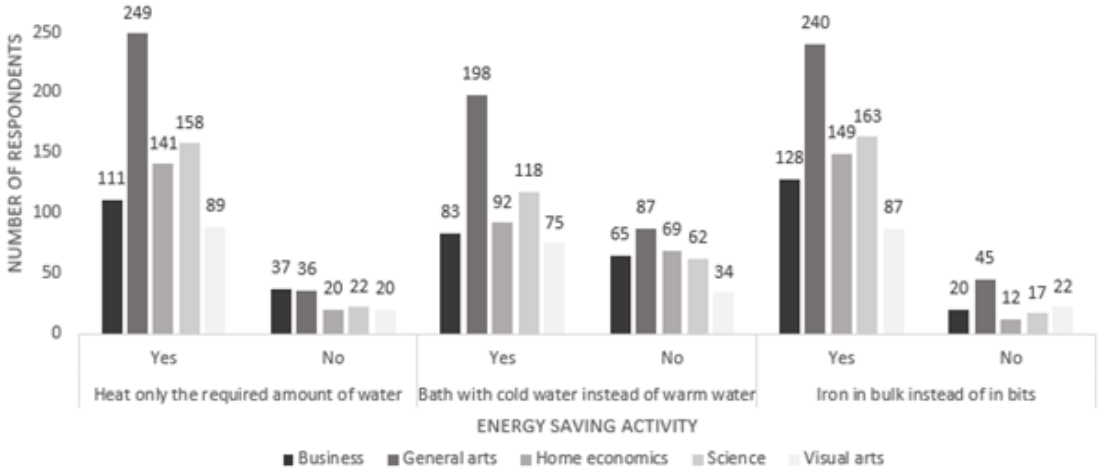

Figure 6. Energy efficiency awareness among programme of study in the use of heating loads

3.3. Energy efficiency awareness relating to the use of electronic devices

Here, it was determined whether the students knew that switching off electronic appliances at the sockets, when they are not in use is an energy conservation measure. It was also found out if they were aware that not keeping computers on standby but rather shutting them down helps to save energy.

Figure 7 shows the responses received, based on gender. Almost 93% of the males indicated knowledge of the fact that switching off electronic appliances at the socket help save energy. A higher percentage (97.2%) of the females knew this. With regards to saving energy by not keeping computers on standby, the percentages are 78.5% for males and 82.9% for females. Here too, the females showed greater awareness.

Figure 8 also shows, based on study level, the responses received for the same questions. With regards to saving energy by switching off appliances at the sockets, SHS2 students demonstrated slightly higher level of awareness than the rest with a percentage of 95.9%. The percentages for SHS1 and SHS3 are 95.7% and 92.5% respectively. Pertaining to

not keeping computers on standby, the percentages of students who answered in the positive are 82.9%, 81.6% and 80.9% for SHS1, SHS2 and SHS3 respectively. Thus, the SHS1 students showed greatest average awareness in the issues assessed.

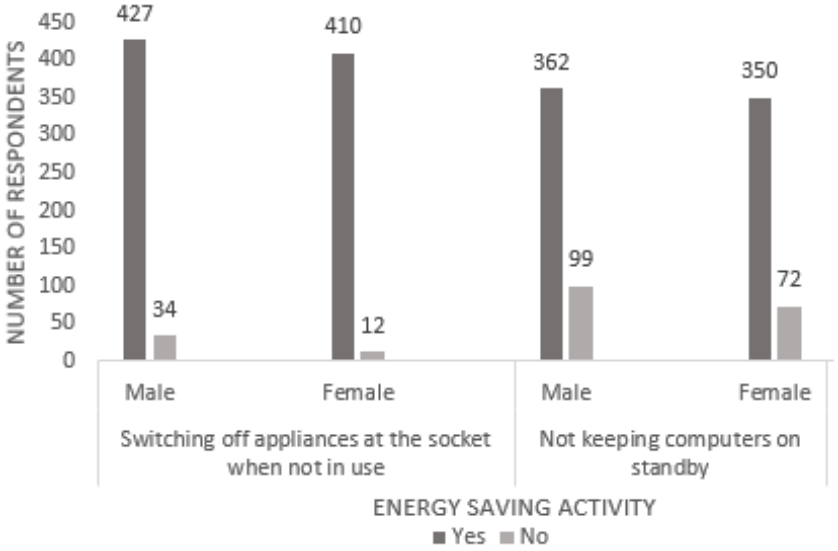

Fig. 7: Awareness in the use of electronic loads, based gender

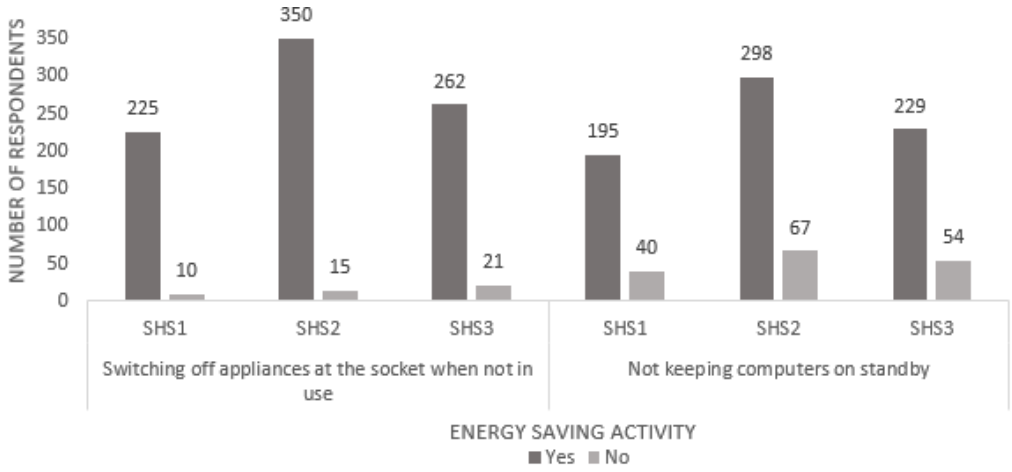

Fig. 8: Awareness in the use of electronic loads, based on study level

Figure 9 highlights the knowledge levels about the energy saving activities, based on the programme of study. Here, 91.9% of Business students, 95.8% of General Arts students, 97.5% of Home Economics students, 96.7% of Science students and 89.0% of visual Arts students knew that switching off electronic appliances at the sockets conserves energy. The percentages who indicated awareness of the fact that not keeping computers on standby saves energy are: 75.7%, 80.7%, 87.0%, 87.0% and 73.4% for students studying Business, General Arts, Home Economics, Science and Visual Arts respectively. The results suggest that most students have knowledge of the issues asked, with the Home Economics students showing the highest average awareness.

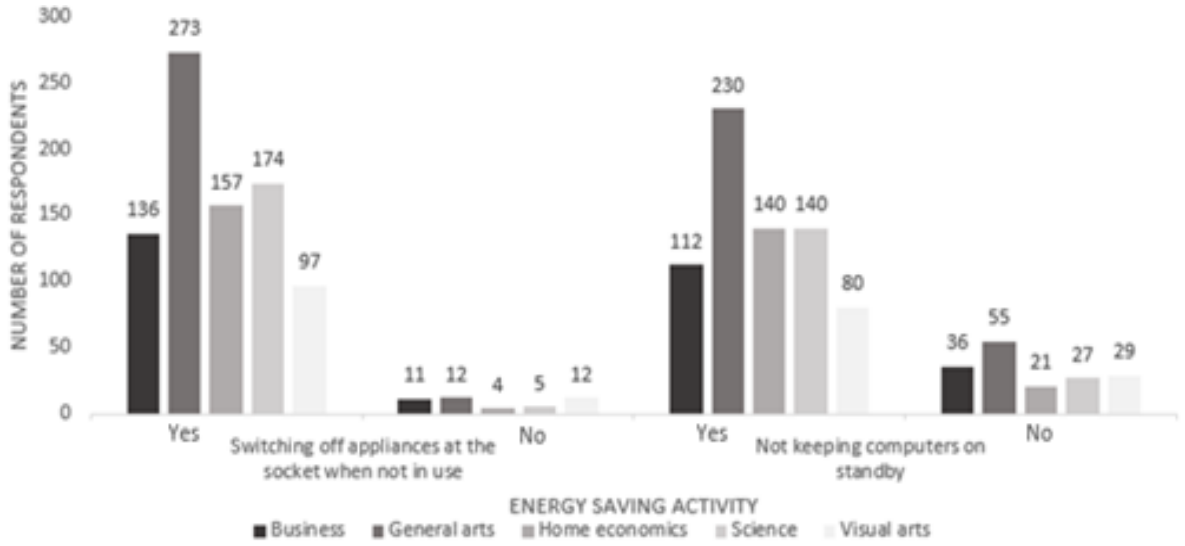

Fig. 9 Awareness in the use of electronic loads, based on programme of study

3.4. Energy efficiency awareness in the use of lighting

As shown in *figure 10*, most male and female students know that putting light bulbs off when there is adequate natural light will help save energy. The specific percentages are 91.1% and 96.2% for males and females respectively. Again, the females showed greater awareness.

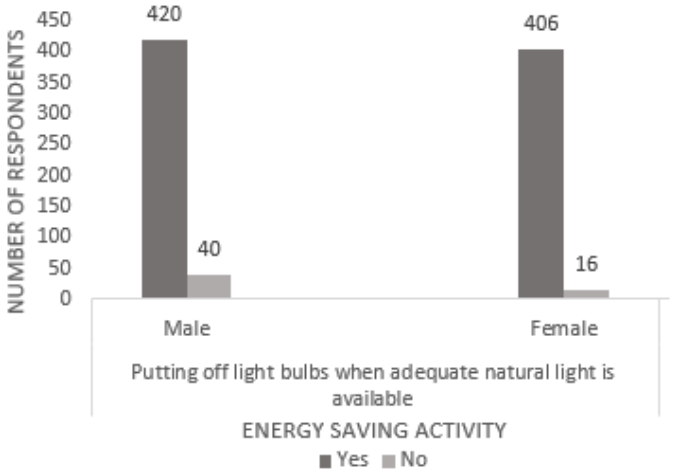

Fig. 10: Awareness in the use of natural lighting to save energy, based on gender

In terms of study levels, 90.6% of SHS1 students, 93.7% of SHS2 students and 95.4% of SHS3 students knew that switching off light bulbs when not needed saves energy, as shown in *figure 11*. The level of awareness is very high among all study levels, with SHS3 students having the highest level.

The percentage levels of awareness based on programme of study were found to be 92.6%, 93.3%, 82.6%, 97.2% and 87.2% for Business, General Arts, Home Economics, Science and Visual Arts programmes respectively. *Figure 12* highlights this. Here, the Science students showed the highest level of awareness.

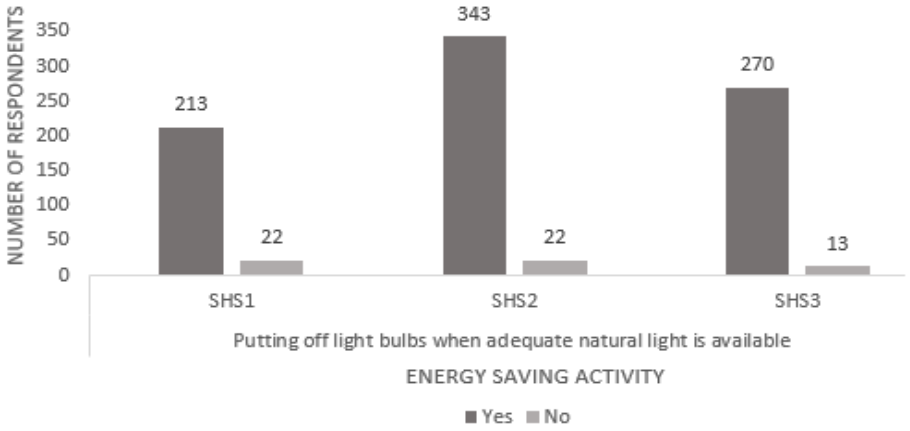

Fig. 11: Awareness in the use of natural lighting to save energy based on study level

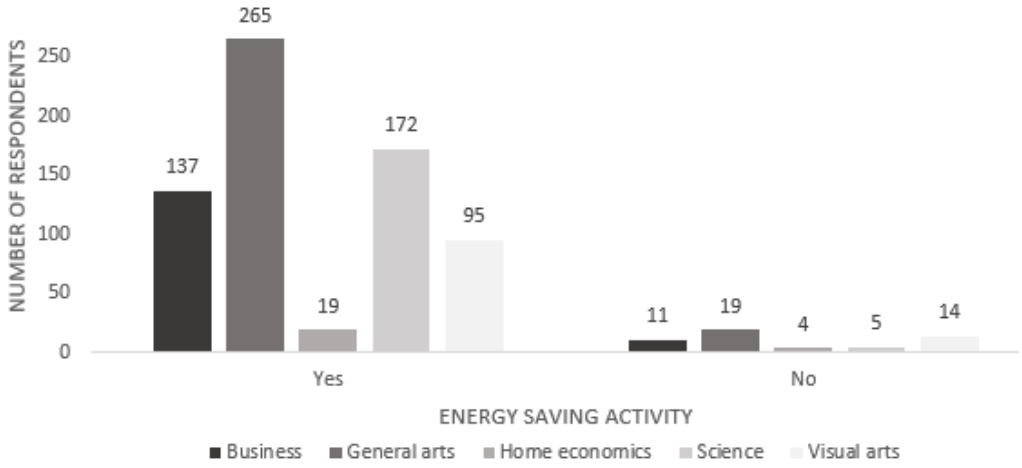

Fig. 12: Awareness in the use of natural lighting to save energy based on programme of study

3.5. Knowledge and practice of energy efficiency in the purchase of consumer items

Here, the basis for the students buying or encouraging their parents or friends to buy various consumer items was determined. It was determined whether the students (i) knew that light emitting diode (LED) bulbs use less energy than compact fluorescent lamps (CFLs), (ii) buy LED bulbs instead of CFLs, (iii) check the energy consumption of appliances before purchase, (iv) buy appliances that have the highest number of energy stars, and (v) buy new refrigerators instead of used ones. In Ghana, energy star labels are embossed on various appliances to indicate their efficiencies. The more the stars in a label on an appliance, the higher its efficiency. Also, there is a government policy that discourages the purchase of used refrigeratiors. Table 2 shows the percentages of respondents that answered in the affirmative. In Table 2, NR is the number of respondents.

Both gender showed high level of knowledge and practice in the areas assessed, except buying appliances with the highest number of energy stars. The male students showed greater knowledge and practice with regards to knowing that LED bulbs use less energy than CFLs, buying LED bulbs instead of CFLs, buying new refrigerators instead of used ones and

checking the energy consumption of appliances before purchase. On the other hand, the females showed greater awareness in buying appliances that have energy star labels as well as buying those with the highest number of energy stars. Averagely, the females had the highest level of awareness. Based on study levels, SHS1 students had the highest average awareness for the areas assessed. In terms of programme of study, Home Economics students showed that highest average awareness

Table 2: Knowledge and practice of energy efficiency in purchase of consumer items

	NR	*Know that LED bulbs use less energy than CFLs*	*Buy LED bulbs instead of CFLs*	*Check energy consumption of appliances before purchase*	*Buy appliances that have the highest number of energy stars*	*Buy new refrigerators instead of used ones*
		Yes(%)	Yes(%)	Yes(%)	Yes(%)	Yes(%)
Male	461	70.3	76.1	82.4	56.2	83.7
Female	422	69.0	70.1	81.8	57.1	82.2
SHS1	235	68.5	74.5	83.8	64.3	83.4
SHS2	365	69.0	72.1	83.0	52.1	81.9
SHS3	283	71.4	73.9	79.5	56.2	84.1
Business	148	68.9	70.9	73.6	51.4	79.7
General Arts	285	67.7	71.2	83.2	55.1	86.7
Home Econ.	161	72.0	79.5	88.8	68.9	82.0
Science	180	67.8	71.7	84.4	53.9	80.6
Visual Arts	109	75.2	75.2	77.1	54.1	83.5

3.6. Engagement in energy saving activities

The motivation for students to help their schools to save energy was determined. The motivations provided for students to select from are: (i) to reduce bill payments, (ii) to reduce the demand on the national grid, (iii) to protect the environment, and (iv) it is the right thing to do. Students could select multiple reasons.

The percentages of students who selected the various factors are presented in Table 3. It is observed from Table 3 that majority of each of the groupings considered are poised to support energy saving efforts. Here, the males showed higher degree of motivation. In terms of study level, the SHS1 students showed the highest average degree of motivation. Based on programme of study, students of the Visual Arts programme had the highest average level of motivation.

Table 3: Motivation for students to engage in energy saving activities

	NR	*To reduce bill payment*	*To reduce the demand on the national grid*	*To protect the environment*	*It is the right thing to do*
		Yes(%)	Yes(%)	Yes(%)	Yes(%)
Male	461	96.1	73.3	76.4	86.1
Female	422	93.4	64.7	73.7	87.9
SHS1	235	91.5	77.4	74.9	90.2
SHS2	365	94.0	65.2	75.9	87.7
SHS3	283	98.6	67.5	74.2	83.4
Business	148	91.2	63.5	71.6	85.1
General Arts	285	95.1	62.5	73.7	87.4
Home Econ.	161	97.5	78.9	78.9	88.8
Science	180	93.3	67.8	70.0	84.4
Visual Arts	109	97.2	82.6	86.2	89.9

The reasons why they would not support energy saving efforts was also determined. The factors provided for them to select from were: (i) I do not pay the bill, (ii) It will not change the amount I pay, (iii) I do not have knowledge about energy conservation, (iv) I feel it is not critical, (v) There is no motivationto do that, and (vi) It is not convenientfor me. The results obtained are presented in Table 4.

Table 4: Reasons for non-involvement in energy saving activities

	NR	*I do not pay the bill*	*It will not change the amount I pay*	*I do not have knowledge about energy conservation*	*I feel it is not critical*	*There is no motivationt o do that*	*It is not convenientf or me*
		Yes(%)	Yes(%)	Yes(%)	Yes(%)	Yes(%)	Yes(%)
Male	461	49.7	49.7	46.6	36.9	52.9	39.0
Female	422	37.4	42.9	38.2	21.3	45.3	28.0
SHS1	235	46.4	47.7	39.1	28.5	49.4	34.5
SHS2	365	44.9	50.4	51.2	34.2	52.3	38.4
SHS3	283	40.3	40.3	34.3	24.0	45.2	27.2
Business	148	42.6	38.5	35.8	26.4	47.3	26.4
Gen. Arts	285	37.9	46.7	48.4	31.6	44.9	27.7

	NR	*I do not pay the bill*	*It will not change the amount I pay*	*I do not have knowledge about energy conservation*	*I feel it is not critical*	*There is no motivationt o do that*	*It is not convenientf or me*
		Yes(%)	Yes(%)	Yes(%)	Yes(%)	Yes(%)	Yes(%)
Home Eco.	161	44.1	52.8	48.4	37.9	52.8	31.7
Science	180	42.2	38.9	25.0	23.9	46.1	20.0
Visual Arts	109	63.3	59.6	56.9	59.6	63.3	50.5

It can be seen from Table 4 that not a high percentage of the students, in all categories, would not support energy saving efforts for the reasons indicated. The females are least concerned about factors that would not make them support energy saving efforts. In terms of study level, SHS2 students expressed least concern, while based on programme of study, Science students expressed least concern.

3.7. Awareness of causes of electric shocks and electric fires

The knowledge of students pertaining to possible causes of electric shocks was determined. Tables 5a and 5b show the percentage levels of awareness. The tables show that a high percentage of the students (in all categories) are aware of the causes of electric shocks and electric fires. The only exception is awareness of the fact that plugs with only two prongs can cause electric shock. It is worth noting that standard sockets in Ghana use three prongs, with the third prong being connected to a local earth. In terms of average level of awareness, the groups with the superior percentages are males, SHS1 and Visual Arts.

Table 5a: Awareness of the causes of electric shocks and electric fires

	NR	*Connecting appliance cables directly to sockets*	*Overloading extension cables*	*Frayed or cracked cables, or exposed conductors*	*Flickering light bulbs and lights that dim when you use certain appliances*	*Plugs that spark when you try to plug them in*
		Yes(%)	Yes(%)	Yes(%)	Yes(%)	Yes(%)
Male	461	85.9	93.1	92.2	73.1	85.5
Female	422	80.1	93.8	91.5	70.6	87.9
SHS1	235	88.1	94.0	89.8	77.9	90.6
SHS2	365	83.0	92.1	93.4	70.4	87.4
SHS3	283	79.2	94.7	91.5	68.9	82.3

	NR	*Connecting appliance cables directly to sockets*	*Overloading extension cables*	*Frayed or cracked cables, or exposed conductors*	*Flickering light bulbs and lights that dim when you use certain appliances*	*Plugs that spark when you try to plug them in*
		Yes(%)	Yes(%)	Yes(%)	Yes(%)	Yes(%)
Business	148	73.6	87.8	87.2	69.6	80.4
Gen. Arts	285	86.7	94.4	93.0	70.2	86.7
Hom. Eco.	161	84.5	95.0	92.5	77.6	89.4
Science	180	82.6	95.0	92.8	67.2	87.2
Vis. Arts	109	72.3	93.6	92.7	78.9	90.8

Table 5b: Awareness of the causes of electric shocks and fires

	NR	*Plugs with only two prongs*	*Outlets that buzz, crackle or hiss*	*Circuit breakers and fuses that trip or short constantly*	*Light switches that are hot to touch*	*Electrical wires and fuse boxes that feel hot to touch*
		Yes(%)	Yes(%)	Yes(%)	Yes(%)	Yes(%)
Male	461	61.8	71.4	72.2	82.9	82.6
Female	422	50.0	70.4	71.8	83.4	85.8
SHS1	235	62.1	76.2	75.3	88.1	88.9
SHS2	365	55.1	68.5	73.7	82.5	82.5
SHS3	283	52.7	69.6	67.1	79.9	82.3
Business	148	55.4	69.6	64.2	79.1	81.1
Genera Arts	285	53.0	69.8	69.1	83.9	83.5
Home Econ.	161	57.8	70.2	82.0	86.3	88.2
Science	180	53.3	68.9	68.3	79.4	80.0
Visual Arts	109	67.9	68.9	81.7	88.1	90.8

3.8. Awareness of preventive measures against electric shocks and electric fires

The level of awareness regarding preventive measures against electric shocks and electric fires was also determined. The preventive measures considered and the results obtained are presented in Tables 6a and 6b. The tables show that most students (of all categories) are aware of preventive measures against electric shocks and electric fires. The females showed greater average awareness while in the other categories, SHS1 and Home Economics students had the highest average awareness.

Table 6a: Awareness of preventive measures to avoid electric shocks and fires

	NR	*Make sure all electrical outlets are fitted and tight to the wall*	*Do not tamper with electrical plugs*	*Replace any frayed or cracked electrical cords*	*Use extension cords as a temporary measure*	*Keep electrical cords away from water, heat sources and high traffic areas*
		Yes(%)	Yes(%)	Yes(%)	Yes(%)	Yes(%)
Male	461	90.2	88.3	88.1	74.4	92.2
Female	422	91.5	89.1	85.5	78.0	95.5
SHS1	235	92.8	91.1	90.6	80.9	95.3
SHS2	365	89.3	88.8	83.6	73.2	93.7
SHS3	283	91.2	86.9	88.0	76.0	93.9
Business	148	87.2	85.1	83.1	73.0	89.9
Gen. Arts	285	93.7	88.4	83.5	76.1	93.0
Home Econ.	161	91.9	88.8	89.4	84.5	96.3
Science	180	90.0	91.1	92.2	71.1	95.0
Visual Arts	109	88.1	89.9	88.1	76.1	95.4

Table 6b: Awareness of preventive measures to avoid electric shocks and fires

	NR	*Ensure socket outlets have child safety covers or spring-latch covers*	*Utilize three-prong plugs when possible*	*Disconnect appliances from socket outlets when not in use*	*Disconnect appliances before cleaning them*	*Use earth leakage breakers/ ground fault interrupters*
		Yes(%)	Yes(%)	Yes(%)	Yes(%)	Yes(%)
Male	461	86.1	77.4	89.2	93.1	77.4
Female	422	87.4	71.8	93.6	94.3	70.6
SHS1	235	90.2	78.7	90.6	95.3	76.2
SHS2	365	85.2	75.6	91.8	94.0	71.8
SHS3	283	85.9	70.3	91.2	91.9	75.6
Business	148	81.8	68.9	87.2	89.2	73.0
General Arts	285	85.3	71.9	91.9	96.1	71.9
Home Econ.	161	91.3	83.2	95.0	95.7	73.9
Science	180	87.8	77.8	91.7	92.8	76.1
Visual Arts	109	89.0	72.5	89.0	91.7	78.9

4. CONCLUSION

This work has evaluated the levels of awareness of senior high school students on issues that bother on electric energy conservation, electric safety and electric fires. The study evaluated the levels of awareness based on three categories namely, gender, programme of study and academic study level. The study revealed that the students have very high levels of awareness (more than 75% in most cases) of electric safety, electric fires, and energy savings issues related to the use of refrigerators, electronic devices, heating loads and lighting. Again, a very high percentage are inclined to factors that would motivate them to support institutional efforts to conserve electrical energy. A low percentage leaned towards factors that would not make them support energy saving efforts. The female students indicated greater average level of awareness than their male counterparts. In terms of level of academic study, SHS1 students showed highest average level of awareness. With regards to programme of study, students of the Home Economics programme (a programme that is almost entirely done by females) showed the greatest average level of awareness. The findings presented will positively influence the approach to electric energy related campaigns in secondary schools.

ACKNOWLEDGMENT

The authors thank the KNUST research fund (KRef) for providing financial support for the work.

REFERENCES

[1] F. Ahmad and S. Iqbal, *Reducing electricity consumption in educational institutes: a case study on aligarh muslim university*, Proceedings IEEE Students' Conference on Electrical, Electronics and Computer Science, pp. 34-38, 2012.

[2] E. J. Gago, T. Muneer, K. Knez and H. Koster, *Natural light controls and guides in building energy saving for electrical lighting and reduction of cooling loads*, Renewable and Sustainable Energy Reviews, vol. 1, pp.1-13, 2015.

[3] M. S. Safe, *School Fires*, Topical Fires Research Series, vol. 8, Issue 1, pp. 1-6, 2007.

[4] P. Wade, D. Teeman S. Golden, R. Wilson and V. Woodley, *The impact of school fires, a study of the wider economic and social impacts on school and the local community*, LGA Educational Research Report, pp. 1-49, 2007.

[5] H. Aktamis, *Determining energy saving behavior and energy awareness of secondary school students according to socio-demographic characteristics*, Educational Research and Reviews, vol. 6, no. 3, pp. 243-250, 2011.

[6] G. Fragidis and D. Olschewski, *Consumer awareness and engagement for energy efficiency eolutions*, Cleopa White Paper Series, 2015.

[7] E. Ç. Altuntaş and S. L. Turan, A*wareness of secondary school students about renewable energy sources*, Renewable Energy, vol. 116, part A, pp. 741-748, 2018.

OPTIMIZING THE USE OF GREEN ENERGIES, AN APPLICATION TO CROP IRRIGATION

Toufik **SEBBAGH**[1], Ridha **KELAIAIA**[1], Assia **ABDELOUAHED**[2] and Abdelouahab **ZAATRI**[3]

[1]*LGMM Laboratory, Université 20 Aout 1955 - Skikda, Skikda, Algeria*

[2] *Department of Civil Engineering, Université 20 Aout 1955 - Skikda, Skikda, Algeria*

[3] *Universityy of Constantine 1, Constantine, Algeria*

t.sebbagh@univ-skikda.dz

Keywords: optimization, irrigation, renewable energy

Abstract*: This paper assesses the optimal farmland that can be irrigated by a predetermined renewable energy system. The optimal irrigated surface from an agriculture area, cultivated by potatoes and tomatoes and powered by a PV system is studied. Two scenarios are discussed: the constraints applied to the first scenario is the limited surface of the agricultural area. While in the second scenario, the surface cultivated with tomatoes must be at least ¼ the surface cultivated with potatoes. Linear programming based on the Simplex algorithm is used to solve the optimization problem. The obtained results show that for the specified cultivating area, and for 10 panels at hand, an optimal surface of about 5.6 ha and 4.7 ha for the first scenario and the second scenario, respectively can be satisfied.*

1. INTRODUCTION

Energy is key in human lives. When converted into different forms, energy sources can power all important utilities, like water or electricity. Renewable energy systems (RESs) are systems that use energy coming from natural resources and are naturally replenished [1]. They are major components to reduce harmful greenhouse effect and to deal with depleting energy sources [2].

RESs are used in two modes: grid-connected or stand-alone. They can be used uniquely or in mixtures. Optimization techniques such as cost minimization [3, 4], production maximization [5] and storage optimization [6] are applied to RESs to deploy them in the best possible way.

The combination of renewable energy power generation and agriculture activities is a natural response to supply sustainable green electric power to agriculture. Crop irrigation is one of the main agriculture applications, it can promote the conservation of farmland and halt the degradation of grassland.

The application of optimization techniques to crop irrigation using RESs is widely covered in the literature. Campana et al. [7] investigated the geospatial distribution of grassland to implement photovoltaic water pumping systems. They used a spatially explicit optimization model of RESs based on cost minimization to assess the optimal location to implement the photovoltaic water pumping (PVWP) system. A drip irrigation system powered by renewable energy and diesel genset is proposed by [8], in which the levelized cost of energy based on the net present cost is optimized using Genetic Algorithms (GA). Authors in [9] used GA to find the optimal size of PVWP systems for irrigation. Their objective was to maximize the annual profit. Tsang and Jim [10] noted that green roof irrigation lacks reliable and cost-effective water conservation measures and employed neural network and fuzzy logic trained by real-time weather variables to develop an optimal irrigation strategy. Authors of [11] integrated a technique for order performance by similarity to ideal solution (TOPSIS) method with analytic hierarchy process (AHP) method to optimally size a PVWP with respect to the economic respect.

All the above publications studied the optimization duty from one side; it concerns the optimization of the energetic system to achieve some goals and/or benefits such as maximizing the energy generated by the systems and minimizing the cost of the energy obtained. But what if people do not have capitals to finance the required size of the system? This study was conducted as a result of an investigation involving several farmers in the region of El Hadaiek, concerning the replacement of diesel generators used for irrigation with renewable energy systems. One of the major concerns is their limited capital to power the irrigation system using the local abundant renewable energy sources.

This paper investigates the use of a fixed size photovoltaic system to optimally irrigate a farmland. The paper presents an application on crop irrigation where the hypothesis is that a farmer has predefined and limited energy system components. The objective is to maximize the surface that can be irrigated with an already sized system. The rest of the paper is organized as follows: the methodology followed in this work is presented in section 2, section 3 gives the case studied, results and discussions are given in section 4 and section 5 concludes the paper.

2. METHODOLOGY

The conceptual framework applied to identify the optimal surface that could be irrigated by the PVWP system is depicted in *fig. 1*. The methodology is divided into three

main steps:

Step 1: Meteorological data (irradiations, wind speed, humidity, ambient temperature, effective rainfall) are collected using the FAO CLIMWAT software [12].

Step 2: These data are then used in one hand, with the technical characteristics of the PV panels to calculate the energy produced by the PV system according to eq. (3). In the other hand, these are used with the crops properties and the soil characteristics to estimate the irrigating water required (IWR) for each crop with the FAO CROPWAT software.

Step 3: deals with the resolution of the optimization problem using the simplex algorithm.

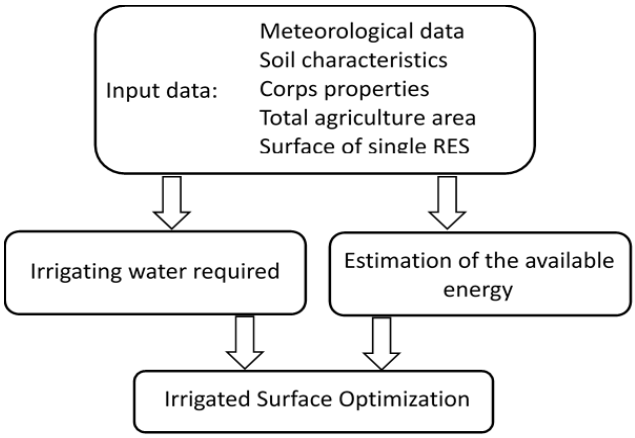

Fig. 1: conceptual framework to assess the optimal farmland irrigated by PVWP system

The calculation of the IWR is assessed using the meteorological data such as wind speed, ambient temperature, the solar irradiations at the crop surface, the effective rainfall and the crop properties as the evapotranspiration, the crop coefficient and the soil type. The IWR is estimated using the CROPWAT software.

The calculation of the equivalent hydraulic and electric energies required to pump the necessary volume of water is detailed is section 2.1. The energy generated by the PV system is calculated using the solar irradiations, the ambient temperature and the PV panel characteristics such as the active surface and the efficiency. The estimation of the energy produced by the PV generator is detailed in Section 2.2.1.

The calculation of the optimal farmland to be irrigated is assessed using the following data: the energy produced by the PV system, the electrical energy required to pump the daily volume of irrigating water required, and the surface of the parcel to be irrigated. The formulation of the optimization problem is detailed in section 2.2.2.

2.1. Load Profile

In this application, the system must power a motor-pump to pump the IWR. The electric Energy required ($E_{elec.}$) is given as:

$$E_{elec.} = \frac{E_h}{\eta} \quad (1)$$

where: η: the efficiency of the motor-pump; E_h(Wh/day): is the required hydraulic energy which is related to the daily water needs and the hydraulic head and it can be calculated by:

$$E_h = \frac{g*\rho*V*h}{3600} \quad (2)$$

g: gravity, ρ: water density (1000 kg/m^3), V: daily required water volume (m^3), h: total head (m).

2.2. System Modelling

2.2.1. PV model

The daily electrical energy produced by the PV system is given according to [13] by the following formula:

$$E_{PV} = F_m.\left[1 - \gamma.\left(T_c - T_{c,ref}\right)\right].\eta_g.A.G(\beta) \quad (3)$$

where: E_{PV}: is the daily electrical energy produced by the PV system ($in\frac{KWh}{m^2}/day$), F_m: is the coupling factor, γ: is the cell temperature coefficient, T_c: is the daily average cell temperature during the sunshine hours.

$$T_C = T_a + (NOCT - 20) * \frac{G}{800} \quad (4)$$

$T_{c,ref}$: cell temperature at reference conditions, η_g: generator efficiency at reference temperature, A: the active surface of the generator ($in\, m^2$), $G(\beta)$: is the daily average irradiation incident on the module inclined by β.

2.2.2. Problem formulation:

The problem of the optimal exploitation of the energy generated by a fixed size standalone RES to maximize the surface irrigated by this system can be discussed as follows.

Consider that a RES can generate an amount $E_{PV}(t)$ of energy. This system is used to satisfy a costumers demand D. This demand can be estimated as the amount of energy necessary to pump the volume of water (V_i) required to irrigate different parcels cultivated by some crops. These parcels have a surface $S_i(t)$ and may have different total heads.

The optimization problem can be formulated as:

$$\begin{cases} Max\ S(t) = \sum_{i=1}^{n} S_i\,(t) \\ ST: \\ \sum_{i=1}^{n} E_i(t).\frac{S_i(t)}{S_u} \le E_{PV}(t) \\ S_i(t) \ge 0 \end{cases} \quad (5)$$

$E_i(t)$: is the electrical energy required to pump the irrigating water for parcel (i), expressed in Wh/ha.

$$E_i(t) = \frac{1}{\eta}.\frac{g.\rho.V_i(t).h_i}{3600} \quad (6)$$

$V_i(t)$: is the IWR for crop (i) (in m^3/ha), S_u: is the unit surface assumed to be 1 ha.

Substitute (6) in (5):

$$\begin{cases} Max\ S(t) = \sum_{i=1}^{n} S_i\,(t) \\ ST: \\ \sum_{i=1}^{n} \left(\frac{1}{\eta}.\frac{g.\rho.V_i(t).h_i}{3600}\right).\frac{S_i(t)}{S_u} \le E_{PV}(t) \\ S_i(t) \ge 0 \end{cases} \quad (7)$$

2.2.3. Simplex method:

The simplex method [14, 15] is used to solve the optimization problem of this study. It is a basic and efficient computational algorithm for solving linear programming problems, introduced in 1947/48 [14]. The flowchart of the simplex algorithm is presented in *figure 2*.

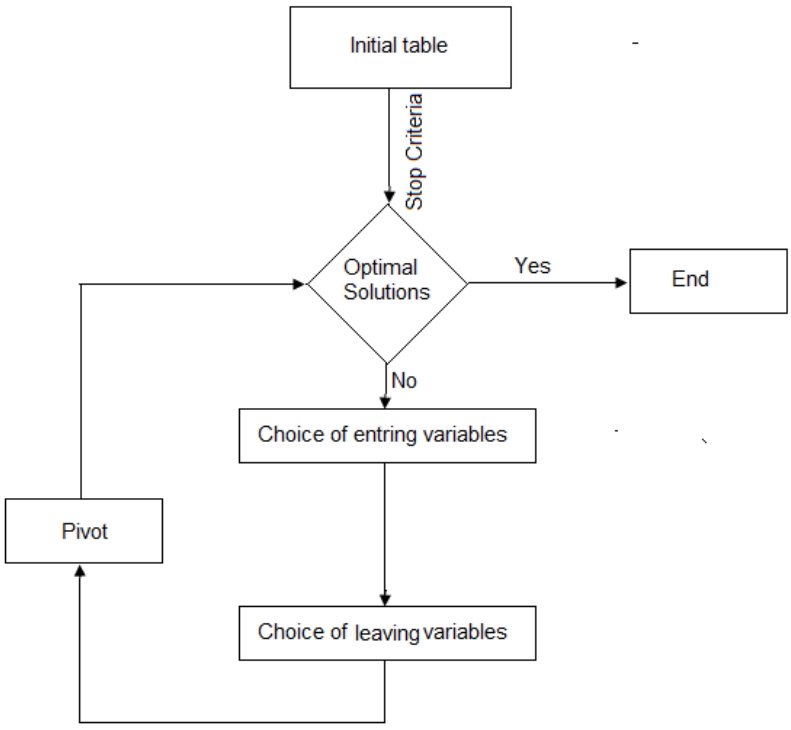

Fig. 2: Flowchart of the Simplex algorithm

3. CASE STUDY

Consider that 2 crops have to be irrigated. The IWR for crop 1 is $V_1(t)$, and for crop 2 is $V_2(t)$. This required water varies within the age of the crop, the meteorological data and, the soil properties. $S_1(t)$ and $S_2(t)$ are the surfaces of the cultivated crops: 1 and 2 respectively.

If these two crops are selected to be potatoes and tomatoes, the IWR for these two crops when cultivated in the region of Skikda, Algeria (Latitude: 36.8762, Longitude: 6.90921) is evaluated using the software CROPWAT. The meteorological data used is obtained from the FAO CLIMWAT. Table 1 illustrates the annual variations of meteorological data in a typical year in the specified area. The IWR for different age stages is represented in figure 3. The cultivation period is supposed to begin on May, 6th.

Table 1: Meteorological properties of the selected site [12].

Month	*Min Temp °C*	*Max Temp °C*	*Humidity %*	*Wind km/day*	*Sun hours*	*Rad MJ/m²/day*	*ETo mm/day*
January	*7.1*	*13.8*	*76*	*156*	*3.4*	*7.3*	*1.20*
February	*7.1*	*14.3*	*69*	*156*	*4.8*	*10.4*	*1.67*
March	*8.8*	*17.1*	*76*	*190*	*6.3*	*14.9*	*2.29*
April	*10.0*	*18.8*	*75*	*138*	*6.8*	*18.1*	*2.85*
May	*13.2*	*21.6*	*77*	*138*	*8.7*	*22.4*	*3.67*
June	*16.6*	*25.0*	*69*	*138*	*9.6*	*24.3*	*4.52*
July	*19.3*	*28.2*	*74*	*138*	*11.3*	*26.2*	*5.08*
August	*20.5*	*28.8*	*75*	*147*	*10.2*	*23.3*	*4.72*
September	*18.8*	*26.6*	*76*	*147*	*8.7*	*18.7*	*3.69*
October	*15.0*	*22.7*	*79*	*138*	*6.0*	*12.5*	*2.30*
November	*11.6*	*18.2*	*74*	*147*	*4.2*	*8.3*	*1.60*

Tab. 1 shows that the cultivation period is characterized by:

- High ambient temperature values, the highest min and max values appear in the month of August with a maximum mean daily average of 24.6°C.
- The highest radiation reaches 26.2 MJ/m²/day (7277,8 Wh/m^2/day), in July.
- An important sunshine duration with a maximum of 11.3h in July.

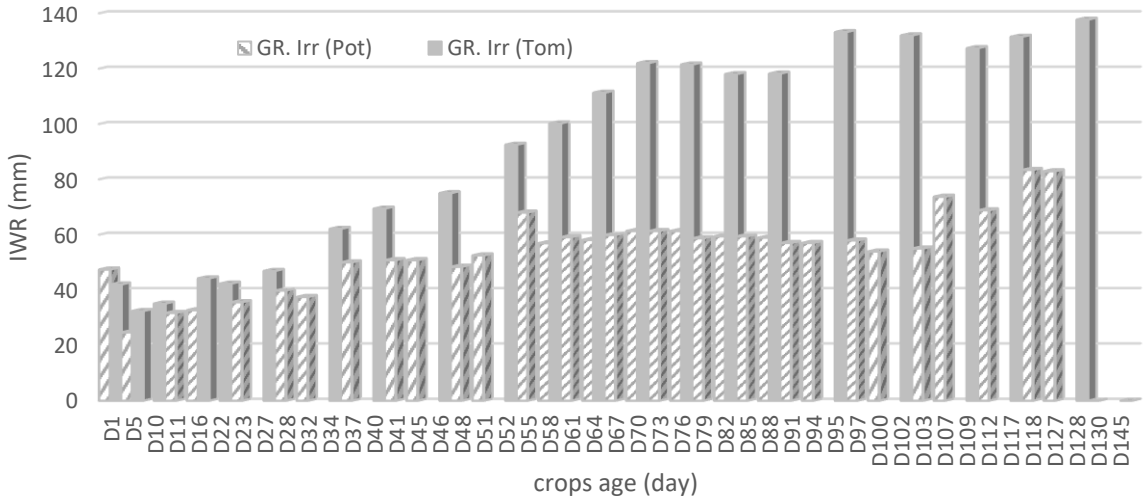

Fig. 3: Irrigating water required of the two crops during the crop life cycle

Fig. 3 presents the irrigating water required by the two crops during the different stages of life cycle.

During the 145 days that represent the cycle life period the following observations can be made:

- ✓ Tomatoes need more water than potatoes during the life cycle except in the first day.
- ✓ 45 rounds of irrigation must be scheduled where 9 times the two crops are irrigated on the same day.
- ✓ IWR increases with the age of the two crops.

To power the irrigating system, a stand-alone Photovoltaic system constituted by 10 (Sunmodule Plus SW 250 poly) panels are used. The Technical characteristics of the used panels are presented in Table 2.

Table 2: Technical characteristics of PV panels.

Item	*Value*
P_{max}	*250 Wc*
U_{OC}	*38.0 V*
U_{mpp}	*30.5 V*
I_{Sc}	*8.88 A*
I_{mpp}	*8.27 A*
Dimensions	*1675/1001/31 (mm)*
weight	*21.2 kg*
Cell numbers	*60*
Cell technology	*Polycrystalline silicon*
Cell dimensions	*156/156 (mm)*

4. RESULTS AND DISCUSSIONS

Two scenarios are discussed within this case study, where the maximum bound is fixed to 10 ha for the entire surface (i.e. $S_1 + S_2$) in the first one. However, another constraint is imposed to the model presented in (7).

4.1. Scenario 1

In this scenario the number of panels available is fixed at 10, the maximum surface to be irrigated is fixed at 10 ha. The problem formulated in (7) becomes:

$$\begin{cases} Max\ S(t) = S_1(t) + S_2(t) \\ ST: \\ \left(\frac{1}{\eta}.\frac{g.\rho.V_1(t).h_1}{3600}\right).S_1(t) + \left(\frac{1}{\eta}.\frac{g.\rho.V_2(t).h_2}{3600}\right).S_2(t) \le E_{PV}(t) \\ S_1(t) + S_2(t) \le 10 \\ S_i(t) \ge 0 \end{cases} \quad (8)$$

Fig. 4 illustrates the optimization results. The optimal surface depends on the quantity of water required by the crop. The surface irrigated on the fifth day (D5) represents the most optimal surface can be irrigated by the system, this surface is equal to 5.6 ha cultivated by potatoes. The PV system generates 9493 Watts and the pumping system pumps a volume of about 138.3 m^3 of water.

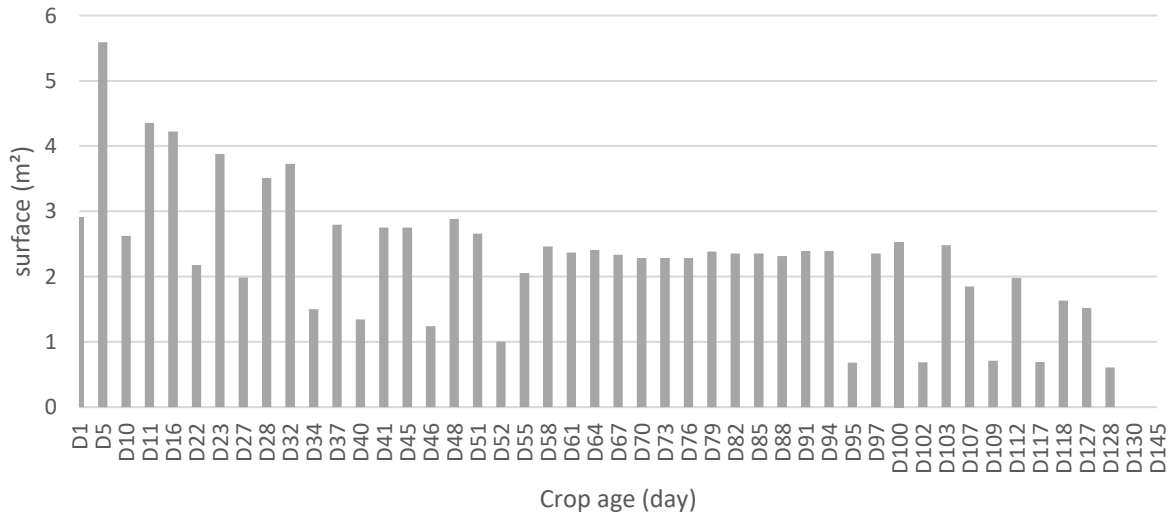

Fig. 4: Optimal surfaces irrigated by the implemented PV system

The repartition of the optimal surfaces that can be irrigated by the system on the two parcels is illustrated in *Fig. 4*. According to this figure, and according to the constraint

imposed, the optimal surface covers most of the lifecycle days surfaces cultivated by potatoes (S_1). This is due to that the irrigating water required by potatoes is less than that required by tomatoes. Twelve cases of optimal surfaces cultivated by tomatoes (S_2) appears in the histogram of the *figure 5* corresponds to the days where irrigation of potatoes is not scheduled.

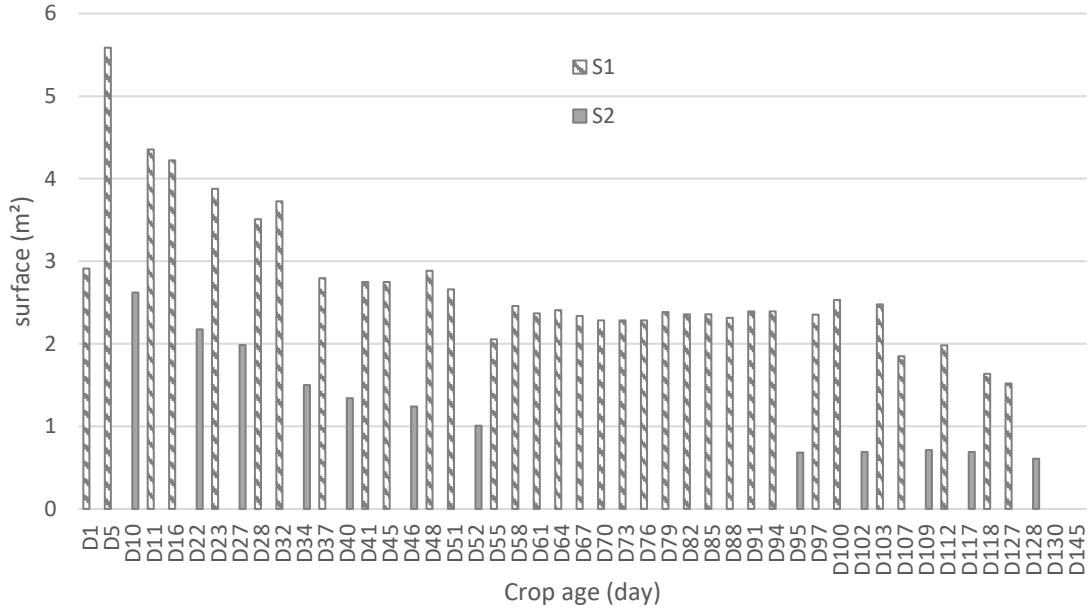

Fig. 5: Repartition of the optimal surface irrigated on the two parcels

4.2. Scenario 2

In this scenario the number of panels available is fixed at 10, the maximum surface to be irrigated is fixed at 10 ha and when the two parcels must be irrigated in the same day, the surface irrigated from the parcel cultivated by tomatoes (S_2) must be at least ¼ the surface irrigated from the parcel cultivated by potatoes (S_1). The optimization problem presented by (6) becomes:

$$\begin{cases} Max\ S(t) = S_1(t) + S_2(t) \\ ST: \\ \left(\frac{1}{\eta}.\frac{g.\rho.V_1(t).h_1}{3600}\right).S_1(t) + \left(\frac{1}{\eta}.\frac{g.\rho.V_2(t).h_2}{3600}\right).S_2(t) \le E_{PV}(t) \\ S_1(t) + S_2(t) \le 10 \\ S_2(t) \ge \frac{1}{4}.S_1(t) \\ S_i(t) \ge 0 \end{cases} \quad (9)$$

Fig. 6 represents the optimization results for all the scheduled irrigation days. In this case, the most optimal surface is always on the fifth day (D5) and compared with that of the first scenario drops to about 4.68 ha, where 3.74 ha is from (S_1) and about 0.93 ha from (S_2)

as detailed in Figure 5. In this case the total volume of water pumped is 122.51 m^3 and the system generates about 9405 watts.

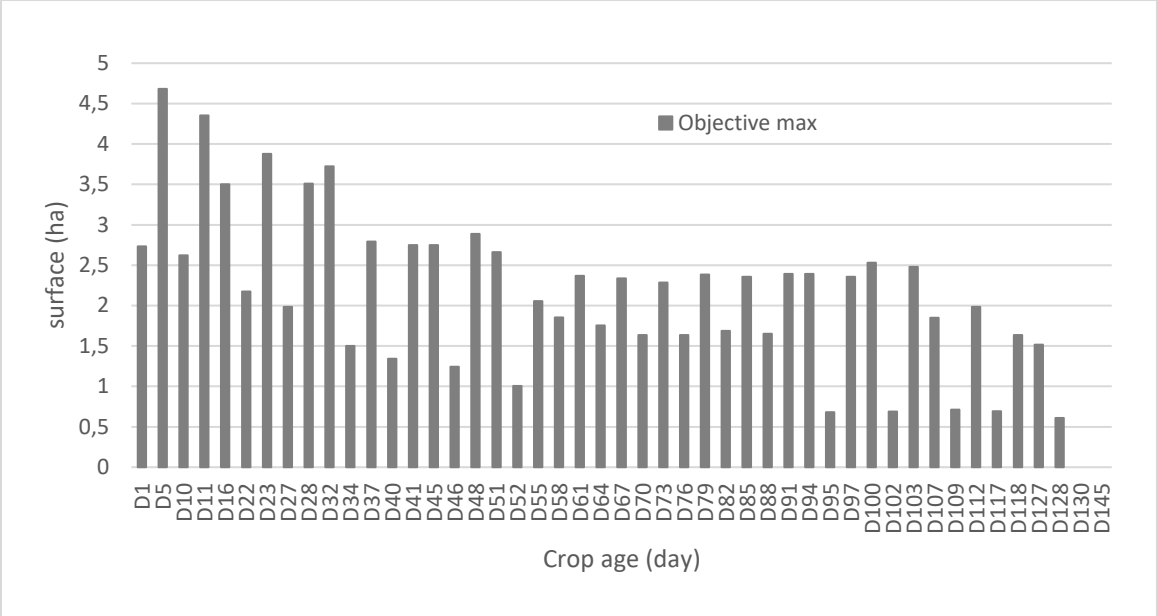

Fig. 6: Optimal surface irrigated by the PV system for the 2nd scenario

The optimal surface irrigated by the system from (S_1) is at the day (D11) with 4.33 ha irrigated by 137.3 m^3 and consumes 9394.3 watts. While the optimal surface irrigated from (S_2) is at the day (D10) with a surface of 2.62 ha, irrigated by a volume of water equal to 91.96 m^3. The pumping system is powered by 9397.4 watts generated by the PV system.

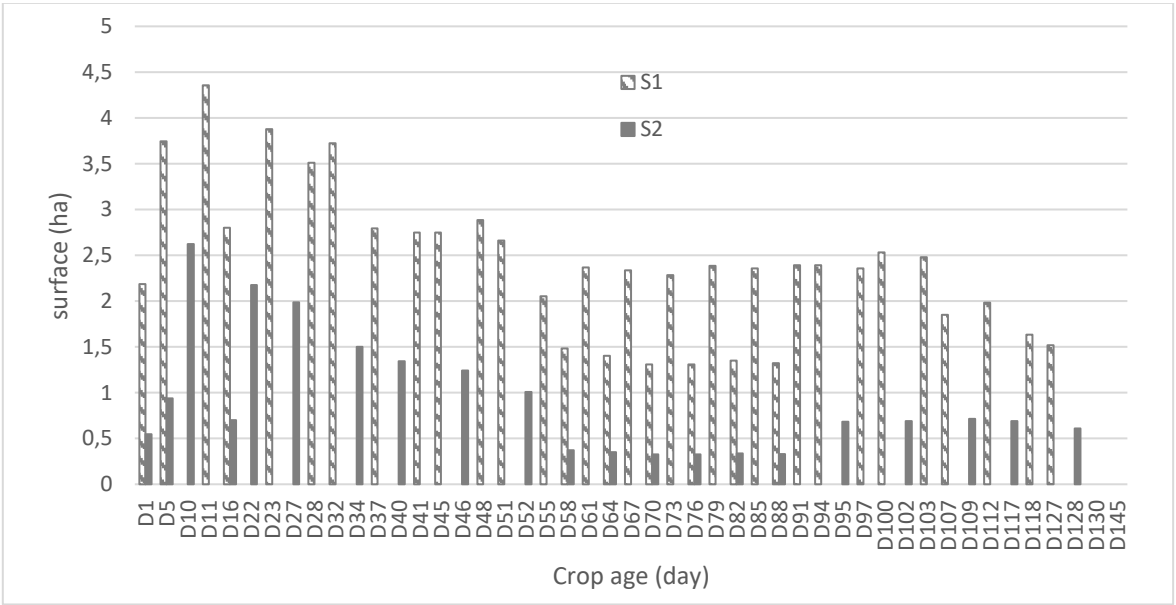

Fig. 7: Repartition of the optimal surface irrigated on the two parcels for the second scenario

Fig. 7 illustrates the repartition of the optimal surfaces that can be irrigated by the

system on the two parcels for the second scenario. The optimal surface irrigated from S1 within this scenario is achieved at the day (D11) with about 4.35 ha. where the irrigation of S1 is not scheduled. Whereas, the optimal surface irrigated from S2 is achieved at the day D10 with about 2.62 ha.

CONCLUSION

The PVWP systems are an alternative solution to the diesel based irrigating systems. It is a clean and renewable-based solution to the sustainable development of the agriculture in Algeria. The optimal sizing of the PVWP systems is an important task to satisfy the costumer's demand. However, the optimal use of the energy produced by the renewable energy systems is required to reduce the costs.

This paper presented a methodical solution to optimize the use of a fixed and predetermined size PV system in the irrigation of crops. The proposed methodology may be applied for different locations, and for several crops.

REFERENCES

[1] R. Baños, F. Manzano-Agugliaro, F. G. Montoya, C. Gil, A. Alcayde, and J. Gómez, *Optimization methods applied to renewable and sustainable energy: A review*, Renewable and Sustainable Energy Reviews, vol. 15, pp. 1753-1766, 2011.

[2] M. Iqbal, M. Azam, M. Naeem, A. S. Khwaja, and A. Anpalagan, *Optimization classification, algorithms and tools for renewable energy: A review*, Renewable and Sustainable Energy Reviews, vol. 39, pp. 640-654, 2014.

[3] L. Noel, J. F. Brodie, W. Kempton, C. L. Archer, and C. Budischak, *Cost minimization of generation, storage, and new loads, comparing costs with and without externalities*, Applied Energy, vol. 189, pp. 110-121, 2017.

[4] M. Majid, H. Sayed Jamal al-Din, and S. Hossein, *Optimal Sizing of an Isolated Hybrid Wind/PV/Battery System with Considering Loss of Power Supply Probability*, vol. - 11, 2017.

[5] X. Wang, A. Palazoglu, and N. H. El-Farra, *Operational optimization and demand response of hybrid renewable energy systems*, Applied Energy, vol. 143, pp. 324-335, 2015.

[6] Y. Zhang, P. E. Campana, A. Lundblad, and J. Yan, *Comparative study of hydrogen storage and battery storage in grid connected photovoltaic system: Storage sizing and rule-based operation*, Applied Energy, vol. 201, pp. 397-411, 2017.

[7] P. E. Campana, S. Leduc, M. Kim, A. Olsson, J. Zhang, J. Liu, F. Kraxner, I. McCallum, H. Li, and J. Yan, *Suitable and optimal locations for implementing photovoltaic water pumping systems for grassland irrigation in China*, Applied Energy, vol. 185, pp. 1879-1889, 2017.

[8] J. Carroquino, R. Dufo-López, and J. L. Bernal-Agustín, *Sizing of off-grid renewable energy*

systems for drip irrigation in Mediterranean crops, Renewable energy, vol. 76, pp. 566-574, 2015.

[9] P. E. Campana, H. Li, J. Zhang, R. Zhang, J. Liu, and J. Yan, *Economic optimization of photovoltaic water pumping systems for irrigation*, Energy Conversion and Management, vol. 95, pp. 32-41, 2015.

[10] S. W. Tsang and C. Y. Jim, *Applying artificial intelligence modeling to optimize green roof irrigation, Energy and Buildings*, vol. 127, pp. 360-369, 2016.

[11] D. H. Muhsen, T. Khatib, and T. E. Abdulabbas, *Sizing of a standalone photovoltaic water pumping system using hybrid multi-criteria decision making methods*, Solar Energy, vol. 159, pp. 1003-1015, 2018.

[12] http://www.fao.org/land-water/databases-and-software/climwat-for-cropwat/en/ (checked on 05/05/2018)

[13] A. HADJ ARAB, M. BENGHANEM, and A. GHARBI, *Dimensionnement de systèmes de pompage photovoltaïque*, Revue des énergies renouvelables, vol. 8, pp. 19-26, 2005.

[14] K.H. Borgwardt, *Introduction. In: The Simplex Method. Algorithms and Combinatorics (Study and Research Texts),* vol 1. Springer, Berlin, Heidelberg, 1987.

[15] R. Fourer, *A simplex algorithm for piecewise-linear programming i: Derivation and proof,* Mathematical programming 33:204–233, 1985.

A MODIFIED VIRTUAL SPACE VECTOR MODULATION TECHNIQUE FOR Z-SOURCE NPC INVERTERS

Francis **EFFAH**[1], Philip **OKYERE**[1], Patrick **WHEELER**[2], Alan **WATSON**[2], Jon **CLARE**[2]

[1] *Kwame Nkrumah University of Scince and Technology, Kumasi, Ghana,* [2] *University of Nottingham, Nottingham, UK.*

fbeffah.coe@knust.edu.gh

Keywords: neutral point, voltage buck-boost, modulation, impedance network

Abstract*: A modified virtual space vector modulation approach for the control of a Z-source neutral point clamped inverter is presented in this paper. This approach works perfectly for the traditional neutral point clamped inverter. In this paper, the effectiveness of the virtual space vector modulation technique in balancing the input capacitor voltages of the Z-source NPC inverter with no low-frequency oscillations superimposed in addition to voltage buck-boost capability is demonstrated through simulations in SABER®. A prototype converter is used to capture experimental results for validation.*

1. INTRODUCTION

Neutral-point-clamped (NPC) inverters are used in both medium-voltage high-power and low-power systems. Their popularity is attributed to merits like better harmonic performance, reduced switching losses, low dv/dt, smaller filter volume, and better electromagnetic compatibility [1]. Unfortunately, the ac peak output voltage that it can synthesize is always less than the input dc source. Thus in many applications a dc-dc boost converter is required at the input stage to meet the required output value. The resulting system becomes more complicated and its control can be difficult [2]. The Z-source NPC (ZNPC) inverter overcomes these limitations. The ZNPC inverter topology has received a lot of attention in the research community and is expected to find application in photovoltaic (PV) power systems [3]. It has also been explored for motor drive applications

such as hybrid electric vehicles [4]. The ZNPC inverter adjustable speed drive (ASD) system has several unique advantages that are very desirable for many ASD applications, such as ride-through capability during sags, reduced line harmonics, improved power factor and reliability, and extending the output voltage range. However, this converter inherits one particular problem of the conventional NPC inverter: unbalanced input capacitor voltages [5, 6].

In many applications, well balanced capacitor voltages are required otherwise increased harmonics and damage of switching devices may result. As a result, there have been much efforts to solve the capacitor voltage balancing problem [7-9]. The capacitor voltage balancing control methods are grouped based on the pulse width modulation (PWM) methods. These include carrier-based sinusoidal PWM (CBSPWM) [10-12], space vector PWM (SVPWM) [8, 13-15], and selective harmonic elimination PWM (SHEPWM) [16]. SVPWM method offers low noise, small ripple, better dc utilization as well as easy implementation in a microcontroller [17] and therefore has attracted more attention.

For the conventional three-level SVPWM, the capacitor voltages can be balanced through adjustment of the redundant small vectors' duration [5, 6, 9, 13, 18]. In [15], an SVPWM-based capacitor voltage controller that uses the direction of load currents was proposed. In this method, redundant voltage vectors were distributed to ensure small current flows through the neutral point (NP) so as to achieve capacitor voltage balance. The idea behind most SVPWM schemes is to select three nearest vectors to form the reference vector. However, these methods are not capable of balancing the capacitor voltages for high modulation index and low power factor [17]. Virtual space vector modulation (VSVM) was proposed to overcome this problem [19].

Several variants of the VSVM technique have been reported in the literature to balance the capacitor voltage of the conventional NPC inverter and some of its derived topologies [17, 19, 20]. Nevertheless, none of these techniques has been verified with the ZNPC inverter in the literature. This creates a research gap since the ZNPC inverter is expected to replace the NPC inverter in most applications where the dc source may not be constant but the output ac voltage needs to be controlled to obtain a favourable value for the load. In this paper the VSVM technique proposed in [19] for controlling the conventional NPC inverter is modified and applied to the ZNPC inverter to verify its effectiveness in modulating this converter. Applying this modified VSVM technique to the ZNPC inverter enables the inverter to perform voltage buck-boost function in addition to balancing input capacitor voltages with all low-frequency oscillations completely eliminated.

The main advantage of the VSVM technique over the conventional SVPWM technique is its ability to eliminate completely low-frequency oscillations of the capacitor voltages. Capacitor voltage oscillation increases the voltage stress on power devices which may lead to premature failure of the converter. However, this benefit in capacitor voltage balance is achieved at the expense of an increased number of commutations compared to the

conventional SVPWM strategy. The increase in commutations is due to the fact that the VSVM technique always employs five different switching states per switching cycle while the conventional SVPWM uses only four for high modulation index and majority of switching cycles. The additional commutations may lead to an increase in switching losses.

In section 2, a brief review of the ZNPC inverter circuit is presented. The modified VSVM technique for controlling this converter is explained in section 3. Simulation as well as experimental results are presented in section 4 to verify the effectiveness of the VSVM technique in modulating the ZNPC inverter.

2. REVIEW OF Z-SOURCE NPC INVERTER

Figure 1 shows the circuit configuration of the ZNPC inverter. The reference is taken as the neutral point, "o". Each output phase leg has three values: $V_i/2$, 0, $-V_i/2$. With operation as a traditional NPC inverter, V_i equals $2V_{DC}$ which is also the maximum output line-to-line voltage obtainable.

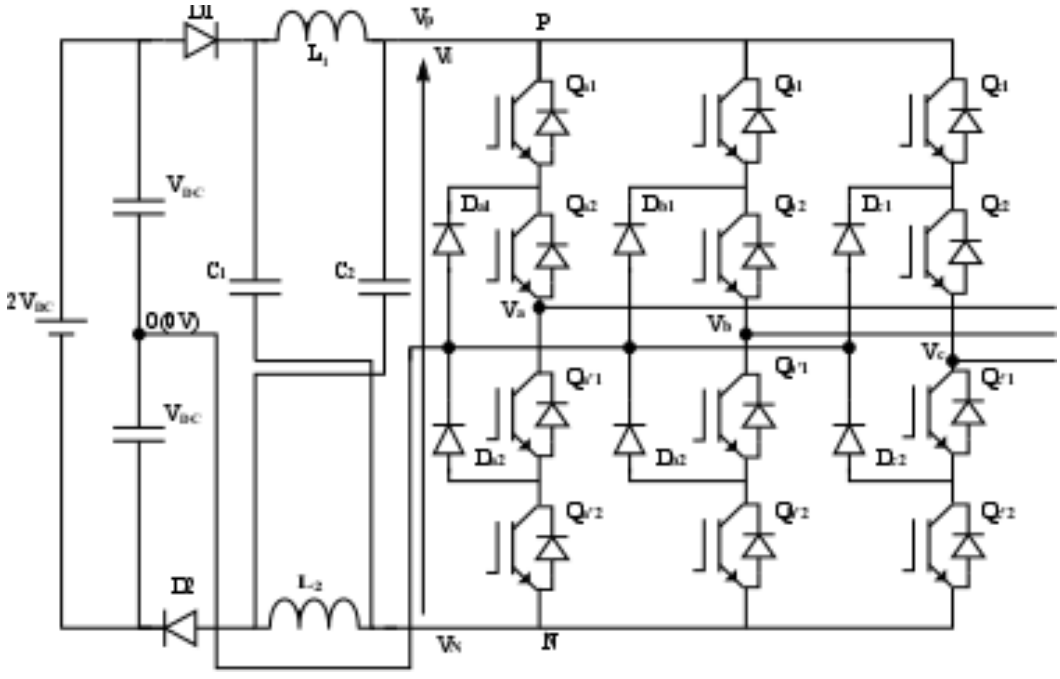

Fig. 1. Z-source NPC inverter

If shoot-through states are introduced into phase legs, an output line-to-line voltage greater than the available dc voltage can be obtained. Thus, ZNPC inverter can step down and step up the output voltage with a single stage structure.

The ZNPC inverter can be operated either with full-shoot-through states or partial-shoot-through states. In this work, partial-shoot-through method is selected since it produces output waveforms with better harmonic content [21].

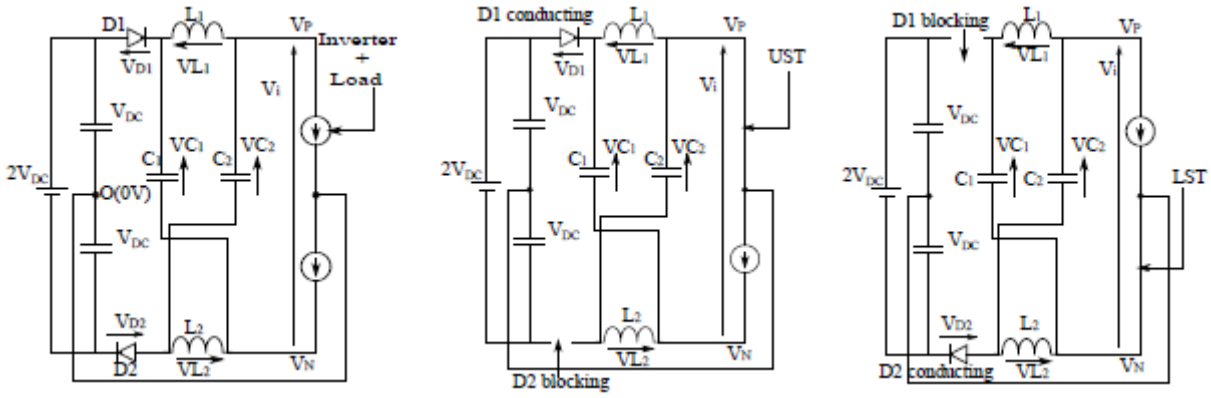

(a) NST state *(b) UST state* *(c) LST state*

Fig. 2. Simplified representation of ZNPC inverter during (a) NST, (b) UST and (c) LST states

Figure 2 shows the simplified equivalent circuits of ZNPC inverter in different states. It is assumed the impedance network is symmetrical. Voltage equations for non-shoot-through (NST) states are given as:

$$V_{L1} = 2V_{DC} - V_{C2} \tag{1}$$

$$V_{L2} = 2V_{DC} - V_{C1} \tag{2}$$

$$V_P = +V_i/2 \tag{3}$$

$$V_N = -V_i/2 \tag{4}$$

$$V_i = V_{C1} + V_{C2} - 2V_{DC} \tag{5}$$

In a similar manner, voltage equations during upper-shoot-through (UST) states are given by:

$$V_{L1} = V_{DC} \tag{6}$$

$$V_P = 0 \tag{7}$$

$$V_N = V_{DC} - V_{C1} \tag{8}$$

and voltage equations for lower-shoot-through (LST) states are given as:

$$V_{L2} = V_{DC} \tag{9}$$

$$V_P = -V_{DC} + V_{C2} \tag{10}$$

$$V_N = 0. \tag{11}$$

Let the switching period be T_{sw} and the combined time of shoot-through states be T_{st}. For symmetrical operation T_{st} is shared equally between UST and LST states. Performing inductor voltage averaging over one switching period, we have:

$$V_{C1} = V_{C2} = V_C = 2V_{DC}.\left\{\frac{1-0.5T_{st}/T_{sw}}{1-T_{st}/T_{sw}}\right\}. \tag{12}$$

Using (12) and (5), the dc-link voltage for NST states is given as:

$$V_{i\_NST} = \frac{2V_{DC}}{1-T_{st}/T_{sw}}. \tag{13}$$

Similarly, putting (12) into (8) and (10), the dc-link voltage for UST and LST states are given by:

$$V_{i\_UST} = V_{i\_LST} = \frac{V_{DC}}{1-T_{st}/T_{sw}}. \tag{14}$$

Obviously, the lower dc-link voltage occurs during LST and UST states when energy is stored in inductors according to (14). This energy is released to capacitors during NST states for voltage boosting. The fundamental ac peak output line-to-line voltage for the ZNPC is given by [21, 22]:

$$\hat{V}_{ll} = m_I.V_{\_NST} = m_I.B.2V_{DC}, \tag{15}$$

where

$$B = 1/(1 - T_{st}/T_{sw}). \tag{16}$$

In (15), $m_I \leq 1$ represents the modulation index whiles $B \geq 1$ represents the boost factor.

3. MODIFIED VSVM APPLIED TO Z-SOURCE NPC INVERTER

In this section, a modified VSVM strategy applied to the ZNPC inverter is presented. This modulation strategy is derived from the VSVM technique proposed in [19] which has

been proved to work very well for the conventional NPC inverter. The VSVM technique in [19] was developed by modifying the conventional SVPWM strategy to mitigate the problem of unbalanced input capacitor voltages. For a conventional SVPWM strategy, the reference vector is formed by selecting three nearest vectors. At times more than one switching state can be used to generate a vector. In such situations a combination of these switching states is used for controlling capacitor voltages.

Figure 3 shows the space vector diagram (SVD) with switching states and associated NP current for a conventional NPC inverter modulated using the conventional SVPWM strategy. The SVD is divided into six sectors (I to VI) and contain twenty-seven switching states classified as zero (V_0), small (V_{S1} to V_{S6}), medium (V_{M1} to V_{M6}) and large (V_{L1} to V_{L6}) vectors. Switching state 'P' means the top two devices of a phase leg are gated on, 'O' means the two middle devices are gated on while 'N' signifies the two bottom devices are turned on. If any output phase leg is in the 'O' state, there will be unequal charging/discharging of the top and bottom input capacitors. This leads to unequal capacitor voltages. To balance capacitor voltages effectively, it is required that average NP current in a switching cycle be zero. The conventional SVPWM technique is unable to achieve this because it uses the NP currents of small vectors to compensate those introduced by the medium vectors and it is not possible for the NP current introduced by the medium vectors to be fully compensated by those introduced by the small vectors. This is especially so when the modulation index is high and the power factor is low.

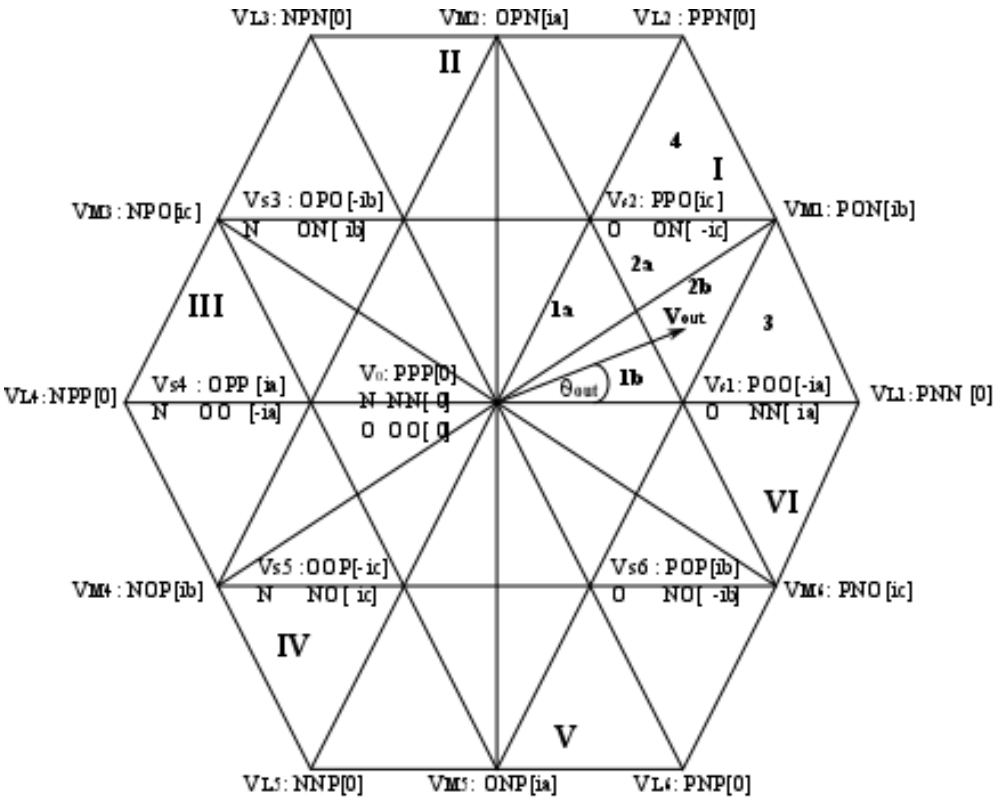

Fig. 3. Space vector diagram of conventional NPC inverter

In the VSVM technique, a new set of virtual vectors is defined to balance the capacitor voltages effectively. These virtual vectors are formed by combining vectors associated with certain switching states of the SVD shown in f*ig. 3*. Then the reference vector in each switching cycle is synthesized with nearest three virtual vectors. The virtual vectors formed have associated average NP currents equal to zero [1, 17, 19]. The virtual vectors for sector I are shown in *fig. 4* where k_5, k_6, $k_7 \in [0, 1]$ and $k_5 + k_6 + k_7 = 1$. Also k_1, k_2, k_3, $k_4 \in [0, 1]$ with $k_1 + k_2 = 1$ and $k_3 + k_4 = 1$. The case shown in *fig.4* represents the situation where $k_5 = k_6 = k_7 = 1/3$ and $k_1 = k_2 = k_3 = k_4 = 1/2$.

- V_{V0} is formed with V_0, which obviously generates a NP current equal to zero because all output terminals are connected to an identical dc-link point, so there is no current flowing in the input capacitors.
- V_{VSi} are obtained from an equal combination of two switching states having the same associated NP current but opposite in sign. For example, if vector V_{VS1} is selected for a period of time t_x, switching state ONN will be active for $0.5t_x$, and POO will be active for the remaining $0.5t_x$. Therefore, the average NP current during t_x will be:

$$\frac{1}{t_x}\{0.5.t_x.(i_a) + 0.5.t_x.(-i_a)\} = 0 \tag{17}$$

- V_{VMi} are obtained from an equal combination of three switching states having an associated NP current equal to i_a, i_b and i_c, respectively, and $i_a + i_b + i_c = 0$. For instance, if vector V_{VM1} is selected for a period of time t_z, switching state ONN will be active for $0.333t_z$, PON will be active for $0.333t_z$, and PPO will be active for $0.333t_z$. Therefore, the average NP current during t_z will be:

$$\frac{1}{t_z}\{0.333.t_z.(i_a) + 0.333.t_z.(i_b) + 0.333.t_z.(i_c)\} = 0 \tag{18}$$

- V_{VLi} are obtained from the switching states that define V_{Li}, all of them having an associated NP current equal to zero.

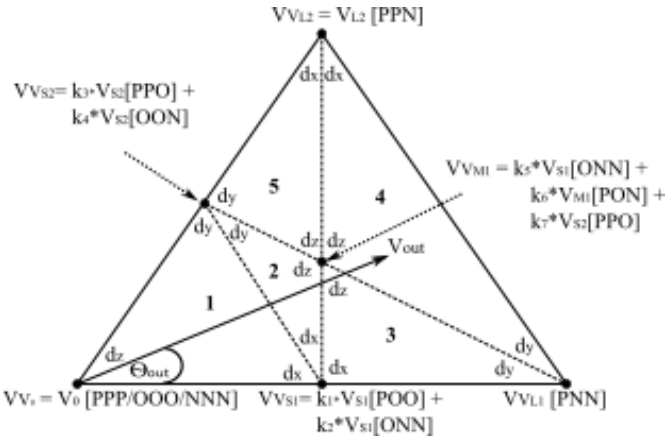

Fig. 4. Virtual space vectors for sector I

The duty ratios of selected virtual vectors in a switching cycle can be calculated as:

$$d_x.V_{V1} + d_y.V_{V2} + d_z.V_{V3} = \vec{V}_{out} \tag{19}$$

$$d_x + d_y + d_z = 1 \tag{20}$$

where V_{Vj} corresponds to the j^{th} selected virtual vector {j=1, 2, 3}. The duty cycles of different switching states forming the virtual vectors can then be determined.

Finally, a decision of the application of different switching states over a switching cycle is made. The order of chosen switching states' is such that connection of each phase to the dc-link points (p, o, n) is symmetrical. For instance, virtual vectors V_{VM1}, V_{VL1} and V_{VL2} are selected to form the reference vector in triangle 4 of sector I. Using the VSVM technique, these virtual vectors are formed from V_{S1} (ONN), V_{S2} (PPO), V_{M1} (PON), V_{L1} (PNN) and V_{L2} (PPN). These vectors can then be applied to the output using the switching sequence: PPO → PPN → PON → PNN → ONN. For a switching period, T_{sw}, the active time of each vector is determined using (21) to (25).

$$t_1[PPO] = k_7.d_z.T_{sw} \tag{21}$$

$$t_2[PPN] = d_x.T_{sw} \tag{22}$$

$$t_3[PON] = k_6.d_z.T_{sw} \tag{23}$$

$$t_4[PNN] = d_y.T_{sw} \tag{24}$$

$$t_5[ONN] = k_5.d_z.T_{sw} \tag{25}$$

In [19], the modification to the VSVM technique is seen in the switching sequence of the vectors applied to the output. The switching sequence is modified by introducing shoot-through states in phase legs of the ZNPC inverter for it to perform voltage buck-boost operation. Only the application of UST and LST states is considered in this work. An UST state means three top devices in a phase leg are turned on while a LST state represents turning on of three lower devices in a phase leg. A PWM switching sequence for achieving this goal is derived as discussed next.

Consider switching sequence PPO → PPN → PON → PNN → ONN for a conventional NPC inverter. An UST state can be inserted in a phase leg provided it is in the "O" state and the other phases are in the "N" or "O" state otherwise there will be a collapse of the output line-to-line voltages. In a similar way, a LST state can be inserted in a phase

leg if it is in the "O" state and the other two phases are in the "P" or "O" state [21]. Based on this reasoning, a LST state is introduced next to PPO (PPL) since this will not affect the output line-to-line voltage. Similarly, an UST is introduced next to ONN (UNN) with no adverse effect on the output line-to-line voltage. No UST or LST state can be introduced next to PON because that will breach the condition for insertion of shoot-through states. The resulting modified PWM sequence for the ZNPC inverter is shown in *fig*. 5 for triangle 4 of sector I.

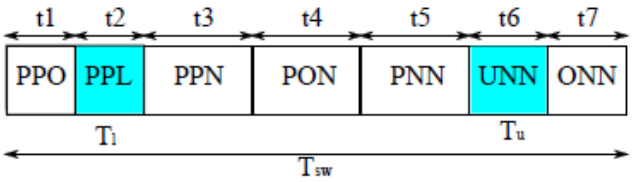

Fig. 5. Example VSVM switching sequence for the ZNPC inverter

4. RESULTS AND DISCUSSION

A simulation exercise in SABER® was undertaken to verify the modified VSVM technique for controlling the ZNPC inverter. The simulation results have been validated experimentally with a laboratory prototype. The parameters used for the simulation and experimental studies are presented in Table 1.

Table 1. Parameters used for simulation and experimental studies

Symbol	Description	Value
$2V_{DC}$	Input dc voltage	120 V
C_{up}, C_{dn}	Input capacitors	100 µF
$L_{1,2}$	Inductors for Z-source network	1 mH
$C_{1,2}$	Capacitors for Z-source network	470 µF
L_{load}	Load inductance	20 mH
R_{load}	Load resistance	10 Ω
f_{out}	Output frequency	50 Hz
f_{sw}	Switching frequency	5 kHz

4.1. Simulation results

The main contribution of this paper is the balancing of input capacitor voltages to eliminate low-frequency oscillations in a ZNPC inverter. The ability of this converter to perform voltage buck-boost function with the introduction of shoot-through states is also demonstrated. These are shown through simulation analysis presented next.

The circuit diagram of the model used for the simulations as well as the experimental validation is shown in *fig.1*. The converter is supplied with a dc voltage of 120 V via two series connected input capacitors. A Z-source network comprising two inductors, two capacitors and two diodes connects the input capacitors to the NPC circuit. The NPC circuit comprises three phase legs with each leg consisting of four IGBTs with anti-parallel diodes and two clamping diodes. An R-L load consisting of 10 Ω resistors and 20 mH inductors was used. The ZNPC inverter was initially operated as a conventional NPC inverter using the VSVM technique described earlier with a modulation index of 0.9 and shoot-through ratio of 0, respectively. With this mode of operation, the output line-to-line voltage is expected to have a fundamental component of 0.9 x 120 = 108 V. This is obvious as shown in *fig. 6 (a)* with a peak fundamental component of 106.6 V.

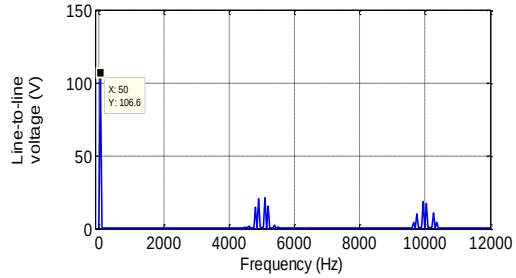

(a) FFT of line-to-line voltage, see (15)

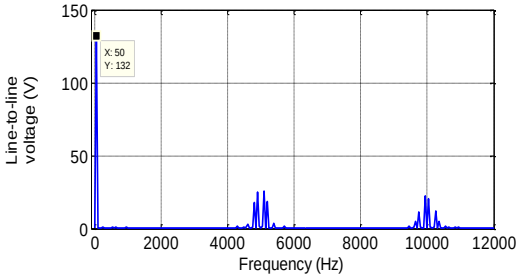

(a) FFT of line-to-line voltage, see (15)

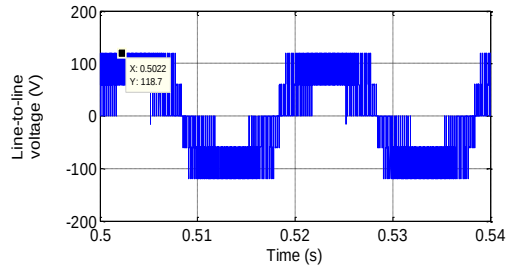

(b) Line-to-line voltage

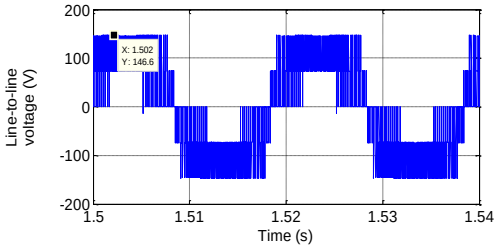

(b) Line-to-line voltage

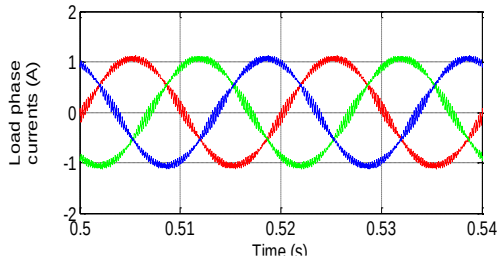

(c) Load phase currents

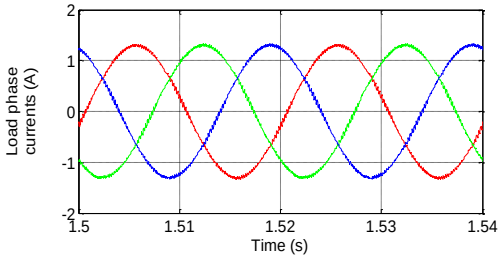

(c) Load phase currents

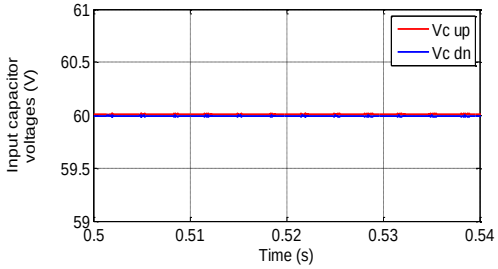

(d) Input capacitor voltages

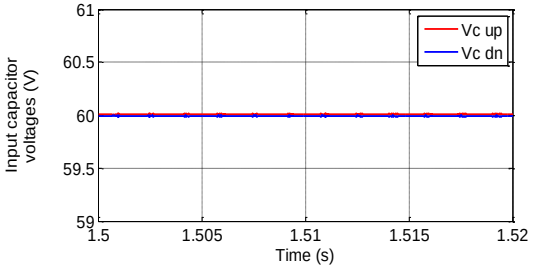

(d) Input capacitor voltages

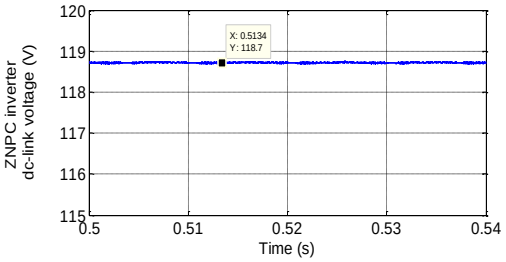

(e) DC-link voltage seen by NPC circuit, see (13)

Fig. 6. Simulation results for voltage-buck operation

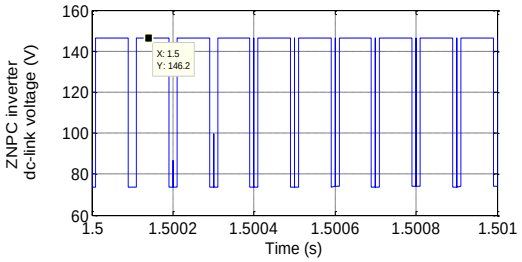

(e) DC-link voltage seen by NPC circuit, see (13) and (14)

Fig. 7. Simulation results for voltage-boost operation

The dc-link voltage appearing at the output of the Z-source network is clearly not stepped up and the output line-to-line voltage has a peak value of 118.7 V (*fig. 6(b)*) taking into consideration the voltage drops in the diodes. The corresponding load currents are shown in *fig. 6(c).* The voltages of the input capacitors are also shown in *fig. 6(d)* where it is noted that they are well balanced with no low-frequency oscillations superimposed on them. Similarly, the dc-link voltage seen by the NPC inverter circuit stands at 118.7 V as expected (*fig. 6(e)*).

For voltage-boost operation, shoot-through states are inserted into selected phase legs as described earlier. Here the modulation index is maintained at 0.9 while shoot-through ratio is set to 0.2. This gives a boost factor of 1/0.8 (= 1.25) and hence the peak fundamental output line-to-line voltage expected is 108 x 1.25 (= 135 V). *Figure 7* shows the boosted waveforms. The FFT of the output line-to-line voltage shows a fundamental value of 132 V (*fig. 7(a)*). A boosted dc-link voltage of 146.6 V is shown in *fig. 7(b).* The corresponding boosted load currents are shown in *fig. 7(c).* The input capacitor voltages are shown in *fig. 7(d)* where it is clear that they are well balanced with all low-frequeny oscillations eliminated completely. The Z-source network output voltage is shown in *fig. 7(e).* This clearly shows two levels of 146.2 V and 73.1 V, respectively, in accordance with (13) and (14).

4.2. Experimental results

To validate the simulation work carried out in section 4.1 an experimental prototype converter was set up. A 120 V dc supply was used to power the ZNPC inverter. The Z-source network comprises two inductors and two capacitors connected in an X-shape between the dc source and the back-end NPC circuit. The NPC circuit consists of three APTGL60TL120T3G NPC modules comprising four series-connected IGBTs with anti-parallel diodes and two clamping diodes. Heat sinks are attached to the IGBT modules for cooling purposes. Converter modulation is implemented using a DSP and an FPGA with a

series of circuits which allow information such as gate drive signals and measurement signals to be transferred to and from the power PCB board. *Figure 8* shows a schematic of the entire system used for the converter control. Experimental results were taken with a LeCroy Waverunner 6050 oscilloscope using a combination of differential voltage and current probes.

First, a buck mode of operation was commanded by using a modulation index and shoot-through ratio of 0.9 and 0 respectively. For this mode, the expected peak value of the fundamental output line-to-line voltage is limited to 0.9 x 120 (= 108 V). *Figure 9(a)* shows the experimental waveform for this condition with an actual value of 105 V. It is clearly seen that this matches well with the simulation result presented earlier. *Figure 9(b)* shows the output line-to-line voltage where a peak value of 117.7 V is recorded. The corresponding load currents are shown in *fig. 9(c).* This result matches well those shown in *fig. 6(c).* The waveforms for the input capacitors are shown in *fig. 9(d).* The result clearly shows balanced capacitor voltages with no low-frequency oscillations. Finally, *fig. 9(e)* shows the ZNPC inverter dc-link voltage which obviously matches that of simulation shown in *fig. 6(e).*

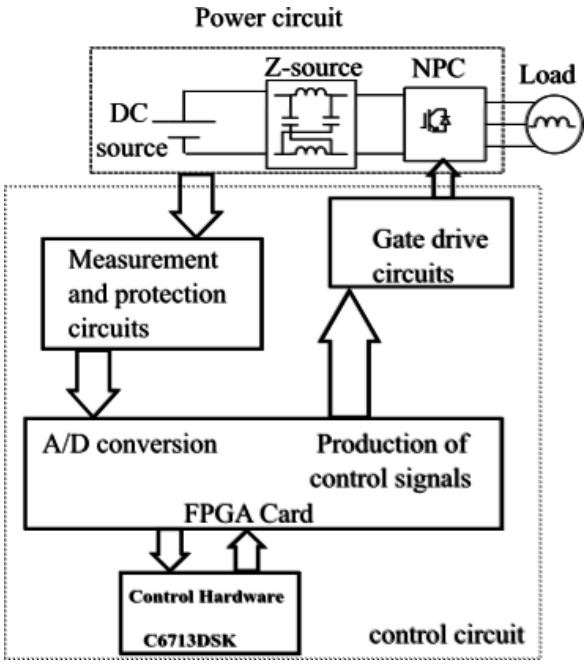

Fig. 8. Schematic of experimental set up

To command voltage-boost operation, the modulation index was maintained at 0.9 while the shoot-through ratio was set to 0.2. The boosted waveforms are shown in *fig. 10*. In these plots, we observe that there is a close matching with the simulation results. *Figure 10(a)* shows the boosted fundamental output line-to -line voltage with a peak value of 129.9 V. The corresponding output line voltage is shown in *fig. 10(b).* The associated boosted currents are shown in *fig. 10(c),* while the input capacitor voltages are shown in *fig. 10(d),* respectively. The boosted ZNPC inverter dc-link voltage is also presented in *fig. 10(e).*

These results clearly confirm effectiveness of the VSVM algorithm in balancing the input capacitor voltages of the ZNPC inverter in addition to voltage buck-boost operation.

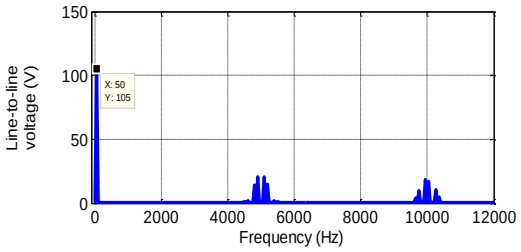

(a) FFT of line-to-line voltage, see (15)

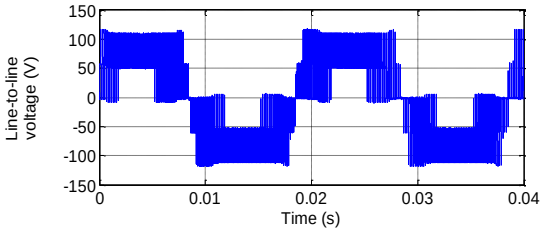

(b) Line-to-line voltage

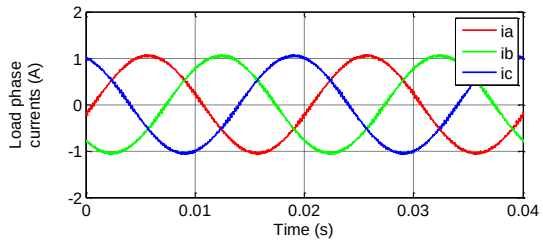

(c) Load phase currents

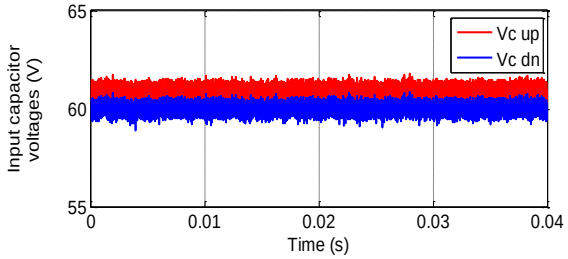

(d) Input capacitor voltages

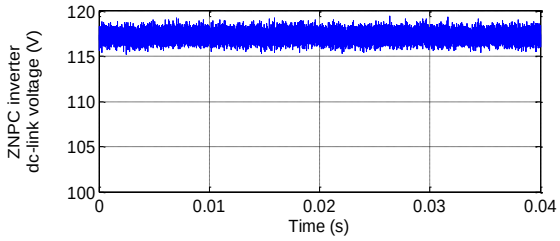

(e) DC-link voltage seen by NPC circuit, see (13)

Fig. 9. Experimental results for voltage-buck operation

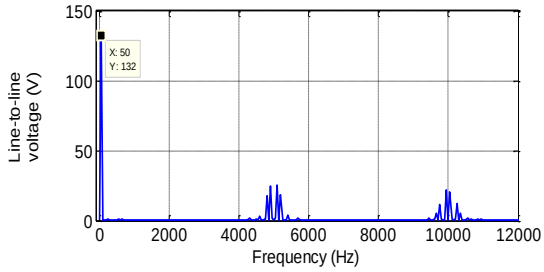

(a) FFT of line-to-line voltage, see (15)

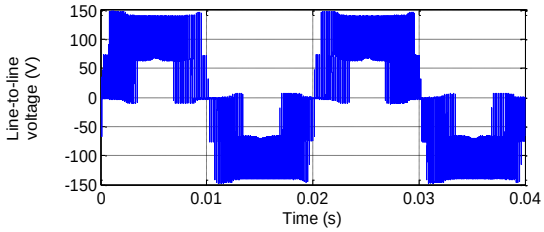

(b) Line-to-line voltage

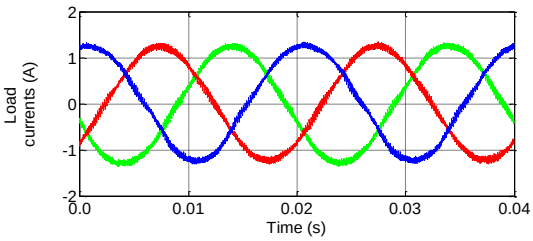

(c) Load phase currents

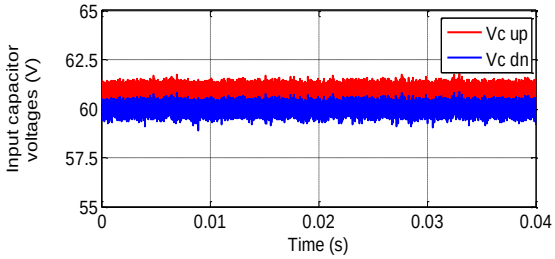

(d) Input capacitor voltages

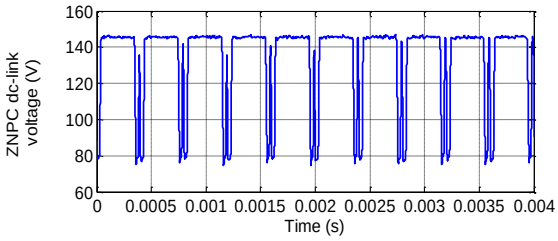

(e) DC-link voltage seen by NPC circuit, see (13) and (14)

Fig. 10. Experimental results for voltage-boost operation

5. CONCLUSIONS

A modified virtual space vector modulation approach used to control a Z-source neutral point clamped inverter has been presented. The ability of this converter to perform voltage buck-boost function has been verified. Balancing of the input capacitors of this converter by the modified virtual space vector modulation technique has also been confirmed through simulations and validated experimentally. The approach used here is superior to the conventional SVPWM in balancing the input capacitor voltages by eliminating completely all low-frequency oscillations on the capacitor voltages which may lead to premature failure of the converter. This benefit is however achieved at the expense of more switching commutations.

REFERENCES

[1] X. Wu, G. Tan, Z. Ye, G. Yao, Z. Liu, and G. Liu, *Virtual-Space-Vector PWM for a Three-Level Neutral-Point-Clamped Inverter with Unbalanced DC-Links*, IEEE Trans. Power Electron., vol. 33, no. 3, pp. 2630-2642, Mar. 2018.

[2] X. Li, W. Zhang, C. Du, X. Wu, and D. Xu, *Neutral point voltage control for three-level fuel cell power conversion system*, in Proc. 2nd IEEE Int. Symp. Power Electron. Distrb. Gen. Syst., pp. 122-128, Jun. 2010.

[3] H. Abu-Rub, A. Iqbal, S. Moin Ahmed, F. Z. Peng, Y. Li, G. Baoming, *Quasi-Z-source inverter-based photovoltaic generation system with maximu power tracking control using ANFIS*, IEEE Trans. Power Electron., vol. 4, no. 1, pp. 11-20, Jan. 2013.

[4] O. Ellabban, J. V. Mierlo, P. V. den Bossche, *Z-source inverter for vehicular applications*, in Proc. IEEE Vehicular Power and Propulsion Conference (VPPC), pp. 1-6, 6-9 Sept. 2011.

[5] W. Chen, H. Sun, X. Gu, and C. Xia, *Synchronized space-vector PWM for three-level VSI with lower harmonic distortion and switching frequency*, IEEE Trans. Power Electron., vol. 31, no. 9, pp. 6428-6441, Sep. 2016.

[6] Y. Zhang, J. Li, X. Li, Y. Cao, M. Sumner and C. Xia, *A method for the suppression of fluctuations in the neutral-point potential of a three-level NPC inverter with capacitor-voltage loop*, IEEE Trans. Power Electron., vol. 32, no. 1, pp. 825-836, Jan. 2017.

[7] A. Choudhury, P. Pillay, and S. S. Williamson, *Modified dc-bus voltage balancing algorithm for three-level neutral-point-clamped (NPC) IPMSM drive for electric vehicle applications*, IEEE Trans. Ind. Electron., vol. 63, no. 2, pp. 761-772, Feb. 2016.

[8] A. Choudhury, P. Pillay, and S. S. Williamson, *DC-Bus voltage balancing algorithm for three-level neutral-point-clamped (NPC) traction inverter drive with modified virtual space vector*, IEEE Trans. Ind. Appl., vol. 52, no. 5, pp. 3958-3967, May. 2016.

[9] J. Lyu, W. Hu, F. Wu, and K. Yao, *Three-level saddle space vector pulse width modulation strategy based on two-level space vector pulse width modulation for neutral-point-clamped*

three-level inverters, IET Power Electron., vol. 9, no. 5, pp. 874-882, Sep. 2016.

[10] Z. Mohzani, B. P. McGrath, and D. G. Holmes, *A generalized natural balance model and balance booster filter design for three level neutral point clamped converters*, IEEE Trans. Ind. Appl., vol. 51, no. 6, pp. 4605-4613, Nov. 2015.

[11] K. Wang, L. Xu, Z. D. Zheng, and Y. Li, *Capacitor voltage balancing of a five-level ANPC converter using phase-shifted PWM*, IEEE Trans. Power Electron., vol. 30, no. 3, pp. 1147-1156, Mar. 2015.

[12] A. Videt, P. L. Moigne, N. Idir, P. Baudesson, and X. Cimetiere, *A new carrier-based PWM providing common-mode current reduction and DC-bus balancing for three-level inverters*, IEEE Trans. Ind. Appl., vol. 54, no. 6, pp. 3001-3011, Dec. 2017.

[13] Y. Jiao, F. C. Lee, and S. Lu, *Space vector modulation for three-level NPC converter with neutral point voltage balance and switching loss reduction*, IEEE Trans. Power Electron., vol. 29, no. 10, pp. 5579-5591, Oct. 2014.

[14] G. J. Tan, Q. W. Deng, and Z. Liu, *An optimized SVPWM strategy for five-level active NPC (5L-ANPC) converter*, IEEE Trans. Power Electron., vol. 29, no. 1, pp. 386-395, Jan. 2014.

[15] B. Jacob, M. R. Baiju, *A new space vector modulation scheme for multilevel inverters which directly vector quantize the reference space vector*, IEEE Trans. Ind. Electron., vol. 62, no. 1, pp. 89-95, Jan 2015.

[16] S. R. Pulikanti, M. S. A. Dahida, and V. G. Agelidis, *Voltage balancing control of three-level active NPC converter using SHE-PWM*, IEEE Trans. Power Del., vol. 26, no. 11, pp. 258-267, Jan. 2011.

[17] C. Hu, X. Yu, D. G. Holmes, W. Shen, Q. Wang, F. Luo, and N. Liu, *An improved Virtual Space Vector Modulation Scheme for Three-Level Active Neutral-Point-Clamped Inverter*, IEEE Trans. on Power Electron., vol. 32, no. 10, pp. 7419-7434, Oct. 2017.

[18] A. R. Beig, S. Kanukollu, K. A. Hosani, and A. Dekka, *Space-vector-based synchronized three-level discontinuous PWM for medium-voltage high-power VSI*, IEEE Trans. Ind. Electron., vol. 61, no. 8, pp. 3891-3901, Aug. 2014.

[19] S. B. Monge, J. Bordonau, D. Boroyevich, and S. Somavilla, *The nearest three virtual space vector PWM – a modulation for the comprehensive neutral-point balancing in the three-level NPC inverter*, IEE, Power Electronics Letters, pp. 11-15, 2004.

[20] S. W. Gui, Z. J. Lin, and S. H. Huang, *A varied VSVM strategy for balancing the neutral-point voltage of dc-link capacitors in three-level npc converters*, Energies, vol. 8, no. 3, pp. 2032-2047, Aug. 2015.

[21] F. B. Effah, P. Wheeler, J. Clare, and A. Watson, *Space-Vector-Modulated Three-Level Inverters With a Single Z-Source Network*, IEEE Trans. Power Electron., vol. 28, no. 6, pp. 2806-2815, Jun. 2013.

[22] P. C. Loh, F. Gao, F. Blaabjerg, and S. W. Lim, *Operational analysis and modulation control of three-level Z-source inverters with enhanced output waveform quality*, IEEE Trans. Power Electron., vol. 24, no. 7, pp. 1767-1775, Jul. 2009.

MODELING AND ELECTRICAL CHARACTERIZATION OF MOSFETs 'EKV MODEL' USING MATLAB

Abdelkrim **MOSTEFAI**[1], Hamza **ABID**[1], Smail **BERRAH**[2]
[1]*Applied Materials Laboratory, University of Sidi Bel Abbes, 22000- Sidi Bel Abbes, Algeria*
[2]*LMER Laboratory, University of A/Mira of Bejaia, Bejaia, Algeria*
mostakrimo@yahoo.fr

Keywords: MOSFET, EKV model, CMOS, MATLAB, Transconductance gm, Methodology g_m/I_D.

Abstract*: The miniaturization of MOS transistors has increased the integration density and speed of operation of the circuits. This miniaturization has led to parasitic phenomena that degrade the current-voltage characteristics. The EKV MOSFET Model resolves this problem, this component enables to progress in miniaturization. This paper presents a simulation of MOSFET 'EKV model' using Matlab to identify the different output and transfer characteristics, transconductance g_m, Methodology g_m/I_D, etc.*

1. INTRODUCTION

The reduction of the metal–oxide–semiconductor field-effect transistor (MOSFETs) sizes is accompanied by the reduction of the gate oxide thickness; different scaling limits for MOSFETs have been discussed [1, 2, 3, 4, 5]. In this context, it must have a model which is continuous in all regime of operation: weak or strong inversion. In 1995, Enz, Krummenacher and Vittoz proposed a mathematical model of metal-oxide semiconductor field-effect transistors (MOSFET) valid in all regions of operation: weak, moderate, and strong inversion so called EKV model [6] which is intended for circuit simulation and analog circuit design.

This paper describes the electrical characterization and modeling for the EKV MOSFETs model using MATLAB.

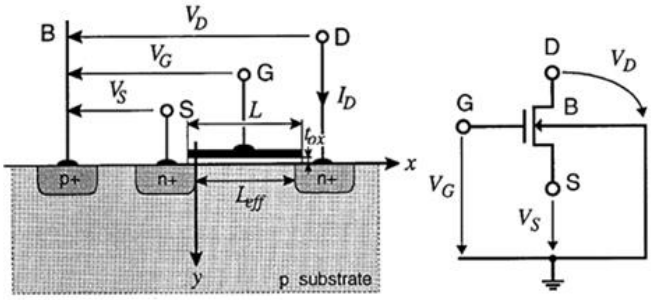

Fig. 1. Cross-section of an idealized n-channel MOS transistor and the corresponding symbol [7].

2. CONTINUOUS MODEL 'EKV MODEL'

The simulation of analog circuit, it is essential to dispose a model which is continuous in all regime of operation (weak, moderate and strong inversion). An EKV model developed in work of Enz, Krummenacher and Vittoz (the so-called "EKV model") solves the problem; EKV calculated the drain current as the combination of a forward current controlled by the source, and a reverse current controlled by the drain. All terminal voltages are called to the local substrate; therefore the inherent device symmetry is conserved. The EKV Mosfet Model is a mathematical model of metal-oxide semiconductor field-effect transistors (MOSFET) which is intended for circuit simulation and analog circuit design.

The following figure presents the log I_D–V_{GS} characteristics of a standard MOSFET.

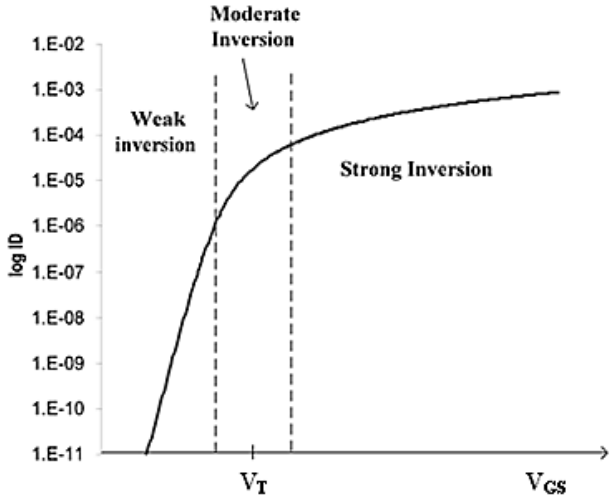

Fig. 2. Discontinuity of the I_{DS} (V_{GS}) characteristics at $V_{GS} \cong V_T$.

Their basic equation for drain current (in saturation) is given by [7,8,9,10] :

$$i = q^2 + q \Rightarrow i = \frac{I_D}{I_S} \Rightarrow I_D = i.I_S \tag{1}$$

$$I_S = 2nU_T^2\mu_n C_{ox}\frac{W}{L} \tag{2}$$

With $U_T = (KT/q)$

The pinch-off voltage V_P is a positive number defined as the value of the channel potential for which the inversion charge is zero in a non-equilibrium state. V_P depends on the gate voltage V_G and represents the voltage applied to the channel to equilibrate the effect of V_G. V_P is related to V_G and V_{TO} by:

$$\frac{V_P - V}{U_T} = 2(q-1) + log(q) \tag{3}$$

$$\Rightarrow q = invq\left(\frac{V_P - V}{U_T}\right) \Rightarrow V_P = \frac{(V_{GS} - V_{TO})}{n} \tag{4}$$

$$V_P = \frac{(V_{GS} - V_{TO})}{n} \;\Rightarrow\; V_{GS} = n.V_P + V_{TO} \tag{5}$$

The following figure presents the Inversion charge density vs. channel voltage.

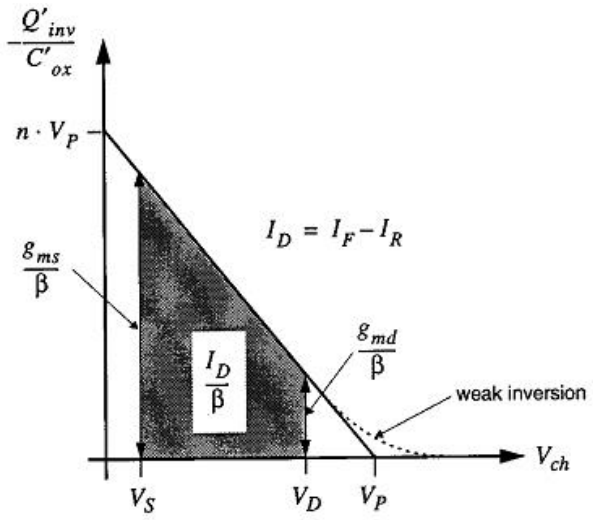

Fig. 3. The Inversion charges density vs. channel voltage.

$$I_D = \overbrace{\beta.\int_{V_S}^{\infty}\left[-\frac{Q'_{inv}(V_{ch})}{C_{ox}}\right].dV_{ch}}^{=I_F\ forward\ current} - \underbrace{\beta.\int_{V_D}^{\infty}\left[-\frac{Q'_{inv}(V_{ch})}{C_{ox}}\right].dV_{ch}}_{=I_R\ reverse\ current} \tag{6}$$

$$I_D = I_F - I_R \tag{7}$$

$$I_D = 2n\mu_n C_{ox}\frac{W}{L}\left(\frac{KT}{q}\right)^2\left[\left\{ln\left[1+exp\left(\frac{V_P - V_S}{\frac{2KT}{q}}\right)\right]\right\}^2 - \left\{ln\left[1+exp\left(\frac{V_P - V_{DS}}{\frac{2KT}{q}}\right)\right]\right\}^2\right] \quad (8)$$

On the other hand, $V_S = 0$, $V_{DS} < V_P$ and $V_{GS} > V_T$ (*i.e.* the transistor is operating in the non-saturated regime). In that case the exponential terms are much larger than unity, and one can write:

$$I_D = 2n\mu_n C_{ox}\frac{W}{L}\left(\frac{KT}{q}\right)^2\left[\left(\frac{V_P}{\frac{2KT}{q}}\right)^2 - \left(\frac{V_P - V_{DS}}{\frac{2KT}{q}}\right)^2\right] \quad (9)$$

$$I_D = \frac{1}{2}n\mu_n C_{ox}\frac{W}{L}[2V_{DS}V_P - V_{DS}^2] \quad (10)$$

$$I_D = \frac{1}{2}n\mu_n C_{ox}\frac{W}{L}\left[2\frac{(V_{GS} - V_T)V_{DS}}{n} - V_{DS}^2\right] \quad (11)$$

$$I_D = \mu_n C_{ox}\frac{W}{L}\left[(V_{GS} - V_T)V_{DS} - \frac{1}{2}nV_{DS}^2\right] \quad (12)$$

With

i: normalized drain current

I_S: specific current

I_F: forward normalized current

I_R: reverse normalized current

V_P: pinch-off voltage

U_T: thermal voltage

We will now study the transconductance *gm* of this model. Transconductance is the most important parameter for MOSFETs. The equation for *gm* is given by:

$$g_m \equiv \frac{\partial I_D}{\partial V_{GS}} \quad (13)$$

Transconductance *gm* (in strong inversion) is given by:

$$g_m \equiv \sqrt{2\mu C_{ox}\frac{W}{L}I_D} \quad (14)$$

Transconductance *gm* (in weak inversion) is:

$$g_m \equiv \frac{I_D}{nU_T} \tag{15}$$

Table 1. Main EKV intrinsic model parameters for first and second order effects and defaults values and units where applicable [15,16].

Name	*Description*	*Units*
COX	*Gate oxide capacitance*	*F/ m²*
VTO	*Nominal threshold voltage*	*V*
GAMMA	*Body effect factor*	*V^1/2*
PHI	*Bulk Fermi potential(2x)*	*V*
KP	*Transconductance parameter*	*A/V²*
THETA	*Mobility reduction coefficient*	*1/V*
UCRIT	*Longitudinal critical field*	*V/m*
XJ	*Source & drain junction depth*	*m*
DL	*Channel length correction*	*m*
DW	*Channel width correction*	*m*
LAMBDA	*Depletion length coefficient*	-
LETA	*Short channel effect coefficient*	-
WETA	*Narrow width effect coefficient*	-

Table 2. extraction procedure for the EKV model, sequence specifying device sizes, state (SI: strong, MI: moderate, WI: weak inversion, co.: conduction, sat.: saturation) and extracted parameters.

Device sizes	*Characteristics*	*Conditions*	*parameters*
Parameter Extraction			
Matrix W/L	I_D *vs.* V_G *gm vs* V_G	*WI*	*DL, DW*
Wide/long	I_D *vs.* V_S V_P *vs.* V_G I_D *vs.* V_G	*SI sat.* *MI sat.* *SI sat.@*V_S	I_S *VTO, GAMMA, PHI* *KP, THETA*
Wide/short	I_D *vs.* V_S V_P *vs.* V_G I_D *vs.* V_D	*SI sat.* *MI sat.* *SI co.-sat.*	I_S *LETA* *UCRIT, LAMBDA*
Narrow/long	I_D *vs.* V_S V_P *vs.* V_G	*SI sat.* *MI sat.*	I_S *WETA*

Table 3. Summary of basic DC simulation model equations [15,16].

Description	*Equation*
Pinch-off voltages	$V_P = V'_G - PHI - \gamma'.(\sqrt{V'_G + \left(\frac{\gamma'}{2}\right)^2} - \frac{\gamma'}{2})$ $V'_G = V_G - VTo + PHI + GAMMA.\sqrt{PHI}$
Slope factor	$n = 1 + \frac{GAMMA}{\sqrt{V_P + PHI}}$
Transconductance, mobility reduction	$\beta = KP.\frac{W_{eff}}{L_{eq}}.\frac{1}{1 + THETA.V_P}$
Effective length & width	$L_{eff} = L + DL, W_{eff} = L + DW$
Channel length modulation & velocity saturation	$L_{eq} = L_{eff} - \Delta L + \frac{V'_{DS}}{UCRIT}$ $\Delta L = LAMBDA.L_C.In(1 + \frac{V_R}{L_C.UCRIT})$ $L_C = \sqrt{\frac{\varepsilon_0 \varepsilon_{si}}{COX}}.XJ$ $V_D - V_S \le V'_{DS} \le V_{DSS}$ $0 \le V_R < V_D - V_S - V'_{DSS}$ *V'_{DS} and $V_R$are continuous functions, V_{DSS} and V'_{DSS} depend on bias, L_{eff}, UCRIT and LAMBDA*
Short & narrow channel effects	$\gamma' = GAMMA - \frac{\varepsilon_0 \varepsilon_{si}}{COX}.\left[\frac{LETA}{L + DL}.\sqrt{V_D + PHI} + \left(\frac{LETA}{L + DL} - \frac{3.WETA}{W + DW}\right).\sqrt{V_S + PHI}\right]$
Drain current and specific current	$I_D = I_F - I_R$ $I_{F(R)} = \begin{cases} I_S.exp\left[(V_P - V_{S(D)})/U_T\right] (WI) \\ I_S.\left[(V_P - V_{S(D)})/2U_T\right]^2 (SI) \end{cases}$ $I_S = 2.n.\beta.U_T^2 \quad U_T \equiv k.T/q$

3. RESULTS AND DISCUSSION

EKV MOSFET model is implemented under matlab m-file (program code), to plot different curves, from detailed model in section 2 (**CONTINUOUS MODEL 'EKV MODEL'**). *Figure 4* and *5* represent the output and transfer characteristics of EKV MOSFET model. *Figures 6* represent the Transconductance g_m as a function of drain current (I_D). *Figures 7* and *8* represent the transconductance efficiency g_m/I_D [11,12] as a function of normalized drain current ($I_D/(W/L)$) and inversion coefficient *(I_C), $I_C = I_D/(I_0 (W/L))$.*

Output and transfer characteristics (*figure 4* and *5*), transconductance *gm* (*figure 6*), transconductance efficiency *gm/I_D* [11,12] (*figure 7* and *8*) of EKV MOSFET model are

important concepts for analog CMOS for the following reasons:

- Method g_m / I_D which allows a rapid initial sizing in all operating regions [18].
- Enable to envisage MOSFET operation over a continuum of inversion levels [13].
- Little touches to make.
- Adopt simple rules for MOSFET sizing in all operating regions [18].
- Relatively reliable calculations: approach a few tens of percent.
- Enable to clearly choose an operating region, which is extremely useful, because each exploitation region possesses distinct characteristics which may or may not be advantageous for a given application.

The results in this work, in good agreement with previous results on Extraction Parameters and electrical characteristic for MOSFETs using various techniques applied to various MOSFETs models [14,15,16,17,19].

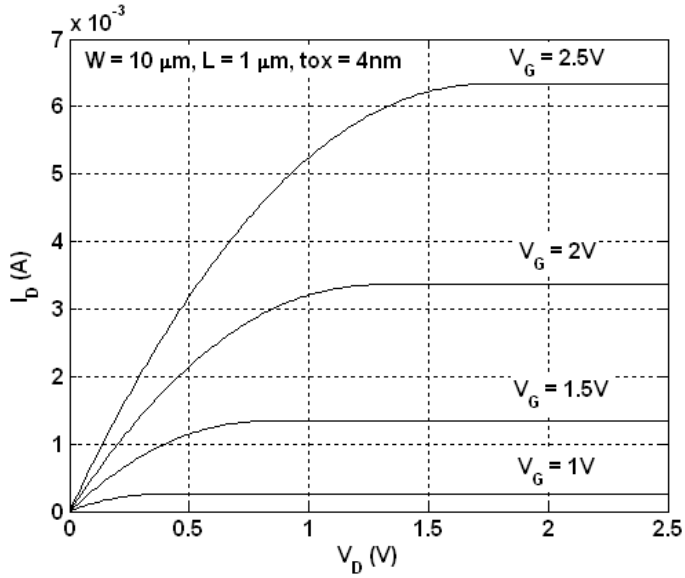

Fig. 4. output characteristics I_D vs. V_D of a short n-channel devices, V_S=0V.

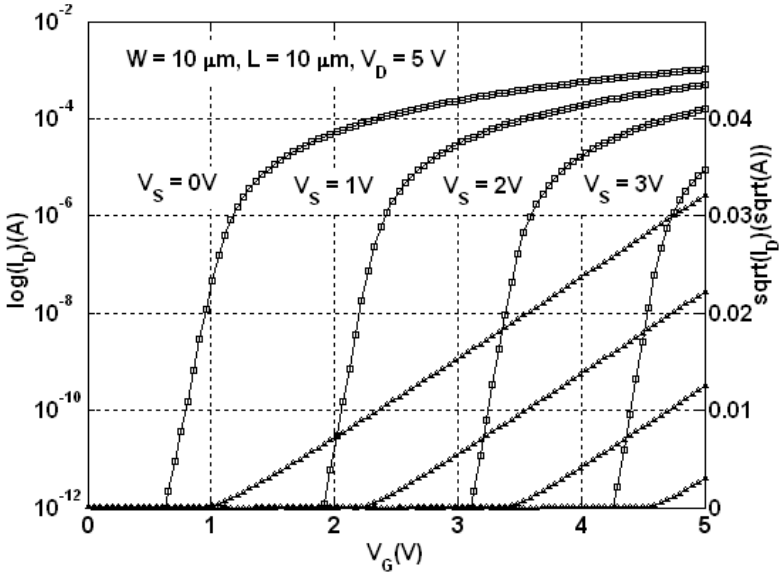

Fig. 5.a) Transfer characteristics log(I_D) & $\sqrt{I_D}$ vs. V_G of n-channel devices, - long-channel

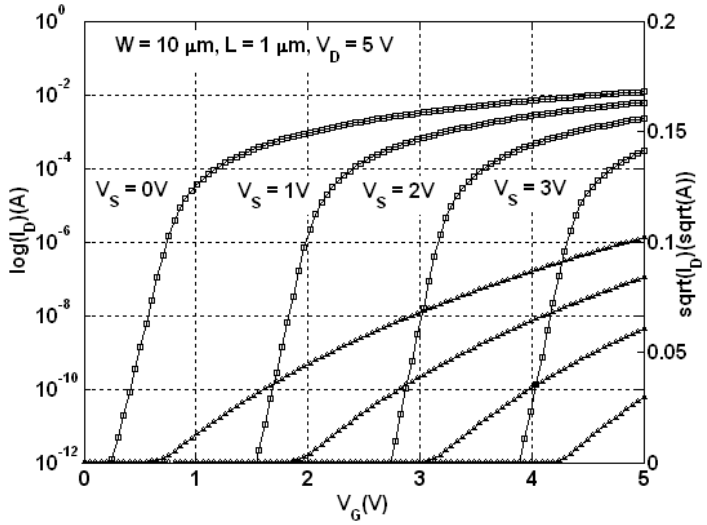

Fig. 5.b) Transfer characteristics log(I_D) & $\sqrt{I_D}$ vs. V_G of n-channel devices, - short-channel.

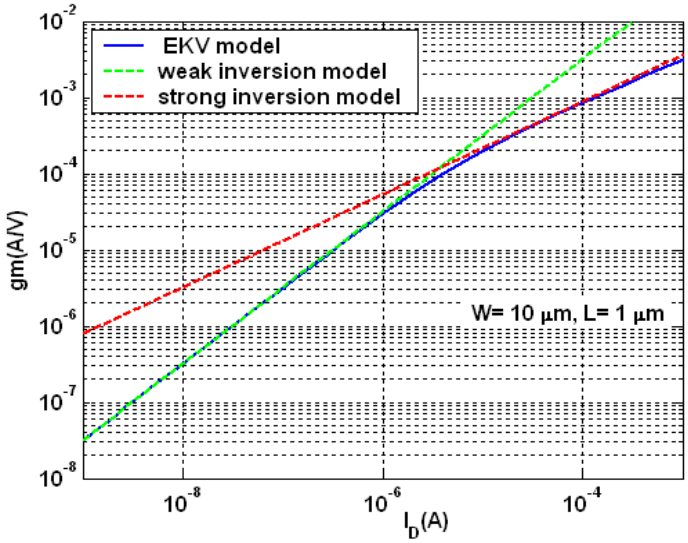

Fig. 6. MOSFET Transconductance gm vs. Drain Current I_D

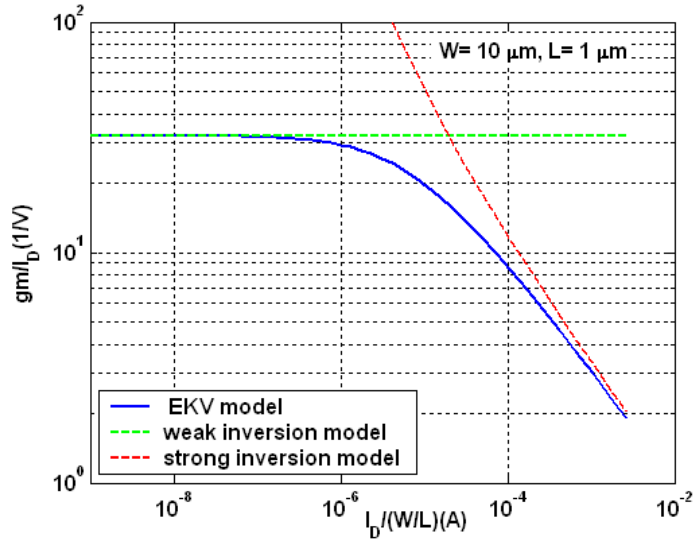

Fig. 7. MOSFET Transconductance Efficiency vs. Normalized Drain Current.

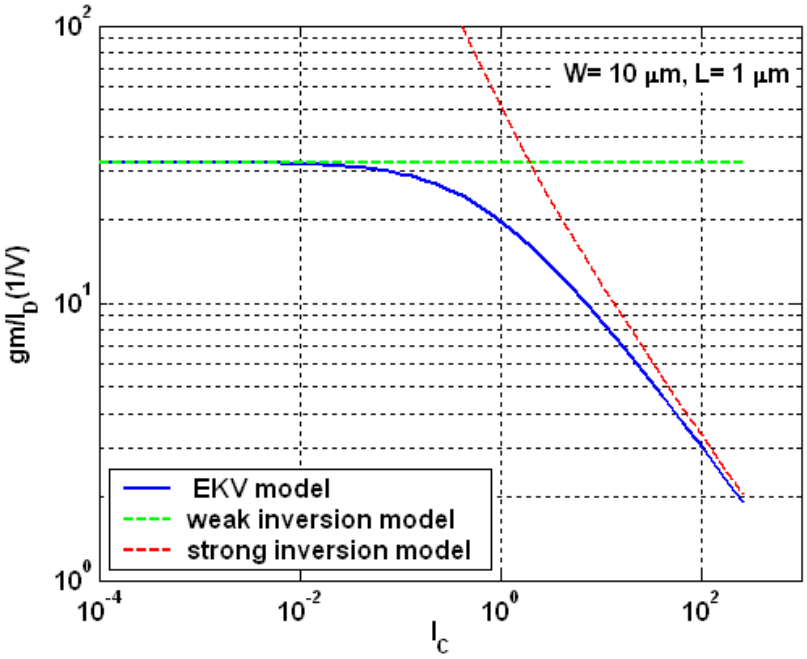

Fig. 8. MOSFET Transconductance Efficiency vs. Inversion Coefficient (I_C).

4. CONCLUSIONS

This paper describes the output and transfer characteristics, the transconductance efficiency, and the transconductances of EKV MOSFET model using Matlab. The EKV model is mathematical model of metal–oxide–semiconductor field-effect transistor (MOSFETs) valid in all regions of operation: weak, moderate, and strong inversion, utilized for circuit simulation and analog circuit design, prepares the path for sizing CMOS circuits suitable for sub-micron low-voltage, low-power circuits. It provides accurate modeling with relates a small signal of parameters to a large signal quantity, does not vary with transistor widths and controls the mode of operation.

REFERENCES

[1] Y. Taur, *CMOS design near the limit of scaling*, IBM Journal of Research and Development, Vol. 46, n°2, pp. 213-220, 2002.

[2] D.J. Frank et al, *Device Scaling Limits of Si MOSFETs and Their Application Dependencies*, Proceedings of the IEEE, Vol. 89, n°3, pp. 259-288, 2001.

[3] D.J. Frank, *Power-constraint CMOS scaling limits*, IBM Journal of Research and Development, Vol. 46, pp. 235-244, 2002.

[4] S. Oda, D. Ferry, *Silicon Nanoelectronics*, Ed. CRC press book, 2005.

[5] J. Wang, M.S. Lundstrom, *Does source-to-drain tunneling limit the ultimate scaling of MOSFET*, Technical Digest. IEEE International Electron Devices Meeting (IEDM), pp. 707-710, 2002.

[6] J.P. Colinge, C.A. Colinge, *Physics of Semiconductor Devices*, Ed. Springer Science -Business Media, 2002.

[7] C. Enz, F. Krummenacher, E.A. Vittoz, *An analytical MOS transistor model valid in all regions of operation and dedicated to low-voltage and low current applications*, Analog integrated circuits and signal processing, Vol. 8, n°1, pp. 83-114, 1995.

[8] C.C. Enz, *The EKV model: a MOST model dedicated to low-current and low voltage analogue circuit design and simulation*, in G.A.S Machado (Ed.), *Low-Power HF Microelectronics: A Unified Approach*, Institution of Electrical Engineers and Technology, pp. 247-300, 1996.

[9] C. Enz, E. Vittoz, *CMOS Low-Power Analog Circuit Design*, Proceeding of IEEE ISCAS, pp. 79-133, 1996.

[10] G.A.S. Machado, C.C. Enz, M. Bucher, *Estimating Key Parameters in the EKV MOST Model for Analogue Design and Simulation*, Proceeding of IEEE International Symposium on Circuits and Systems, pp. 1588-1591, Seattle, Washington, 1995.

[11] F. Silveira, D. Flandre, P.G.A. Jespers, *A gm/I_D based methodology for the design of CMOS analog circuits and its application to the synthesis of a silicon-on-insulator micropower OTA*, IEEE Journal of Solid-State Circuits, Vol. 31, n°9, pp. 1314-1319, 1996.

[12] W. Rivas-Torres, and Z.S. Roth, *Determination and Study of MOSFET Technology Current*, Canadian Journal on Electrical and Electronics Engineering, Vol. 4, n°2, pp. 75-82, 2013.

[13] D.M. Binkley, M. Bucher, and D.P. Foty, *Design Oriented Characterization of CMOS over the Continuum of Inversion Level and Channel Length*, Proceeding of the 7th International Conference on Electronics, Circuits and Systems (ICECS'2K), pp. 161-164, 2000.

[14] S.C. Terry, J.M. Rochelle, D.M. Binkley, B.J. Blalock, D.P. Foty, M. Bucher, *Comparison of a BSIM3V3 and EKV MOSFET model for a 0.5 um CMOS process and implications for analog circuit design*, IEEE Transactions on Nuclear Science, Vol. 50, n°4, pp. 915-920, 2003.

[15] M. Bucher, C. Lallement, C.C. Enz and F. Krummenacher, *Accurate MOS Modelling for Analog Circuit Simulation Using the EKV Model*, Proceeding of IEEE International Symposium on Circuits and Systems, Vol. 4, pp. 703-706, 1996.

[16] M. Bucher, C. Lallement, C. Enz, F. Theodoloz and F. Krummenacher, *The EPFL-EKV model equations for simulation, v2.6*, Electronics Laboratories, Swiss Federal Institute of Technology, Lausanne (EPFL), 1997.

[17] M. Bucher, C. Lallement and C. Enz, *An efficient parameter extraction methodology for the EKV MOST Model*, Proceeding of IEEE International conference on Microelectronic Test Structures (ICMTS), Vol. 9, pp. 145-50, 1996.

[18] P.G.A. Jespers, *The gm/I_D Methodology, A Sizing Tool for Low-voltage Analog CMOS Circuits*, Ed. Analog circuits and signal processing series, Springer Science+Business Media, 2010.

[19] R.R. Harrison, *MOSFET operation in weak and moderate inversion*, EE 5720, University of Utah.

ENVIRONMENTAL IMPACT OF ELECTRICITY

Mihaela **ŞTEŢ**
North University Centre of Baia Mare, Technical University of Cluj Napoca
mihaela.stet@cunbm.utcluj.ro

Keywords: energy, pollution, electricity, environment

Abstract*: Electricity is justly considered today as an indispensable factor of existence and development of society. Besides its incontestable benefits, there can be revealed some forms of environmental impact that, to a greater or lesser extent, create concern amongst specialists, as well as among the general public. The paper proposes an analysis of the impact on the environment of the electricity, starting from the different forms of production of electric energy, presenting also the negative environmental effects of transport, distribution, and use of electricity.*

1. INTRODUCTION

Since the beginning of electricity production and its use, the benefits of electricity have been worldwide recognized. Gradually, however, a number of shortcomings, negative effects accompanying electricity from the extraction and exploitation of energy resources to its use have been revealed.

Over time, highlighting negative effects has generated measures and solutions to reduce the negative impact on the environment. This paper reveals, in a structured form, the types of impacts associated with the generation, transport, distribution and use of electricity.

The methodology of this study combines different methods, mainly literature review, classification, data analysis and problem identification.

2. FORMS OF ENVIRONMENTAL IMPACT OF ELECTRICITY

There are many forms of impact that the energy sector produces on the environment. Of these, an important part is due to electricity, their presence being identified in the energy production phases, but also in the stages of transport, distribution and use.

The most well-known negative effects are on air, water and soil, both because their detection is easy, and because these contaminated environmental factors can substantially amplify the effects of pollution.

In addition to the thermal power plants that affect these environmental factors to a large extent, other forms of energy production have been identified that have negative environmental influences, even if they are not at the size of those caused by the thermal power plants.

Other forms of impact are also associated with activities in the electricity sector, such as noise pollution, vibration, visual pollution, waste generation and electromagnetic pollution (Table 1).

Table 1. Forms of environmental impact

Environmental impact forms / Types of activities	Air pollution	Water use and pollution	Land use and soil pollution	Noise	Vibration	Visual pollution	Impact on flora and fauna	Use of hazardous materials	Waste generation	Electromagnetic pollution
Thermal power plants	√	√	√				√		√	
Nuclear power plants	√	√						√	√	
Hydropower plants	√		√	√	√		√			
Wind power plants			√	√		√	√			
Solar power plants	√	√	√					√		
Geothermal plants	√		√							
Electricity transport	√	√	√	√		√	√			√

2.1. Air pollution

When talking about the air pollution generated by the energy field, the production in the thermoelectric power plants proves to be the worst for the environment. The amount and the wide range of emissions make this form of production the most commonly nominated in environmental impact assessments of energy. Both in the case of coal-fired power plants, and

hydrocarbon power plants, the air environment factor is the most affected.

The combustion gases of the thermal power stations generate a series of harmful emissions to the atmosphere, of which the greatest harmful effects are sulfur oxides, nitrogen oxides and ash dust.

Istrate and Guşă [1] present a wide range of techniques for the treatment of the gases emitted by the thermoelectric power plants, grouping them into three main categories:

- Pre-combustion treatment technologies;
- During combustion treatment technologies;
- Post-combustion treatment technologies.

In relation to pollutants being treated, the authors distinguish as procedures for the reduction of pollution the desulphurization, denitrification and reduction of solid emissions from combustion gases [1] (Table 2).

Table 2. Treatment techniques of emissions of thermal power plants

Treatment techniques of gaseous emissions	Type of purification techniques	Example of specific procedures
Sulphur oxides emissions treatment	Physicochemical desulfurization processes	Sulfur dioxide neutralization reactions with basic substances
	Treatment of fuels in pre-combustion phase	• Washing of coal • Hydrodesulfurization
	Combustion of powdered coal	• Limestone Additive Process
	Combustion in fluidized bed	• Combustion in stationary fluidized bed • Combustion in circulating fluidized bed
	Dry procedures	• With active coke or copper oxide • With calcium compounds • With nahcolite and trona
	Semi-dry procedures	• Semi-dry NIRO procedure • Mixt procedure
	Wet procedures	• With alkaline adsorbent • Ammonia absorption procedures • With alkaline-earth adsorbent • Hybrid procedure
Nitrogen oxides emissions treatment	Primary methods of reducing nitrogen oxide emissions	- burning in stairs, non-stoichiometric burning, optimal sizing of the furnace
	Secondary reduction methods	• Dry procedures • Wet procedures
Reduction of solid emissions	Use of filters	- mechanical filters, - acoustic filters; - wet filters, - electrostatic filters, - filters with bags made of woven or non-woven material.

Even though solar power production does not pollute air, the production of equipment and devices generates some greenhouse gas emissions. They have to be mentioned, even if

their values are much lower than other technologies. Emission estimates for photovoltaic systems in these stages are between 30 and 85 grams of carbon dioxide per kilowatt-hour.

Open loop geothermal systems generate emissions of carbon dioxide, ammonia, methane, boron, and hydrogen sulfide, which in the atmosphere are converted to sulfur dioxide, but their volume is substantially lower than that of thermal power plants.

Even hydropower plants face in operation with certain greenhouse gas emissions, the size of which varies according to the nature of the land, the size of the storage lake, and the climatic area in which they are built. So, flooding the land leads to vegetation decomposition, which leads to methane and carbon dioxide, reaching emissions of over 200 grams of carbon dioxide per kilowatt-hour [2].

Regarding the power transmission companies, they can pollute air both during construction work (suspended particulates) and during operation. Thus, sulfur hexafluoride pollution can occur due to the leakage of equipment or combustion gases emissions resulting from the generating sets or possible fires or explosions. High voltage overhead lines can cause pollution with ozone and nitrogen oxides due to Corona discharge occurring around active conductors, especially during rainy weather, but the contribution of these pollutants to the diminution of air quality is reduced [3].

2.2. Impact of electricity on water

In what it concerns the impact of electricity on water, two forms of impact can be identified: water pollution, as a result of activities in the chain of extraction, production, transport, distribution, use, and water consumption in these activities, which, in some cases, is significant.

In the case of coal-fired thermal power plants, as well those based-on fuel oil, the water flows consumed are significant, and restituted ones pollute the surface waters.

The energy production based on solar energy is associated with water consumption depending on the technology used. If, in the case of photovoltaic cells, water consumption is specific only to the production process, in that of the solar thermal collectors, it is significant in their operation. The type of equipment and cooling system influences the water consumption. For example, when using wet cooling technology with cooling towers, between 2200 and 2500 liters of water per megawatt hour of electricity are used.

Geothermal production facilities also use water for cooling and re-injection, depending on the technology used and the size of the operation. Water consumption per megawatt-hour is between 6000 - 15000 liters of water.

Also, in the transport of electric energy, can occurred accidentally effects on the water. For example, in the case of an electricity transmission company, the poor maintenance of the water-oil separators or the lack of precipitation caused the concentration of the pollutants in the internal sewerage network of the transformer stations.

2.3. Impact on land use and soil pollution

The transmission of electricity, due to the nature of high-voltage electrical installations, is associated with a significant impact on the environment through field surfaces occupied by power stations and overhead power lines.

Although there are no sources of soil pollution in normal electricity transmission activities, accidental pollution may occur during construction, installation, maintenance, such as leakage of oil, fuel, or some due to leaks, damage, failures of equipment with electro-insulating oil.

The use of solar energy for the production of electricity is also associated with land use, depending on the technology used. In the case of solar energy, the dislocation of the land depends on the technology, the topography of the site and the intensity of the solar resource.

Estimates for photovoltaic systems range from 3.5 to 10 hectares per megawatt, while estimates for concentrator collectors are between 4 and 16.5 hectares per megawatt. In order to reduce the impact, some solutions have been proposed, such as location on brownfields, lanes of the electric lines or buildings [4].

Use of wind energy to produce electricity is also associated with the impact on land use due to the location of wind turbines and the corresponding infrastructure. This is even more significant in the case of offshore facilities, thanks to bigger turbines than onshore facilities.

The lands affected by a geothermal system depend on the energy conversion system, power capacity, resource reservoir properties, wells and piping systems. the type of cooling system, the facilities required for operation [5]. However, land use for geothermal wells, pipelines and power plants is low compared to land use for other extractive energy sources such as oil, gas, coal and nuclear.

Another problem faced by geothermal systems is the land subsidence risk due to the removal of water from geothermal reservoirs. The use of open systems without the return of energy effluents in the source aquifer can lead to land drainage / compaction or surface water pollution. Restitution of water is often problematic when the water is exposed to atmospheric air or the water temperature exceeds> 50 ° C (in case of seasonal storage) [6]. Also, hydrothermal plants, the enhanced geothermal systems, are exposed to earthquake risk [5].

Hydropower plant construction and land flooding can lead to loss of forest lands, dislocation of cropland areas, erosion and sedimentation in reservoirs, soil degradation through construction. Land topography and size of generators influence the land area required to build a hydropower plant.

2.4. Noise pollution

Sounds, depending on their intensity, duration and frequency, can be considered one of the forms of pollution. Infrasound and ultrasound, at certain intensity levels, may be dangerous for humans, but also for other forms of existence.

The various activities in the energy sector are generating noise that can affect the employees of the companies involved, but also the population in the vicinity of the noise sources.

Installations and constructions specific to the transport of electricity generate noise due to the Corona discharge phenomenon around the overhead power lines, as well as the noise caused by the operation and vibration of the electrical installations. Also, during the construction of these installations, noise levels can be exceeded due to the operation of the equipment.

Intermittent, short-lived noise caused by flashover of insulating chains or switching action nearby the switching action may also be noted.

During operation, the noise generated by the operation of a wind farm creates pollution sound. The operation of wind turbines is associated with the noise produced by them: aerodynamic, generated by the turbine blade movement, and mechanical, due to the turbines themselves by their components.

2.5. Impact on vegetation and wildlife

There are a series of pollutants generated by the thermoelectric power plants with direct effects on the human body, like oxides of nitrogen, sulphur oxides, some heavy metals, carbon monoxide (respiratory diseases). Sulphur dioxide, sedimentary dusts, as well as different combinations of chlorine and hydrogen have direct effects on the vegetation. Carbon dioxide and nitrogen dioxide contribute to the greenhouse effect.

Sulfur dioxide contributes to the formation of acid rain with harmful effects on vegetation, forests, crops, watercourses and lakes. Acid particles formed can cause lung and heart disease [7].

Near the very high voltage lines, genetic and reproduction changes have been observed in some plant species.

A problem faced by hydropower developments is that of retention in accumulation lakes of sediments and increase of nutrient volumes. This leads to the multiplication of aquatic weeds that endanger the existence of other species of aquatic flora and fauna.

There is a risk that, at certain periods of the year, if the amount of water stored in the reservoir is high, some portions of the downstream river to be dried, with negative effects on animal and plant species. The risk is also amplified by the evaporation process that is more

pronounced in the reservoir area.

Due to the excess atmospheric humidity in the area, climatic disturbances can be caused by lowering the average zonal temperature and frequent foggy weather.

There are number of studies that have analyzed the effects of wind turbines on fauna, especially on birds whose habitats are affected. Changes in air pressure due to turbine blades have also been identified, with effects on their existence. But the most severely affected are by the collisions with the moving wind turbines. Negative effects have also been identified on fish and marine fauna [8].

Although the negative effects of the hydrokinetic systems have not yet been identified, there are some hypotheses about the potential impact on the environment. The need for extended marine space for wave energy equipment or the possible damage caused by these to aquatic habitats, as well as possible changes in salinity and hydrology can pose dangers to marine life.

Wave energy devices and associated cables can have negative impact, interfering with movements of whales and other large animals. More, they can alter sediment transport affecting benthic habitats, beach geomorphology, and intertidal ecology [9].

2.6. Visual pollution

Visual pollution is primarily determined by electricity transmission activities. In the same category, wind turbines are also registered.

As well, under certain lighting conditions, wind turbines can create the so-called shadow flicker effect [8].

2.7. Electromagnetic pollution

High and very high voltage installations cause the appearance of an electromagnetic field around them, the intensity of which varies with distance and voltage.

In the case of installations, constructions and equipment used in energy transport, the phenomenon of electrical induction can be revealed in metallic structures not connected to the earth and, also, radio interference phenomena.

In a study, Popescu [10] points out that because of parasitic radiation of high voltage lines, transformation points, radio-TV transmitters, radars, communications systems may pose dangers to the human body, especially organs slightly irrigated with blood (eye, bile, spine, etc.). The effect of electromagnetic fields on biological organs is dependent on the intensity and frequency of the field. He highlights the occurrence of the thermal and electrochemical effects.

According to the European legislation, transposed in Romanian legislation, two categories of effects of the electromagnetic field on the human body can be identified: direct

and indirect effects, *figure 1*.

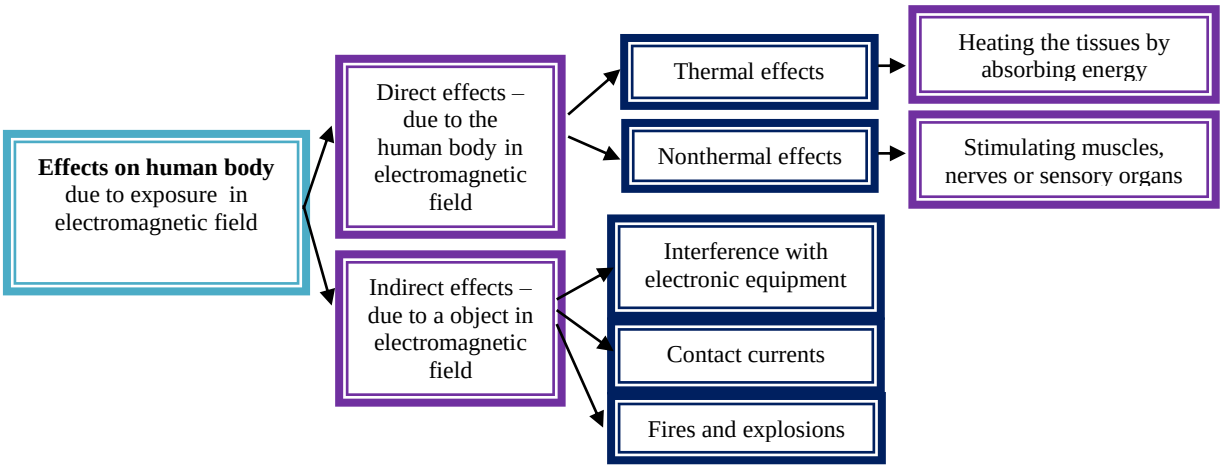

Fig.1 Effects of exposure of human body in electromagnetic field

In what it concerns electromagnetic influences on the environment, Nicolaescu [11] also groups them into two categories. In the category of direct influences of the electromagnetic field, there are ecological perturbations on plants and animals, pollution by the electromagnetic induction effect, as well as by the accidents it can produce. As indirect influences, the author highlights noise pollution, indirect environmental pollution, air ionization, and radio-TV broadcast disruptions.

2.8. Use of hazardous materials

In the production of photovoltaic panels, several hazardous materials are used, depending on the cell type, such as acetone and acids: sulfuric, nitric and hydrochloric. They also contain a few toxic materials.

The potentially hazardous elements (Hg, B, As and Cl) produced in the geothermal solution are largely injected back into the production tank.

2.9. Waste generation

Among the activities in the energy sector, the largest generators of waste are the thermoelectric power plants. They generate solid and liquid waste, with negative effects on soil and water.

Of the solid waste, the most important are slag, ash and various compounds used in the purification processes. Liquid waste results from the treatment of the water used in the thermal circuit, the cooling water, the leakage from the main circuit, and the liquid lubricant residue.

Although electricity transport activities do not generate waste, the occasional existence of waste as a result of certain maintenance or construction works can be highlighted. If some

of these can be considered non-hazardous, there is also a range of hazardous waste for the environment: hazardous electric and electronic equipment, waste oil, accumulators, batteries, sludge from water-oil separators, various materials contaminated with hazardous substances, etc. [3].

Another major source of waste is represented by the nuclear power plants. In Romania radioactive waste is classified into six groups: exempt waste, transition, very low activity. low and medium activity of short life, respectively long life and high activity waste. The last 4 types have storage restrictions, requiring special high depth deposits to provide radiological barriers between radioactive substances and the environment [12].

Nuclear reactors used in the production of electricity produce radioactive waste not only during operation, but also after their shutdown or decommissioning. The author presents several radioactive waste management solutions: reducing the amount of radioactive waste by compaction or using a wet air pollutant filtering installation in combination with a liquid radioactive waste treatment facility that can treat the resulting mud instantly; or by accumulation in special tanks.

3. CONCLUSIONS

In the energy sector specific activities, a wide range of impact forms can be highlighted both during the construction of installations and facilities, as well as during the operating period.

If the negative influences identified during the construction phase are present for a limited period, relatively short, in the case of influences during the operating period, they are maintained over the lifetime of the equipment.

In some situations, the impact can be increased with the depreciation of the installations. For this reason, it is necessary a permanent monitoring of the values of pollution indicators.

In what it concerns the construction of energy facilities and equipment, the legislation of many countries requires that, since the design period to be identified the forms of impact they will generate in construction and operation, as well as measures to diminish these negative influences.

In order to identify, to analyse the negative effects produced and to find suitable solutions, there are necessary collaborations between specialists from different fields: electrical engineering, medicine, biology, geology, chemistry, physics and statistics.

REFERENCES

[1] M. Istrate, M. Guşă, *Impactul producerii, transportului şi distribuţiei energiei electrice asupra mediului*, Ed. AGIR, Bucureşti, 2000.

[2] Union of Concerned Scientists UCS, *Environmental Impacts of Hydroelectric Power* https://www.ucsusa.org/clean_energy/ accesed at 10.10.2018.

[3] Compania Națională de Transport al Energiei Electrice CNTEE Transelectrica SA, *Informația privind mediul,* București, www.transelectrica.ro.

[4] Union of Concerned Scientists UCS, *Environmental Impacts of Solar Power*, *Science for a healthy planet and safer world*, https://www.ucsusa.org/clean_energy/ accesed at 10.10.2018.

[5] National Renewable Energy Laboratory (NREL), *Renewable Electricity Futures Study*, 2012.

[6] R. Gavriliuc, and R. Zeghici, *Aplicații geotermale pentru încălzire și răcire centralizată*, Workshop GeoDH Bucuresti, 16 aprilie 2013.

[7] National Research Council (NRC), *Hidden costs of energy: Unpriced consequences of energy production and use*, Washington, DC: National Academies Press, 2010, Online at http://www.nap.edu/catalog.php?record_id=12794.

[8] Union of Concerned Scientists UCS, *Environmental Impacts of Wind Power*, Science for a healthy planet and safer world, https://www.ucsusa.org/clean_energy/ accesed at 10.10.2018.

[9] G. Cada, et all, *Potential Impacts of Hydrokinetic and Wave Energy Conversion Technologies on Aquatic Environments,* Fisheries, 2007, 32:4, pp 174-181.

[10] H. Popescu, *Poluarea electromagnetica in poligoane de trageri si in campul tactic*, Research regarding bio-electromagnetic interaction and the biological impact of human exposure to radiofrequency and microwaves electromagnetic fields, Project under the National Research Program CEEX 2005 from the Romanian Ministry of Education and Research, 2005, http://www.armyacademy.ro/, accessed at 25.11.2018.

[11] A. Nicolaescu, *Protecţia mediului – Lucrări practice de laborator*, Timişoara, 2003.

[12] C. M. Ciobanu, *Analiza situației deșeurilor radioactive produse de centralele nucleare,* Romanian Journal of Building Services, Revista Română de Instalații Volume 1 / No. 1 / 2015 / www.rjbs.ro, 2015.

INSTRUCTIONS FOR AUTHORS

Name **SURNAME**[1], Name **SURNAME**[2], **...**

[1] *Affiliation of 1st author,* [2] *Affiliation of 2nd author, ...*

Email of 1st author, Email of 2nd author, ... (it is compulsory only for the first author)

Keywords: List 3-4 keywords *(aligned to the left, 10 pt. bold, separated by commas; please choose keywords from IEEE Approved Indexing Keyword List)*

Abstract: *Abstract of max. 200 words, justify, 10 pt. italic.*

1. INTRODUCTION

The paper must be written in English. It shall contain at least the following chapters: introduction, research course (mathematical algorithm); method used; results and conclusions, references.

1.1. Fonts

Use DIN A4 Format (297 x 210 mm) MSWord format. Margins: top, bottom, left and right 2.5 mm each. The text should be written on one side of the page only. Use Times New Roman fonts, line spacing 1.3. The font formats are: paper title: 14 pt, bold, italic, capital letters, author's name(s): 12 pt, regular for name and 12 pt., bold, for surname; Affiliation: 11 pt., italic; key words: 10 pt., bold; Abstract: 10 pt., italic, word Abstract in 10 pt., bold; chapter titles (do not use automatic numbering): 12 pt., bold, capital letters; subtitles: 12 pt., bold, lower case letters; subsubtitles: 12 pt., italic, lower case letters; body text: 12 pt., regular; tables and figures caption: 11 pt.; italic; references: author 11 pt.; regular, title 11 pt. italic, year, pages, ... in regular.

1.1.1. Number of pages

The number of pages is not restricted.

2. FIGURES AND TABLES

Figures have to be made in high quality, which is suitable for reproduction and printing. Don't include photos or color prints if there are not clearly intelligible in gray scale option. Place figures and tables at the top or bottom of a page wherever possible, as close as possible to the first reference to them in the paper. Use either *fig. 1* or *figure 1* when necessarily.

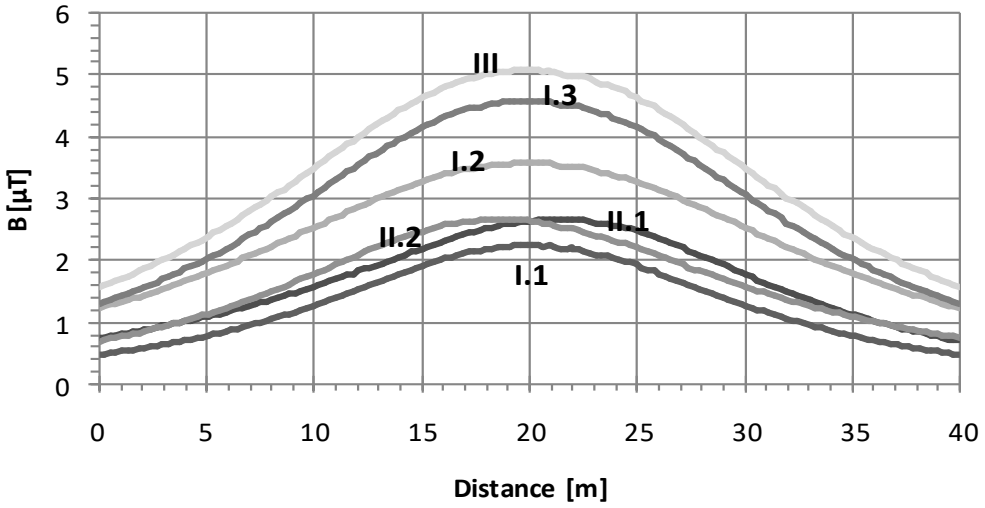

Fig. 1. Magnetic flux density at 1 m above the ground

Table 1. Transposing principle

	Circuit											
	1	*2*	*1*	*2*	*1*	*2*	*1*	*2*	*1*	*2*	***1***	***2***
1/3	*R*	*T*	***R***	***R***	*R*	*S*	*R*	*T*	*R*	*S*	***R***	***R***
line	***S***	***S***	*S*	*T*	*S*	*R*	*S*	*R*	*S*	*T*	***S***	***S***
length	*T*	*R*	*T*	*S*	***T***	***T***	*T*	*S*	*T*	*R*	***T***	***T***
1/3	*T*	*S*	***T***	***T***	*T*	*R*	*T*	*S*	*T*	*R*	***T***	***T***
line	***R***	***R***	*R*	*S*	*R*	*T*	*R*	*T*	*R*	*S*	***R***	***R***
length	*S*	*T*	*S*	*R*	***S***	***S***	*S*	*R*	*S*	*T*	***S***	***S***
1/3	*S*	*R*	***S***	***S***	*S*	*T*	*S*	*R*	*S*	*T*	***S***	***S***
line	***T***	***T***	*T*	*S*	*T*	*S*	*T*	*S*	*T*	*R*	***T***	***T***
length	*R*	*S*	*R*	*T*	***R***	***R***	*R*	*T*	*R*	*S*	***R***	***R***
Name	***I.1***		***I.2***		***I.3***		***II.1***		***II.2***		***III***	

3. EQUATIONS

Equations are centred on page and are numbered in round parentheses, flush to right margin.

$$a = b + c \tag{1}$$

Between equations, not interfered by text, there is only one empty line:

$$a = b + c \tag{2}$$

$$a = b + c \tag{3}$$

In text respect the following rules: all variables are italic, constants are regular; the references are cited in the text between right parentheses [1], the list of references has to be arranged in order of citation.

REFERENCES

[1] International Commission on Non-ionizing Radiation Protection, *Guidelines for limiting exposure to time-varying electric, magnetic and electromagnetic fields (Up to 300 GHz)*, Health Physics, vol. 74, no. 1, pp. 494-522, 1998.

[2] A. Marincu, M. Greconici, *The electromagnetic field around a high voltage 110 KV electrical overhead lines and the influence on the biological systems*, Proceedings of the 5th International Power Systems Conference, pp. 357-362, Timisoara, 2003.

[3] Gh. Hortopan, *Compatibilitate electromagnetică*, Ed. Tehnică, 2005.